◧ NTNU
Norwegian University of
Science and Technology

Stochastic Mooring Analysis of Aquaculture Installations

Malin Bjørkøy

NTNU Trondheim
Norges teknisk-naturvitenskapelige universitet
Institutt for marin teknikk

MASTER THESIS SPRING 2017

for

Stud. tech. Malin Bjørkøy

Stochastic Mooring Analysis of Aquaculture Installations
Stokastisk analyse av forankringssystemer for havbruksanlegg

Background

The aquaculture industry has grown significantly the latest years and driven by increased use of advanced marine technology and competence. Extensive development and research projects have resulted in increased focus on safety and consistent structural design of the aquaculture installations.

At present, keywords such as larger installations in more exposed and tougher areas together with stricter design requirements have posed demanding challenges to the industry. A consequence is the demand for new and more optimal design of cage and mooring systems. At the same time, the risk of fish escape must be reduced. Hence, small scale model tests in combination with more advanced numerical simulations are required.

The background and documentation of today's load- and material factors for design of structural components such as mooring lines are unclear. Of special interest is the variability of characteristic load effects and the inherent safety levels of present rules and regulations.

Scope of Work

1) Review relevant literature and describe briefly the state-of-art concepts for aquaculture installations like cage and mooring systems. Relevant equipment and hardware components shall be included.

2) Give an overview of the Norwegian rules and regulations, in particular the aspects in NS9415 that relates to structural design of cage and mooring system.

3) Familiarize with the simulation program FhSim and describe the theory that is relevant for design and behavior of cage collars and mooring systems.

4) Establish a FhSim model of a selected cage and mooring system. The selected concept shall be the same as studied during the project work. Simulations of selected cases shall be performed and reported. In particular, numerical simulation results of mooring line tension shall be estimated and compared for different models of environmental force models; irregular vs regular waves and the effect of interaction between waves and current.

5) Propose a method to calculate the annual distribution of mooring line tension when there is lack of simultaneous environmental data (waves and current). Establish the annual distribution of tension for irregular waves with current and compare the distributions with different ways to calculate characteristic tension. Indicate levels of probability exceedance of the different ways to calculate characteristic tension including load factors required in the regulations. Describe how probability of overload failure can be estimated by using an appropriate model for tension strength of a synthetic fiber line.

6) Conclusions and recommendations for further work.

General information

The thesis shall build on the project work report "Structural Design and Behaviour of Aquastructure Installations". The work scope may change or prove to be larger than initially anticipated. Subject to approval from the supervisor, topics may be changed or reduced in extent. In the project the candidate shall present her personal contribution to the resolution of problems within the scope of work.

Theories and conclusions should be based on mathematical derivations and/or logic reasoning identifying the various steps in the deduction.

The candidates should utilise the existing possibilities for obtaining relevant literature.

Thesis format
The thesis report shall be organised in a rational manner to give a clear exposition of results, assessments, and conclusions. The text should be brief and to the point, with a clear language. Telegraphic language should be avoided.

The report shall be written in English and edited as a research report including literature survey, description of relevant mathematical models together with numerical simulation results, discussion, conclusions and proposal for further work. List of symbols and acronyms, references and (optional) appendices shall also be included. All figures, tables and equations shall be numerated.
The original contribution of the candidate and material taken from other sources shall be clearly defined. Work from other sources shall be properly referenced using an acknowledged referencing system.

In addition to an electronic version of the report, two paper copies shall be delivered:
- Signed by the candidate
- The text defining the scope included
- In bound volume(s)
- Drawings and/or computer prints which cannot be bound should be organised in a separate folder.

Ownership
NTNU has according to the present rules the ownership of the project results. Any use of the project results has to be approved by NTNU (or external partner when this applies). The department has the right to use the results as if the work was carried out by a NTNU employee, if nothing else has been agreed in advance.

Thesis supervisor:
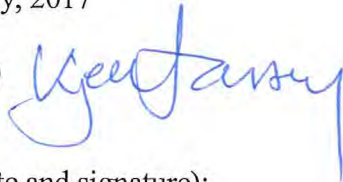Prof. II Kjell Larsen, NTNU/Statoil
Co-supervisor :
CTO Martin Søreide, Aqualine AS

Deadline: June 11, 2017

Trondheim, January, 2017

Kjell Larsen (sign.)
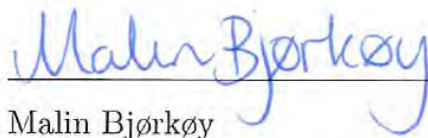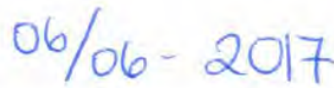
Malin Bjørkøy (date and signature):

Preface

This report presents the results of my Master Thesis, conducted at the Norwegian University of Science and Technology (NTNU), spring 2017, as the final part of my Master of Science in Marine Technology. The following comprise the study of *Stochastic Mooring Analysis of Aquaculture Installations*.

I would like to express my gratitude to my supervisor, Adjunct Professor Kjell Larsen, for valuable guidance, discussions and perspective throughout this process. His enthusiasm for the topic and valuable feedback on my work is highly appreciated. I would also like to acknowledge the cooperation with Aqualine AS, and especially co-supervisor Martin Søreide, CTO in Aqualine. Martin has contributed to this Master Thesis with a topic that is highly relevant for the aquaculture industry, as well as input on the design approaches applied in the industry today.

Martin Føre, associate professor at NTNU and research scientist at SINTEF Ocean, deserves acknowledgement for giving an introduction to the software FhSim and for establishing a simulation model for the purpose of this Master Thesis. Martin has answered questions regarding the simulation software, as well as programming and modelling, and his help is much appreciated.

Malin Bjørkøy

06/06 - 2017

Date

Summary

The aquaculture industry is experiencing rapid growth, which encourages moving the installations to more exposed sites, with harsher environmental conditions. With more exposed sites comes stricter structural requirements, and the response of the installations should be assessed and documented in irregular environmental conditions to capture the realistic behavior of the structures. The variability of environmental loads is not assessed in standard regular analyses, which is the industry's "best practice" today.

Aquaculture installations are designed based on the *partial coefficient method*, which is an ultimate limit state design approach. The procedure is based on requiring that the extreme loads that act on the structure, represented by characteristic load, S_C, must be lower than the minimum strength of the component, represented by characteristic strength, R_C. The partial coefficient method incorporates safety factors for both load and strength, to ensure that the structure meets the design requirements that are necessary to avoid technical failure. Design load, S_D, is then determined by multiplying characteristic load with a load factor, γ_f, and similarly, design strength, R_D, is determined by dividing the characteristic strength with a material factor, γ_m. The load factor depends on the type of design analysis conducted, while the material factor is chosen based on material and component type.

This master thesis focuses on the extreme effects of environmental conditions on a single frame moored cage system. In particular, numerical simulations of mooring line tension were performed in the simulation software FhSim, for different environmental conditions. Stochastic analyses of two sea states with 10 and 50 year return period were performed to determine the annual extreme value distribution of the load in irregular conditions. The extreme value distribution was compared to the distribution of strength, which was assumed normal distributed, and approximated based on the assumption that mean and standard deviation are related to minimum breaking load as $\mu = 1.05 \times MBL$ and $\sigma_x = 1.05 \times 0.03 \times MBL$, respectively.

The resulting distribution of load and strength showed that the curves did not overlap, which indicated that the probability of failure was extremely small. According to the partial coefficient method, characteristic strength is considered equal to minimum breaking load, which represents the 90% quantile of the strength distribution. This implies that a safety level is already inherent in the characteristic strength, before application of the material factor. After applying a material factor of $\gamma_m = 3.0$, the minimum strength of the mooring line became very conservative.

The distribution of load and strength was compared to different approaches for calculating

characteristic load; (i) static analyses with current only, (ii) dynamic analyses in irregular waves, and (iii) dynamic analyses in regular waves. Regular analyses based on the design wave approach gave resulting design load of more than twice as high as the irregular design load, and three times as high as the static design load in current only. The results showed that analyses based on the design wave approach are very conservative compared to irregular and static analyses. This implies that selection of analysis approach has significant impact on the requirements concerning the load the components must withstand, and the suppliers can possibly save money based on which approach they choose to apply.

Interaction between current and waves in irregular environmental conditions were inspected by isolating the response in current only and waves only, and compared to the combination of waves and current. The response analyses revealed a non-linear relationship between the combination of current and waves, and the theoretical summation of current and waves. The non-linearity occurred due to viscous drift, which are second-order effects that arise from the relative velocity between the structure and the fluid. Viscous drift caused both a mean drift force, and slowly-varying motions, which gave a significant increase in mooring line response. Slowly-varying motions are not captured by regular wave analyses.

This report concludes that design analyses should be conducted with longer time series and irregular environmental conditions to be able to study the behavior of fish farms in more realistic sea states and better capture the variability of sea loads. Challenges that comes with more exposed sites must be modelled correctly to ensure that the installations are fit for harsher environmental conditions.

Sammendrag

Havbruksnæringen opplever hurtig vekst, og installasjonene flyttes til mer eksponerte lokaliteter med hardere værkondisjoner. Med mer eksponerte lokaliteter følger strengere krav til strukturdesign, og responsen til installasjonene må vurderes og dokumenteres for irregulære sjøtilstander i tillegg til analysene som gjøres i dag. Variabiliteten til miljølaster er ikke tatt hensyn til i dagens industristandard, som stort sett kun benytter seg av regulære analyser.

Havbruksanlegg designes på bakgrunn av *partielle koeffisienters metode*, som krever at ekstrem last som virker på konstruksjonen, representert ved karakteristisk last, S_C, må være mindre enn minimum styrke av komponenten, representert ved karakteristisk styrke, R_C. Metoden inkluderer sikkerhetsfaktorer for både last og styrke, som skal sikre at konstruksjonen møter designkravet som er nødvendig for å hindre teknisk svikt. Design last, S_D, bestemmes ved å multiplisere karakterisk styrke med en lastfaktor, γ_f, og på samme måte, design styrke, R_D, bestemmes ved å dele karakterisk styrke på en materialfaktor, γ_m. Lastfaktoren avhenger av hvilken type designanalyse som utføres, mens materialfaktoren velges på bakgrunn av materiale og komponenttype.

Fokus for denne mastergraden er effekten av ekstreme miljølaster på en enkel rammeforankret merd. Numeriske simuleringer av strekk i en ankerline ble gjennomført i simuleringsprogrammet FhSim, for ulike sjøtilstander. Stokastisk analyse av to sjøtilstander med 10 og 50 års returperiode ble gjennomført for å bestemme årlig ekstremverdi fordeling av linestrekk i irregulær sjø. Fordeling av styrke ble antatt å være normalfordelt, og tilnærmet ved å anta at middelverdi og standardavvik er relatert til minimum bruddstyrke (MBL) som henholdsvis $\mu = 1.05 \times MBL$ and $\sigma_x = 1.05 \times 0.03 \times MBL$.

Resulterende fordeling av last og styrke viste at de to kurvene ikke overlappet, noe som indikerer at sannsynlighet for feil er ekstremt lav. I følge partielle koeffisienters metode så kan karakteristisk styrke antas å være lik minimum bruddstyrke, som representerer 90% kvantilen for fordelingen. Dette innebærer at karakteristisk styrke allerede inkluderer et visst sikkerhetsnivå, før materialfaktoren er anvendt. Når en materialfaktor på $\gamma_m = 3.0$, benyttes, så vil designstyrken bli veldig konservativ, og ikke reflektere usikkerhet i last siden denne verdien kommer ekstremt langt ut i "halen" til styrkefordelingen.

Fordeling av last og styrke ble sammenlignet med forskjellige måter å bestemme karakteristisk last; (i) statisk analyse med kun strøm, (ii) dynamisk analyse i irregulære bølger, og (iii) dynamisk analyse i regulære bølger. Regulære analyser basert på designmetoden gav designlast som var mer enn dobbelt så stor som den irregulære designlasten, og tre ganger så stor

som resulterende designlast fra statiske analyser i kun strøm. Resultatene viste at analyser basert på designmetoden i regulær sjø er veldig konservative sammenlignet med irregulære og statiske analyser. Dette antyder at valg av analysemetode har betydelig innvirkning på krav til styrke.

Interaksjon mellom strøm og bølger i irregulære sjøtilstander ble studert ved å isolere responsen i kun bølger og kun strøm, og sammenligne med respons fra strøm og bølger kombinert. Responsanalysene viste et ikke-lineært forhold mellom kombinasjonen av bølger og strøm og den teoretiske superposisjonen av kun bølger og kun strøm. Det ikke-lineære forholdet oppstod som følge av viskøs drift, som er en andre-ordens effekt som oppstår på grunn av relativ hastighet mellom konstruksjonen og vannet. Viskøs drift forårsaket både en gjennomsnittlig drift-kraft, samt sakte-varierende krefter, som viste seg å gi en betydelig økning i linestrekk. Sakte-varierende krefter fanges ikke opp i standard regulære analyser, siden to bølger med ulik høyde og amplitude er nødvendig for å få denne effekten.

Denne rapporten konkluderer med at designanalyser bør gjennomføres med lengre tidsserier og irregulære sjøtilstander, for å kunne studere adferden til et havbruksanlegg i mer realistiske kondisjoner, og for å fange variabiliteten i lastene. Utfordringene som kommer med mer eksponerte lokaliteter må modelleres korrekt for å sørge for at installasjonene er tilpasset tøffere sjøtilstander.

Contents

List of Tables

List of Figures

Nomenclature

The most used nomenclature is presented below. Those not included here will be presented when used in the text.

A_{ij}	added mass coefficient
A_W	wave particle acceleration
C_D	drag coefficient
C_L	lift coefficient
C_M	mass coefficient
D	cylinder diameter
d	twine diameter
F_D	drag force
F_e	effective fetch length
F_L	lift force
F_N	normal force
F_R	resultant force
F_T	tangential force
H	wave height
H_{max}	maximum wave height
H_S	significant wave height
k_E	elastic stiffness
k_G	geometric stiffness
k_{tot}	total stiffness
N	number of simulations
n	normal vector
p	hydrodynamic pressure
R	strength of the component
R_C	characteristic strength
R_D	design strength
S	load
$S(w)$	wave spectrum
S_n	solidity
S_C	characteristic load
S_D	design load
T_p	peak period
U_{10}	average wind velocity at 10 meter height
U_A	adjusted wind velocity
U_S	increased current velocity

U_∞	inflow current velocity
V_C	current velocity
V_R	relative velocity
V_r	partial relative velocity
V_S	structure velocity
V_W	wave particle velocity
w_p	peak frequency
x	position vector
ρ	mass density of water
γ	peakedness parameter
γ_m	material factor
γ_f	load factor factor
λ	wave length
μ	mean
σ_x	standard deviation

LIST OF FIGURES

1   Introduction

The introduction will present the background of the research questions investigated in this Master Thesis, and why there is a need to highlighting these topics. The objectives and limitations of the study are presented, together with a presentation of previous work. The structure of the report is introduced at the end for reader guidance.

1.1   Background

Since modern commercial aquaculture begun in Norway in the early 1970's, the industry has experienced rapid development and growth. Aquaculture installations are getting larger, the environmental conditions become tougher, and the fish farms are moved to more exposed sites. This entails stricter requirements for structural design to avoid fish escape, and increased use of advanced technology is essential to meet the new challenges in the industry.

In the Norwegian aquaculture industry, NS9415 is the governing technical standard. The main purpose of this standard is to prevent fish escape due to technical failure and/or improper operation of the marine fish farm. The standard was drafted in 2003, and then revised in 2009. Since then, the industry has experienced rapid development, and it is essential that the technical standard assure the safety of the structures in light of the new challenges the industry opposes.

The design approach applied in the industry today is based on ensuring that the loads imposed on the structure over its lifetime does not exceed the strength of the installation and its components. The background and documentation of today's load – and material factors for design of structural components are unclear. Also, the variability of the load effects is not assessed in standard analyses.

Today, the industry perform design analyses with regular waves as "best practice". As the environmental conditions at fish farm locations get harsher, regular waves will not be sufficient to describe the realistic response of the structure. Improved analyses that address the variability of the environment and uncertainty in estimation of loads should be applied to ensure that the structures are fit for more exposed sites.

1.2   Objective

The main objective of this Master Thesis is to examine whether the technical standard and design procedures applied in Norwegian aquaculture today are good enough to cover the

new challenges the industry face. In this lies the need for studying the effects of irregular environmental conditions, and compare them to the response of the structure in regular waves, to see if irregular conditions have prominent influence on the characteristic loads applied in the design approach. Also, interaction between current and waves must be studied to inspect second-order effects on the response.

In particular, response of mooring lines in different environmental conditions is examined in a simulation study, to inspect the extent of the standard design approaches. A method for determining the annual distribution of extreme mooring line tension when there is lack of simultaneous data is proposed, and used for design checks in terms of varying environmental force models.

1.3 Limitations

The simulation study was limited to inspecting the variability of the extreme tension in one windward mooring line. This component was chosen to illustrate the application of the Two Sea States Approach, and the conclusions made in this report are only valid for the specific system and specific mooring line. Distribution of load and characteristic loads for other components of the fish farm were not examined.

The inspected 10 and 50 year environmental conditions were based on a site survey conducted at Salatskjæra, an exposed location in Frøyhavet. The distribution of mooring line tension is thus valid only for locations with similar sea states.

The level of detail in the description of the relevant theory for this Master Thesis is varying, due to limited time and space. The main focus of this report lie on theoretical concepts that were highly relevant for the simulation study. The report includes a detailed description of sea loads and stochastic analyses, while aquaculture concepts and components are introduced briefly.

1.4 Previous Work

This Master Thesis is a continuation of the topic examined in my Project Thesis conducted during fall 2016. The project thesis *Structural Design and Behavior of Aquaculture Installations* mainly focused on static and dynamic mooring analyses, and regular wave analyses were performed to examine the mooring line tension in different environmental conditions, as well as accidental conditions. Some parts of the project thesis were used as background literature for this Master Thesis. This will be specified in section 1.5.

1.5   Structure of the Report

This report will first introduce the Norwegian aquaculture industry; different concepts, components, and the rules and regulations which applies to the industry today. Then, the theoretical background for performing stochastic mooring analyses is explained. The last part of this report presents the simulation study that was performed, with a detailed description of the applied method, results and discussions of results. The report will end with conclusions and recommendations for further work.

Chapter 2 to 4 gives a brief introduction to the Norwegian aquaculture industry. Chapter 2 presents an overview of different fish farm concepts, their components, how to develop a fish farm as well as some state of the art concepts. This chapter is based on the project thesis. The mooring system of an aquaculture installation and its components is presented in chapter 3, which is also based on previous work. Chapter 4 presents rules and regulations that apply for the Norwegian aquaculture industry.

Chapter 5 introduce design approaches, and presents the *partial coefficient method*, which is the governing design approach applied in the industry today. This chapter is based on previous work, but includes a more detailed explanation of the design procedure and how to determine extreme load effects.

Chapter 6 describe the sea loads that act on a floating fish farm, and how to model these loads for calculation and simulation purposes. Some parts are based on previous work, but this report includes a more comprehensive description of environmental loads and their effects on the response of the structure. Numerical models for determining sea loads are also introduced here.

Chapter 7 describe how dynamic response analyses are conducted, and how the motion of the structure can be described by mathematical expressions. The description of equations of motions is based on previous work.

Chapter 8 gives an introduction to statistical description of waves, stochastic processes and how to determine short– and long-term response of a structure. The theoretical concepts introduced here were used as basis for the simulation study and development of the extreme value distribution.

Chapter 9 presents FhSim, the software used in the simulation study for this Master Thesis. The software framework, key components and generic models are described.

Chapter 10 presents the simulation study that was performed to inspect the structure's behavior in irregular sea. The applied method is presented in detail. The results from the

simulation study are also presented in this chapter and discussed at the end of this report, together with final conclusions and recommendations for further work.

The reader of this Master Thesis is expected to have basic knowledge about marine hydrodynamics and statistics, but no prior knowledge about stochastic analyses are required.

2   Aquaculture Installations

Large scale aquaculture is a relatively new industry in Norway, and the fish farming technology has experienced rapid development in recent years. The combination of new technology and competence has made it possible to increase the size of farming facilities and move the fish farms to more exposed sites, which has made the aquaculture industry an important contributor to the Norwegian economy.

The farming conditions along the Norwegian coastline are favorable due to optimal temperature – and oxygen levels, flow conditions, salinity and wave exposure. The combination of environmental conditions and access to unique technical competence from the offshore industry, has made Norway world leading in aquaculture farming.

Today, several concepts for fish farming facilities are available on the market. The most common construction is the *open fish farm*, which is characterized by free water flow through the plant. *Closed fish farms* are, as the name suggests, closed to the surrounding environment and needs its own water circulation system (Karlsen, 2015).

Fish farms can be located in the surface or be submerged, either partly or fully submerged. This Master Thesis will focus on open surface fish farms. The following sections will present different fish farm concepts within this category, main components of the fish farm, as well as an introduction to development of fish farms. State of the art concepts will be introduced at the end of this chapter.

2.1   Fish Farm Concepts

Floating fish farms comes in various shapes and designs, and the choice of fish farm concept is often based on the amount of fish intended for the farm, as well as the environmental conditions on site.

The conditions on site can be defined according to degree of exposure. *Sheltered sites* represent locations in the inner parts of the fjords, protected from high waves and strong currents, while *exposed sites* have conditions more similar to those offshore. Exposed sites oppose challenges of harsh environmental conditions, such as strong currents, high waves, varying peak period and high wave steepness. Also, longer duration of storms, as well as longer distance from shore makes it more challenging to operate aquaculture installations at exposed sites (Fredheim, 2016).

Fish farm concepts can be categorized according to their structural properties and behavior

in the ocean environment (Fredheim and Langan, 2009):

- Flexible systems

- Hinged connected bridges

- Rigid structures

Different concepts for floating fish farms are presented in the following sections.

2.1.1   Circular Collar Fish Farm

The circular high-density polyethylene (HDPE) collar cage is an example of a flexible system. This concept is illustrated in figure 2.1. The collar is made of plastic pipes, which are welded together into preferred lengths and bent into circles with the desired ring size. Several rings, usually two, are connected to ensure sufficient buoyancy, as well as to serve as working platform for the operational staff. Circular plastic collars have high flexibility, which gives good seakeeping performances in demanding environmental conditions, and is often the preferred concept at exposed sites (Fredheim and Langan, 2009).
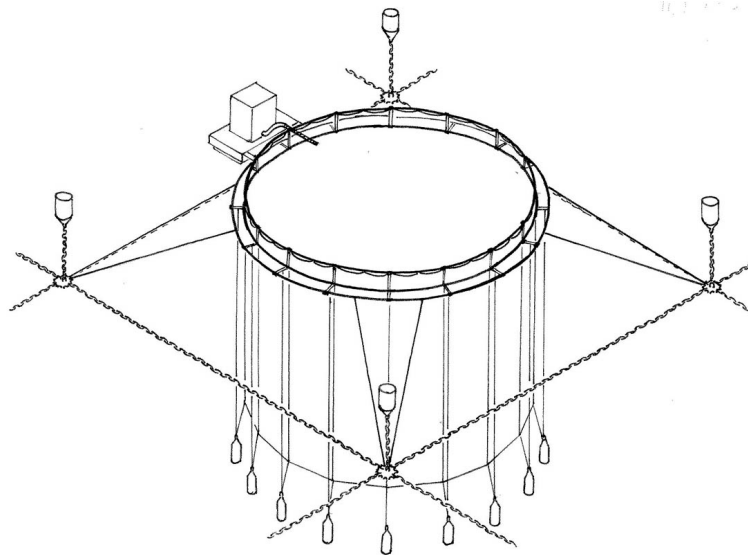
Figure 2.1: Circular collar fish farm (illustration by SINTEF Ocean)

A typical floating fish farm consists of several cages and a global mooring system to keep the farm in position. Circular collar fish farm concepts ensure good water flow conditions due to optimal distance between the collars. This is an advantage concerning available oxygen for the salmon and for avoiding salmon lice. The main disadvantage of this concept is the

working conditions. The working platform does not have room for extra storage, such that additional vessels with auxiliary equipment are needed to perform larger operations at the fish farm. Operational tasks are difficult to perform on the circular collar due to its flexibility, especially in bad weather (Fredheim and Langan, 2009).

2.1.2   Steel Fish Farm

Another fish farm concept is the interconnected hinged steel fish farms, which consist of square cages connected by bridges of steel. The concept is illustrated in figure 2.2. Polyester floatation is connected directly to the steel bridges and provides better flotation capabilities than the circular plastic collars. The interconnected hinged steel fish farms also have better working conditions due to larger and more stable working platforms. This makes the operation of the fish farm easier and safer. Lack of flexibility in the horizontal plane can cause structural problems when the fish farm is exposed to waves and ocean currents, and it is therefore more suitable for sheltered sites (Fredheim and Langan, 2009).
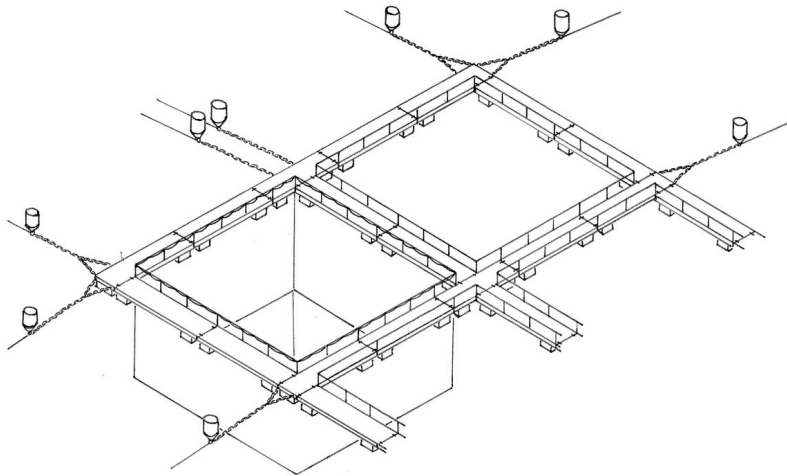
Figure 2.2: Steel fish farm (illustration by SINTEF Ocean)

2.1.3   Catamaran Steel Fish Farm

The catamaran steel fish farm is another concept with hinged connected bridges, which consists of several steel hulls. The hulls provide flotation, while the hinges allow for rotation in the horizontal plane. The hulls are not in direct contact with water, and therefore provide flotation only along one axis. This gives better resistance to displacement forces than the regular steel fish farms. In contrast to circular collar fish farms, the catamaran fish farms have the advantage of good working conditions, with large working platform area suitable

both for storage and for performing daily operations (Fredheim and Langan, 2009). An illustration of the catamaran fish farm is shown in figure 2.3.
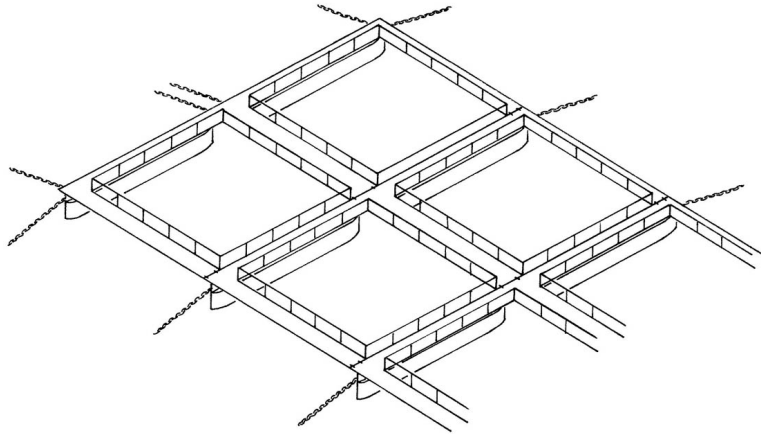
Figure 2.3: Catamaran fish farm (illustration by SINTEF Ocean)

2.1.4 Rigid Steel Fish Farm

Rigid steel fish farm concepts vary within the category. The most common types consist primarily of steel pipes welded together into square collars. Wide working platforms gives good working conditions, in contrast to the circular collar farms. Because these systems are rigid, they are highly impacted by environmental loads and are thus not suitable for exposed sites (Fredheim and Langan, 2009).

2.2 Fish Farm Components

An aquaculture fish farm can consist of several cages, and one farm usually range from 6 to 12 cages, depending on size of the location and amount of fish intended for the location. The three main components of a typical fish cage are the floating collar, the net cage and mooring system. In addition, buoys and weights are needed to provide the necessary buoyancy and to ensure that the net cage remains its desired shape, and hand rails and working platform are included for easier handling (Moe et al., 2007).

Figure 2.4 illustrates a single circular collar cage with its components highlighted. The following sections will briefly describe the main components of a typical fish cage concept.
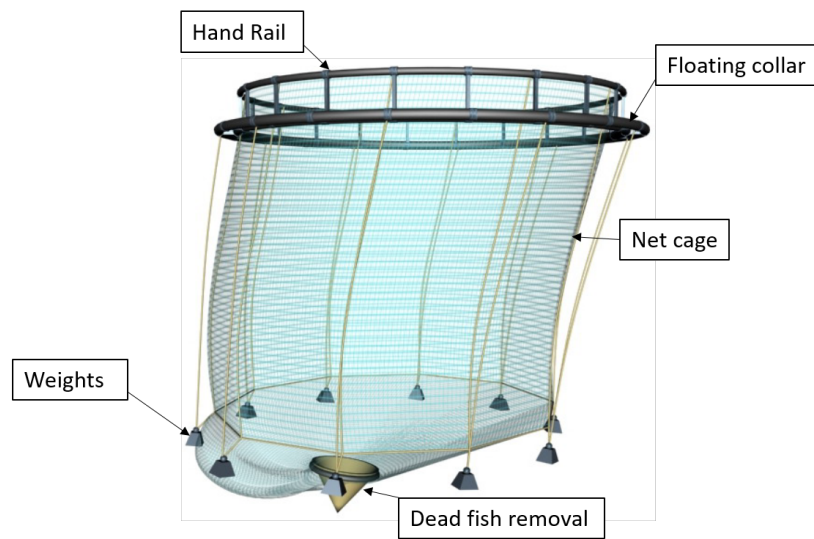
Figure 2.4: Single cage with main components (illustration by SINTEF Ocean)

2.2.1   Floating Collar

The floating collar serves as an attachment point for the net and integrates all parts of the floating fish farm. It provides buoyancy, distributes forces to the mooring system, and serves as a working platform for daily operations (Fredheim and Langan, 2009). The floating collar must also absorb the forces imposed on it. This includes loads that directly affect the collar, but also loads that affect its adjacent parts, such as mooring system, net pen, feeding equipment etc. (Standard Norway, 2009).

2.2.2   Net Cage

The farmed fish is kept in place in a net cage connected to the floating collar. Design of the net cage aim to reduce the risk of fish escape, and ensure fish welfare. The net must also be able to withstand forces from waves and current, as well as manual handling (Karlsen, 2015).

Form and function of the net cage are determined by several parameters, such as shape of the floating collar, necessary net volume, depth and net materials. Depending on collar type, net cages can be circular or square, and they can have vertical or inclined sides. The bottom is usually cone shaped to collect dead fish in the bottom center (Føre, 2016). A circular net cage provides the largest possible net cage volume compared to other shapes, and thus have higher fish capacity. Large volume is also beneficial for increasing the efficiency of operational procedures such as feeding. On the other hand, increased net cage volume implies a larger fish quantum to handle and hence increased consequences in the event of

fish escape (Karlsen, 2015).

Weights are applied to the lower parts of the net to keep the desired shape of the net cage when it is under influence of environmental loads. For circular cages, a filled polyethylene ring, called sinker tube, or separate weights, are used for maintaining the net shape in waves and current (Berstad et al., 2005).

A net cage consists of a system of ropes and netting, designed to transfer and carry forces through the ropes. The material used for netting can be produced of either *knotless netting*, which is knitted bundles of multifilaments, or *knotted netting*, which consists of twines of twisted multifilament bundles connected by knots. In Norwegian aquaculture, knotless netting is the most common type (Moe et al., 2007). The netting is usually made of synthetic fibre such as nylon, HDPE, polyethylene, polyester or Dyneema®. Synthetic fibre is suitable because of its distinct material properties; its rigidity ensures that the netting maintains the desired shape, while the flexibility provides good resistance to environmental forces (Fredheim and Langan, 2009).

The mesh length is an important parameter for the net cage, and is defined as the distance between the center of two opposing knots when the mesh is fully stretched out (Standard Norway, 2009). Choice of mesh length is mainly determined by the size of the fish that is kept in the net cage. Also, the mesh length must be small enough to avoid wild fish from swimming into the net, and at the same time be large enough to ensure good water flow conditions through the net. Selection of mesh size influence the weight of the net cage and cost, as well as the effect of current loads (Karlsen, 2015).

2.2.3   Mooring System

The purpose of the mooring system is to keep the fish farm at its desired position. The main components of the mooring system include ropes, floats and bottom attachments (Fredheim and Langan, 2009). The mooring system is described more closely in chapter 3.

2.3   Fish Farm Development

Development of new fish farms must promote profitability for the farmer and always strive to be a part of a sustainable industry. The main objective when designing aquaculture installations is to ensure sufficient structural integrity to prevent fish escape. The fish farm must be able to withstand environmental loads, be operational, and ensure proper fish welfare. The location of the fish farm must be optimized in terms of water flow, temperature, salinity and available oxygen (Fredheim, 2016).

Fish farms are designed and certified according to the technical requirements provided in the Norwegian standard, NS9415, and all stages of design must coincide with the standard (Fredheim and Langan, 2009). The technical standard set requirements for individual components of the fish farm, as well as requirements for the functionality of the fish farm as a global installation. Rules and regulations that apply for the Norwegian aquaculture industry will be further discussed in chapter 4.

The design process can be divided into three main steps (Søreide, 2016): (i) site survey and specification, (ii) analysis and testing, and (iii) report and planning. Each stage will be discussed briefly in the following sections.

2.3.1 Site Survey and Specification

In order to develop a fish farm, a license must be issued by the relevant authorities. For the farmer to get a license to farm, a site survey must be carried out at the specific site intended for the installation. The aim of the site survey is to map the environmental parameters that will impact the installation in order to calculate environmental loads. Wind velocity, current velocity, and wave parameters can be determined from measurements, statistical data and/or calculations according to NS9415 (Standard Norway, 2009).

The site survey must also include a description of water depth, bottom type and topography. This documentation is mainly used for the anchoring – and mooring analysis (Fredheim, 2016).

Specification of equipment is necessary to perform structural analyses of the installation and the main components shall be carefully documented. The technical standard requires that calculations, material parameters, certificates for parts and traceability are documented for all structural components of the fish farm.

2.3.2 Analyses and Testing

Both structural and hydrodynamic analyses must be carried out for the specific components of the fish farm, as well as for the global installation. These analyses are based on the site survey and ensures that the structure meets the criteria stated in NS9415.

In addition to analyses of loads and loading conditions, risk assessment must be carried out in the design process. Risk assessment includes risk analysis and risk evaluation, and must be performed to ensure the safety of people, fish, and the installation (Standard Norway, 2009). The risk analysis should identify what can go wrong, estimate how likely it is that

something goes wrong, as well as estimate the consequences of the event if something does go wrong. Risk evaluation is carried out to determine which risks that can be tolerated, and which risks that must be further assessed (Rausand, 2013).

Testing of equipment is performed to document the capacity of the installation and its components, and can be conducted as an alternative to mathematical analyses. Both model-tests and full-scale tests are performed to ensure the safety of the installation. Testing can be used to (Standard Norway, 2009):

- Determine component characteristics and/or breaking capacity of the components

- Reduce uncertainty in analytical risk models

- Control the quality of construction parts

- Determine material characteristics

- Inspect fish farms after installation

2.3.3   Reporting and Planning

Reporting and documentation must be done according to NS9415. Reporting is essential for safe and proper operation of the installations. Proper planning of the operations required on the fish farm is conducted to ensure the safety of the people handling the installation, as well as sustainability (Søreide, 2016).

2.4   State of the Art

The aquaculture industry has developed rapidly in recent years. Today, several innovative concepts are being developed to meet new challenges such as more exposed sites, larger installations and stricter government requirements.

2.4.1   Innovation Licenses

In the Norwegian aquaculture industry, there are strict regulations of the amount of fish allowed at a fish farm, as well as the amount of fish allowed in one single net cage. To produce farmed fish, the farmer needs a license, which constrain the maximum allowable production at one site, called *maximum allowed biomass* (MAB). This is described more closely in chapter 4.

The Directorate of Fisheries in Norway can grant special innovation licenses to concepts that have potential for innovation and significant investments. The purpose of the innovation licenses is to enhance technology developments that can contribute to solve challenges in the aquaculture industry. This license can grant permission to farm more than the general maximum allowable biomass for the industry, and the developers can apply for several licenses for one concept (Directorate of Fisheries, 2016).

2.4.2   Ocean Farm 1

Ocean Farm 1 is the first offshore aquaculture installation to be built, and the technical solution is based on semi-submersible offshore concepts. Ocean Farm 1 is designed by Ocean Farming, which is a Research and Development company within the SalMar group. The offshore fish farm will be 250 000 cubic meter and can contain 6240 tonnes of fish (SalMar, 2016). The concept is shown in figure 2.5.

Figure 2.5: Ocean Farm 1 (SalMar, 2016)

Ocean Farm 1 can be installed in areas with a water depth of 100 to 300 meter, which is beneficial both for production and operation. The offshore conditions provide good biological terms for the fish, and the fish farm can be operated autonomously, which implies that heavy marine operations can be avoided. Ocean Farm 1 was granted an innovation license in 2016, and will be tested offshore during the fall of 2017 (SalMar, 2016).

2.4.3   Havfarm 1

The Norwegian company Nordlaks has proposed an aquaculture ship for farming salmon, called Havfarm 1, designed by NSK Ship Design. Havfarm 1 is designed with a capacity

of 10 000 tonnes of salmon, which corresponds to over 2 million fish, and shall withstand significant wave heights of up to 10 meter. The ship farm is planned to be 430 meter long and contain six net cages, each with a surface area of 2500 square meter and 60 meter depth (NSK Ship Design, 2016). The concept is shown in figure 2.6.

Figure 2.6: Havfarm 1 (NSK Ship Design, 2016)

The facility will be equipped with thrusters to optimize the oxygen ratio for the salmon and to assist marine operations. Havfarm 1 is intended to lay at one site for its lifetime of 25 years, and it shall be moored in the bow to provide weather vaning capabilities. This gives great advantages in rough sea. Also, by rotating the farm around the mooring point, the spreading area for waste products is increased (NSK Ship Design, 2016).

The Havfarm 1 concept was granted an innovation license in December 2016 (Directorate of Fisheries, 2016).

3   Mooring System

The purpose of the mooring system is to keep the installation at its correct position and ensure safe position-keeping at all times (Standard Norway, 2009). Design of the mooring system also aim to reduce the risk of fish escape, as a result of technical failure. All main components of the fish farm interact with the mooring system, and the system must therefore be analyzed in regard to the global installation.

This chapter presents mooring concepts and the main components of a frame mooring system.

3.1   Mooring Concepts

Choice of mooring concept is based on size and characteristics of the specific fish farm, as well as weather conditions and bottom topography at site. Mooring is usually done either by independent lines directly moored from the collar to the bottom, or by a grid mooring system. In the case of grid mooring, one or several collars are connected to a mooring frame which is independently attached to the seabed (Fredheim and Langan, 2009).

3.1.1   Independent Mooring

Independent mooring lines are usually applied for interconnected hinged bridge systems.

3.1.2   Frame Mooring

Frame mooring systems are applied for fish farms that consist of circular cages. The mooring frame intend to provide additional horizontal stiffness for the fish farm, since the plastic collars themselves have low horizontal stiffness (Fredheim and Langan, 2009).

The collars are connected to the mooring frame by bridles, such that each cage can move freely inside the frame, independent of the mooring grid. The main mooring frame consists of fiber ropes designed to withstand environmental loads. The mooring frame, bridles, mooring lines, and frame buoys are connected by submerged mooring plates (Karlsen, 2015).

The mooring frame itself is kept at sufficient depth, usually 5-10 meters, such that it won't affect marine operations. This avoids issues such as ropes coming into propellers, and allows for boats to easily pass the installation site (Fredheim and Langan, 2009). An illustration of a frame mooring system and its main components is shown in figure 3.1.
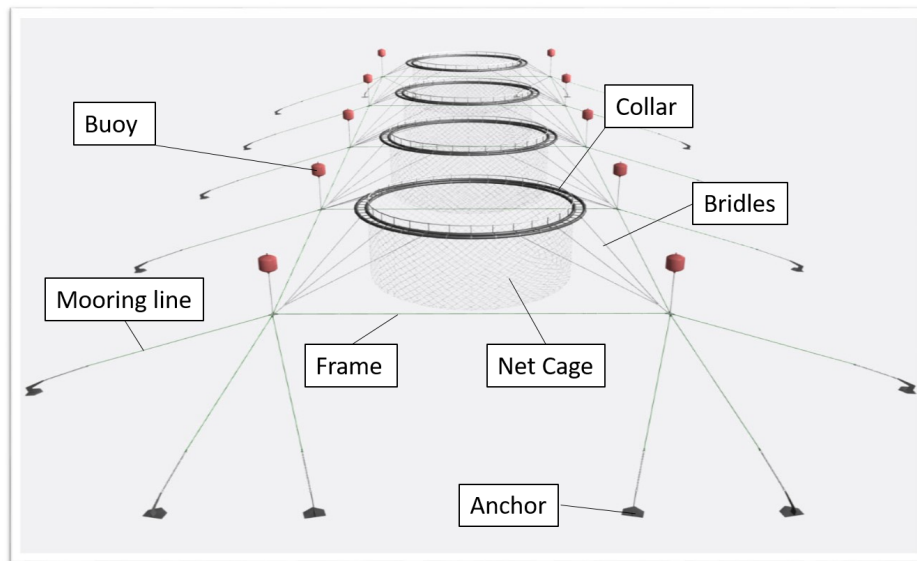
Figure 3.1: Frame mooring layout (illustration by Aqualine)

3.2 Mooring Components

A general mooring system consists of several cables attached to the floating installation at different points with the lower ends of the cables anchored to the seabed (Faltinsen, 1990). The standard frame mooring system consists of synthetic ropes, long link chain, shackles, mooring plates, anchor chain and anchors (Søreide, 2016). The following sections focus on mooring components for a typical frame moored circular collar fish farm as the one shown in figure 3.1.

3.2.1 Mooring Line

Mooring lines are used to attach the installation to the seabed, and to connect the separate cages in a frame moored fish farm. The lines can consist of chain, fiber ropes, or a combination of both. Choice of mooring line material depends on its application, but a combination of chain and fiber rope is the most common option. The mooring frame itself usually consist of fiber rope.

Chain

Chains come in different diameters and with different grades, and choice of chain is based on the strength requirements determined in the dimensioning analysis. Chain has very good abrasion characteristics and provide high geometric stiffness due to weight (Larsen, 2016). This will be further discussed in chapter 7.

Chain links can be either studlink or studless. The studless chain links are most common for permanent mooring (Vryof Anchors, 2010). The bottom attachment usually consists of heavy studless chain to provide good dynamic capabilities and a flexible mooring system. In other parts of the mooring system, lighter chain is usually applied (Standard Norway, 2009).

Synthetic Fiber Ropes

Synthetic fiber ropes has the advantage of high elasticity and low weight. Polyester and polyethylene, which are the most common materials, is close to nylon in strength, but stretches very little. They provide good damping effects and have highly elastic properties (Bai and Bai, 2012). Synthetic mooring lines are easy to handle and install, but doesn't have as good abrasion characteristics as chain (Larsen, 2016).

3.2.2   Connectors

Connectors are applied to ensure safe and reliable connection between the different mooring components.

Shackles

Shackles are used to connect the anchor chain to the anchor, or as a connection between the chain segment and polyester segment of the mooring lines. A shackle consist of a bow that is closed with a pin, and functions as a locking mechanism between two components (Vryof Anchors, 2010). NS9415 require that shackles must be doubly secured, and made of corrosion-resistant material. An example of a shackle configuration is shown in figure 3.2a.

Mooring Plate

The mooring plate is the connection point between the mooring frame, mooring lines, bridles and buoy. It is the most important part of the mooring system, and aim to ensure safe position keeping of the global installation. All ropes are connected to the mooring plate at the mooring frame depth, well below propeller depth, to ensure safe transport around the fish farm. The coupling plate must be designed such that the first yield occurs in a mooring line attachment point rather than in the plate itself (Standard Norway, 2009). A typical mooring plate configuration is shown in figure 3.2b. The buoy is attached in the middle of the plate, while the mooring lines and mooring frame ropes are evenly distributed and connected to the plate by shackles.

(a) Shackle

(b) Mooring Plate

Figure 3.2: Connectors (illustrations by Aqualine)

3.2.3   Bottom Attachment

The bottom attachment transfer loads from the mooring system to the seabed. Choice of bottom attachment type mainly depends on the bottom conditions on site. *Rock pins* are applied for rock bottom, while for sand and clay bottom, *anchors* are the preferred type of bottom attachment.

Rock Pins

Rock pins are hollow steel pipes that can penetrate through rock. Two types of rock pins are used for anchoring; T-pins and eye-pins. T-pins have a T-configuration on top of the pin and shackles can be connected around the bolt stem, while for eye-pins, shackles are connected through a hole at the top of the pin. The rock pin is installed by a piling hammer or vibrator, and it is fastened to the soil either by expanding the steel on the bottom of the pile, or by grout, which makes the pile stick to the rock. A combination of the two fastening methods is usually applied. The holding capacity of the rock pin depends on the strength of the steel, how good attachment it gets with the soil, as well as the strength of the soil itself (SINTEF et al., 2010). A typical T-pin configuration is shown in figure 3.3a.

Anchors

The required dimensions of the anchor depend on the geological conditions on site, and the weight of the installation. The anchor holding power must be sufficient to ensure safe position-keeping, and according to the documentation provided by the manufacturer.

Fluke anchors are the most common anchor type for mooring of fish farms. These anchors are beneficial in terms of high holding-capacity-to-weight ratio. The holding capacity depends on the amount of soil that is displaced by the anchor and the ability of the soil to hold together. This implies that anchors with large fluke and deep penetration gives the highest

holding capacity. Penetration depth is dependent on soil conditions, and must be adapted to the specific site (Vryof Anchors, 2010). An example of a fluke anchor is shown in figure 3.3b.
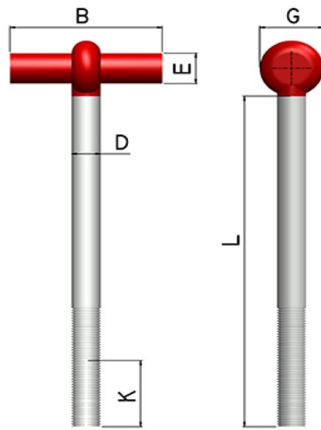
(a) Rock pin

(b) Fluke anchor

Figure 3.3: Bottom attachments (illustrations by Aqualine)

4 Rules and Regulations

The Norwegian aquaculture industry is regulated by the Directorate of Fisheries, which is subject to the Norwegian Ministry of Trade, Industry and Fisheries. The Directorate of Fisheries is the advisory and executive body of the Norwegian authorities and aim to ensure a profitable and sustainable aquaculture industry (Directorate of Fisheries, 2017).

Rules and regulations are essential to ensure safe working conditions and fish welfare in Norwegian aquaculture. Technical standards are an important part of Health, Safety and Environment (HSE) regulations, to protect personnel and public from harm and reduce negative environmental impacts. The rules and regulations also aim to ensure safe and secure structures, and serve as guidelines for the farmers, suppliers, and manufacturers in the industry (Fredheim, 2016).

This chapter will introduce the governing rules and regulations that applies for the Norwegian aquaculture industry, with main focus on the technical regulations.

4.1 The Aquaculture Act

Norwegian aquaculture is subject to the Aquaculture Act, which applies for production of all aquatic organisms. The Aquaculture Act is issued by the Directorate of Fisheries and was first applied in 2006. Its purpose is to ensure that Norwegian aquaculture is profitable and competitive, and that the industry is sustainable and contributes with wealth creation to the local community, as well as to the nation (The Aquaculture Act, 2006).

4.1.1 Aquaculture Licenses

To engage in aquaculture activities, a farming license is required. The license grants permission to produce specific species in restricted areas, and allocation of licenses is given by the Directorate of Fisheries (The Aquaculture Act, 2006).

The license constrains the maximum allowable biomass (MAB) for each company, as well as for the industry as a whole. MAB is implemented to regulate the produced volume of salmon. One MAB equals 780 metric tonnes, but several MAB licenses can be granted for one site, and in general, one fish farm contain between 2340 and 4680 tonnes (Marine Harvest, 2015). Biomass limitations are determined by the carrying capacity of the production site and varies for the different production sites.

The amount of fish in one single cage is also limited by regulations. One cage can only contain 25 kg fish per cubic meter of water, due to sanitary reasons and to ensure fish welfare (Fredheim, 2016).

4.1.2   Environmental Considerations

The environmental aspects of Norwegian aquaculture is mainly regulated by the Aquaculture Act. It states that aquaculture should be done in a sustainable manner in all phases of production, including planning and termination. The law set requirements for e.g. environmental surveillance, protection of specific sites and removal of escaped fish (Norwegian Seafood Council, 2016).

4.2   Technical Regulations

In addition to the Aquaculture act, *technical* requirements for aquaculture installations are specified in separate regulations. The overall objective of the technical rules and regulations applied in Norwegian aquaculture is to prevent fish escape by ensuring sufficient integrity of the installations. Operational integrity, design integrity, as well as technical integrity must be assessed in order to prevent escape (NYTEK, 2011).

Fish escape is a threat to wild stock and nature. Interbreeding of farmed fish and wild stock can introduce new species, which is not suited for wild life. Farmed fish claims food and space, and can possibly transfer pathogens and parasites to the wild stock. Fish escape can also result in significant economic loss for the farmer. Both loss of income due to escaped fish and the cost related to handling of the incident affects the total return, so it is of great interest for the farmer to avoid fish escape (Fredheim, 2016).

Technical regulations in Norwegian aquaculture is set by NYTEK, while NS9415 represent the technical standard of the industry.

4.2.1   NYTEK

NYTEK is the national regulation of technical standards for floating aquaculture installations, issued by the Norwegian Ministry of Trade, Industry and Fisheries.

NYTEK includes regulations for certification and inspection of fish farms. For the farmers to get a license to farm, documentation on the specific locality, mooring analyses and a site certificate is required. All main components, such as the cage, net and mooring system, must

be controlled and verified by an independent third-party inspection company. The purpose of the NYTEK certification is to reduce the risk of technical failure, and to ensure high reliability of the components (NYTEK, 2011).

NYTEK set requirements for all entities involved in the aquaculture industry; the farmers, the manufacturers and suppliers. The farmers are required to provide environmental data for the planned location of the fish farm to get a license, while manufacturers and suppliers is required to certify their products to be allowed to deliver equipment to the farming industry (NYTEK, 2011). NYTEK refers to NS9415 for technical specifications.

4.2.2   NS9415

The Norwegian Standard, NS9415, outlines the technical requirements for design, dimensioning, production, installation and operation of a marine fish farm (Søreide, 2016). NS9415 is applicable to all main components of the farm, such as nets, floating collars, mooring systems and rafts. The standard was drafted in 2003, and then revised in 2009 (Standard Norway, 2009). The specific design requirements include prerequisites for all main components of a fish farm, as well as requirements for the functionality of the global installation. This includes strength analyses, safety limits and lifetime analyses. The standard also specifies which loads to include when dimensioning the equipment and how to calculate the specific loads (Standard Norway, 2009).

As mentioned, the regulations state that a site survey must be performed to be allowed to develop an aquaculture fish farm. The site survey shall provide the information needed to be able to determine the environmental loads on site, and an overview of parameters such as wind, waves and current must be included. These parameters will be used as a basis for calculations of environmental loads that can affect the planned installation (Standard Norway, 2009).

NS9415 also include requirements for use and installation manuals. This is to ensure proper interaction between the main components of the fish farm (Fredheim, 2016).

5   Design of Aquaculture Installations

When designing a marine fish farm, rules and regulations needs to be assessed in all stages of the design process. The overall purpose of a comprehensive design approach is to avoid fish escape because of technical failure. NS9415 set restrictions that applies for all main components of the installation, and specifies design limit states for the individual components, as well as for the global installation. To ensure safe design of the structure, determination of loads, load effects and resistance to the load effects needs to be assessed early in the design process. This should be done in accordance with defined limit states.

This chapter will introduce the concept of limit state design, and describe the partial coefficient method, which is a design approach applied to ensure that the structure meet the load requirements necessary to avoid technical failure.

5.1   Limit State Design Approaches

In early stages of design, it is difficult to predict the loads that will act on the structure during its intended lifetime. *Limit state design* is a method for enabling more accurate structural design by considering the possible loads separately (Curtin et al., 2008). The method is applied to verify that no structural limits can be exceeded due to unpredicted loads and response, improper material properties, inaccurate geometrical data, or product properties (Fredheim, 2016).

Design limit states are introduced to ensure that the structure can handle the loads that will impact the structure over its intended lifetime. According to NS9415, dimensioning of a structure, or part of a structure, should be done in relation to two limit states:

- Ultimate Limit State (ULS)

- Serviceability Limit State (SLS)

Fatigue and accident situations should be seen in regard to the ULS condition (Standard Norway, 2009). The different limit states will be presented briefly in the following sections.

5.1.1   Ultimate Limit State (ULS)

The ultimate limit state (ULS) aim to ensure that the structure, or a specific part of the structure, have sufficient strength when exposed to extreme environmental loads. ULS is usually set equal to the maximum load that the components can withstand without structural

failure. The ultimate limit state shall ensure the safety of people, as well as the safety of the structure itself (Standard Norway, 2009).

5.1.2   Serviceability Limit State (SLS)

The serviceability limit state (SLS) is the limit state for when a structure, or part of a structure, no longer meets the requirements for normal use. This limit state assess the comfort of the people handling and operating the installation (Standard Norway, 2009).

5.1.3   Accidental Limit State (ALS)

The accidental limit state (ALS) is the limit state for when a structure, or part of a structure, is exposed to an accidental load (Standard Norway, 2009). ALS aim to ensure that the system has enough reserve capacity in accident situations. Accidental loads can arise from accidental events, such as collisions, or operational failure, such as improper pretension of the mooring lines (Brown, 2005).

5.1.4   Fatigue Limit State (FLS)

The fatigue limit state (FLS) is the limit state for when a structure, or part of a structure, is exposed to repeated loads during its intended lifetime (Standard Norway, 2009). FLS aim to ensure that the system has enough reserve capacity when the equipment is exposed to cyclic loading. Fatigue depends on load variations over time, and for mooring lines it is especially important to asses loads that vary with wave frequency (Brown, 2005).

5.2   Partial Coefficient Method

Ultimate limit states are important criteria in design of aquaculture structures, and ULS design checks are generally based on extreme load effects. In the aquaculture industry, extreme environmental conditions are represented by waves and current with 10 and 50 year return period. How to determine extreme environmental conditions that cause extreme loads are presented in section 5.2.2.

Fish farms are exposed to random load processes, $S(t)$, as illustrated in figure 5.1. The design procedure aims to ensure that the structure can resist the *maximum* load effect that may cause ultimate failure over the structure's lifetime. This is done by making sure the dimensions of the equipment are adequate and that the material properties are suitable

for the environmental conditions at the specific location of the structure (Naess and Moan, 2012).
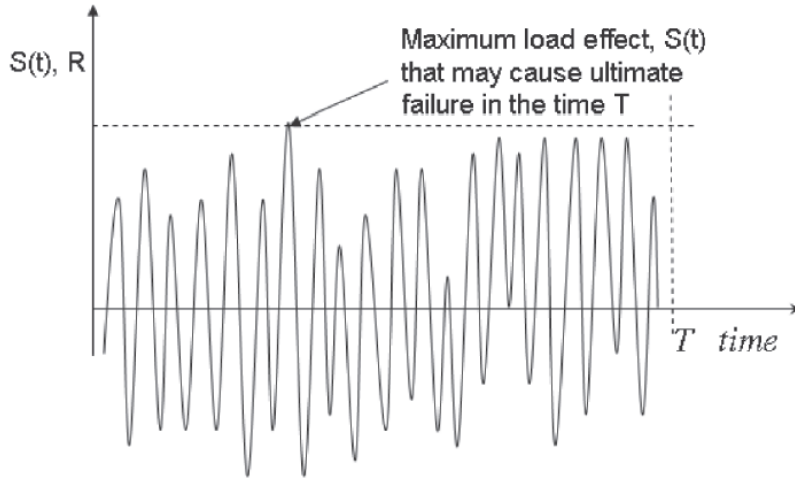
Figure 5.1: Random load process (Naess and Moan, 2012)

The simplest example of an ULS design check approach is the *partial coefficient method*. This procedure incorporates safety factors to ensure that the structure meets the design requirements that are necessary to avoid technical failure. The partial coefficient method is based on requiring that the extreme load effect, S, must be less than or equal to the strength of the component, R (Standard Norway, 2009):

$$S \leq R \tag{1}$$

Safety factors are applied to account for the variability and uncertainty of strength and load effects, which gives:

$$S_C \times \gamma_f \leq \frac{R_C}{\gamma_m} \tag{2}$$

where

S_C	is the characteristic load
γ_f	is the load factor
R_C	is the characteristic strength
γ_m	is the material factor

The characteristic capacity for strength, R_C, is usually determined by equipment testing, and is commonly set equal to the minimum breaking load (MBL) of the component, which corresponds to the 90% quantile of the strength distribution. This will be further introduced in chapter 8. If no test data is available, the distribution of strength could be assumed to follow the normal distribution, with mean value,

$$\mu = 1.05 \times MBL \tag{3}$$

and standard deviation,

$$\sigma_x = 1.05 \times 0.03 \times MBL \tag{4}$$

This is valid for polyester ropes, but can be assumed to apply for polyethylene ropes as well (Hørte and Macke, 2014).

The characteristic load, S_C, is determined from extreme value analyses based on the design limit states (Standard Norway, 2009). This will also be explained in more detail in chapter 8. NS9415 require that two combinations of loads, based on return period, must be assessed when designing a marine fish farm. Table 5.1 presents the combinations of current, wind, and waves that must be controlled in ULS. The most unfavorable of the two load combinations should be used to determine the characteristic load, S_C.

Table 5.1: Combinations of environmental loads, given in return period (years)

Combination	Current	Wind	Wave
1	50	10	10
2	10	50	50

The concept of the partial coefficient method is illustrated in figure 5.2. The curve to the left illustrates the distribution of load, S, and the right curve illustrates the distribution of strength, R. The objective of equation 2 is to ensure that the load does not exceed the strength of the component with a defined probability level. The probability of failure is indicated on the figure by the grey shaded area where the two distribution curves overlap.
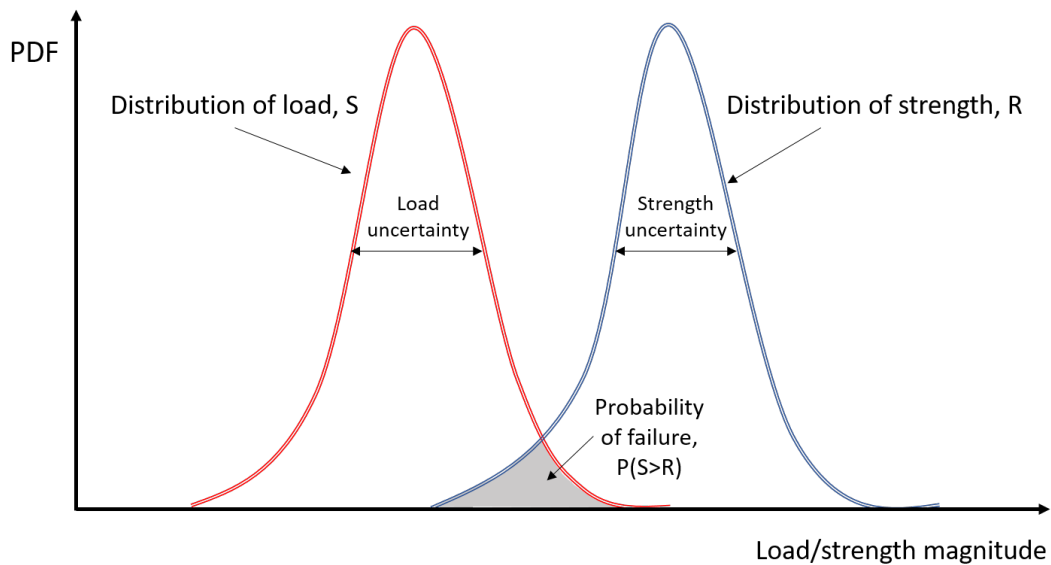
Figure 5.2: Illustration of the partial coefficient method

Probability of failure can be calculated by integrating over the two curves:

$$P_f = P(S > R) = \int_S f_S(s) \, F_R(s) \, ds \tag{5}$$

where $f_S(s)$ is the distribution of load, and $F_R(s)$ is the probability of load being greater than strength, $P(R \leq S)$. Probability distribution will also be explained in more detail in chapter 8.

5.2.1 Safety Factors

Safety factors are applied to ensure that the possible loads imposed on the fish farm do not exceed the capacity of the different components with defined probability, i.e. that the grey shaded area in figure 5.2 is sufficiently small. The safety factors account for uncertainty in loads and response, as well as uncertainties in material properties (Standard Norway, 2009).

The safety factors in NS9415 are adapted from *Eurocode: Basis for Structural Design, NS-EN 1990*, which is the governing standard for the Eurocode series. It establishes principles and requirements for the reliability of constructions, the design of structures and verification of safety (Standard Norway, 2002).

The *load factor*, γ_f, applied in the partial coefficient method accounts for uncertainty in loads. The load factor considers the following (Standard Norway, 2009):

- The possibility of loads deviating from the theoretical values

- The reduced probability of extreme loads acting at the same time

- Uncertainties in modelling and analyses of loads

The load factor is independent of the type of component that is inspected, and all components must be designed in accordance with the load factors provided in NS915. Which load factor to apply in the design check depend on the type of analysis conducted, and the load factors provided in NS9415 are presented in table 5.2.

Table 5.2: Load factors for mooring lines (Standard Norway, 2009)

Type of analysis	Load factor, γ_f
Static analysis	1.6
Quasi-static analysis	$1.15 \times$ DAF
Dynamic analysis	1.15
Accident limit (break in mooring line)	1.0
Spring flood	1.0

The *material factor*, γ_m, accounts for uncertainty in material properties. The material factor considers the following (Standard Norway, 2009):

- The possibility of material strength deviating from the theoretical values

- The possibility that the total material strength for the global installation is less than the material strength for each individual component

- Uncertainties in the modelling of strength

The specific material factor depends on the type of materials and/or components to be designed. NS9415 provide material factors for all the main components of a marine fish farm and the material factors that applies for mooring lines are presented in table 5.3.

Table 5.3: Material factors for mooring lines (Standard Norway, 2009)

Type	Material factor, γ_m
Synthetic rope	3.0
Synthetic rope with knots	5.0
Chains and chain components	2.0
Used chain	5.0
Coupling disks	1.5
Shackles	2.0
Rock bolts and other bottom attachments	3.0

As seen, synthetic rope has a material factor of 3.0, while chain has a material factor of 2.0. Chain has lower material factor due to lower capacity uncertainty, compared to synthetic fiber. The material that is going to be used must be in accordance with the documentation provided by the supplier of the mooring lines, and the material properties must be documented by proper testing (Standard Norway, 2009).

Figure 5.3 illustrates the application of safety factors in the partial coefficient method. S_D represents the *design load*, which is the dimensioning load the structure must be able to resist. R_D represents *design strength*, which is considered representative for the minimum strength of the component. If $S_D > R_D$, equation 2 is not satisfied, and the strength of the component must be increased. For mooring lines, this is typically done by increasing the rope diameter.
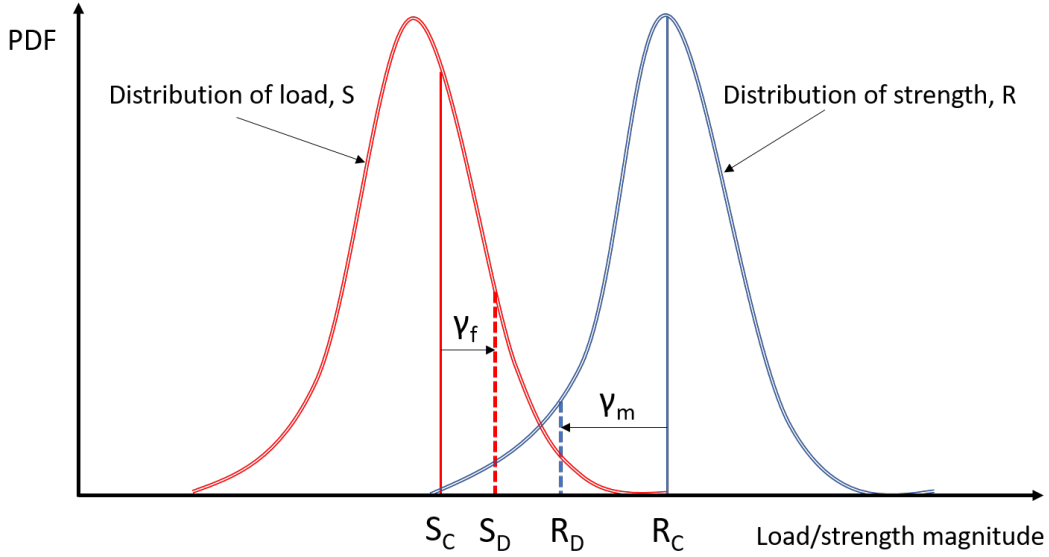
Figure 5.3: Illustration of the effect of safety factors

5.2.2 Determining Extreme Load Effect

For aquaculture fish farms, the extreme load effects from waves and current are the governing forces regarding design purposes. To determine the design load effect, S, wave distribution and environmental conditions at the fish farm's intended locality is examined. The site survey provides the basis for the analysis that is conducted to determine the characteristic load, S_C, that act on the installation. The environmental parameters in the site survey includes significant wave height, H_S, peak period, T_p, and current velocity, V_C, at two different depths, as well as the direction of the different parameters.

Determination of Waves

Dimensioning wave conditions are based on the types of waves representative for the specific locality. *Wind-induced waves* are determined by either wave measurements, or calculations based on effective fetch length. In the case of calculations, wind data from the locality is used, which represent 10 minute average wind velocity at 10 meter height, U_{10}. 50 year significant wave height is determined based on the 50 year wind velocity at the location, and similarly for 10 year significant wave height. The adjusted wind velocity is then determined from (Standard Norway, 2009):

$$U_A = 0.71 \, U_{10}^{1.23} \tag{6}$$

and the dimensioning wave height and peak period is calculated by:

$$H_S = 5.112 \times 10^{-4} \, U_A \, F_e^{\frac{1}{2}} \tag{7}$$

$$T_p = 6.238 \times 10^{-2} \, (U_A \, F_e)^{\frac{1}{3}}, \tag{8}$$

respectively. F_e represent the effective fetch length, which must be determined by a "recognized method" according to NS9415. Alternatively, H_S and T_p can be determined from plots of peak period and significant wave height versus effective fetch length for different wind velocities. These plots are provided in NS9415 and are shown in figure 5.4.

(a) Peak period

(b) Significant wave height
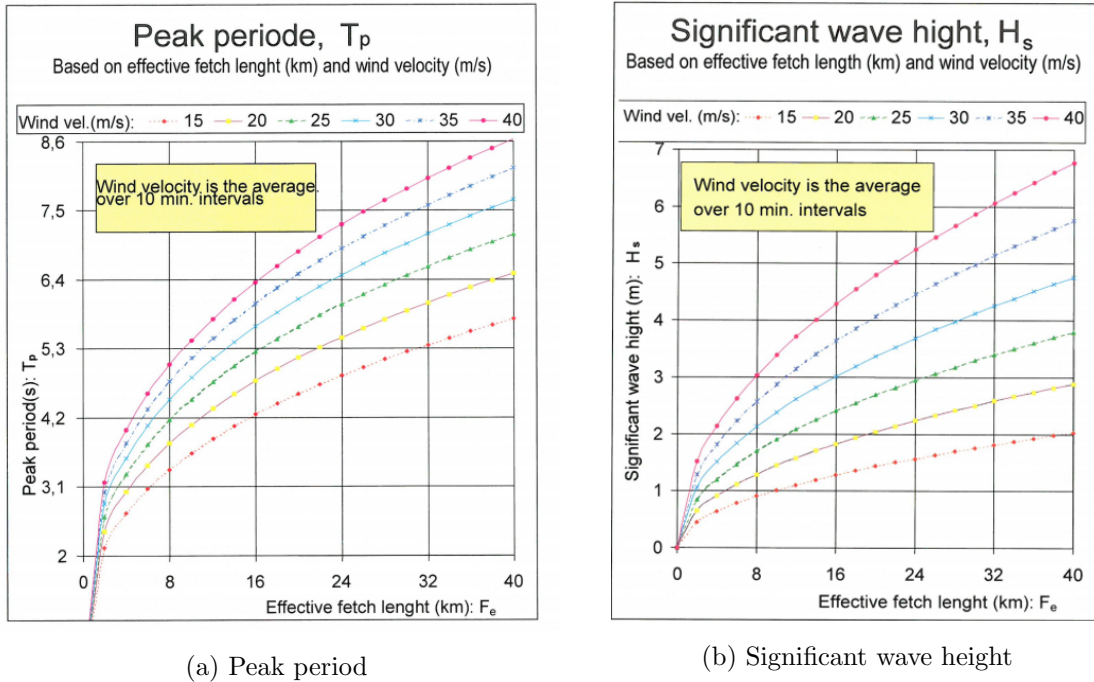
Figure 5.4: T_p and H_S based on effective fetch length (Standard Norway, 2009)

If *ocean swells* occur on site, the dimensioning wave height and peak period is determined from one of the following (Standard Norway, 2009):

- Diffraction and refraction analysis

- Measurements on site

- Other documented methods

Other wave conditions at site, such as ship-generated waves, wave/current interaction or wave reflection, must also be considered if relevant (Standard Norway, 2009).

Analyses could be done based on either irregular or regular sea states. For calculations with irregular sea, the JONSWAP spectrum should be applied with peakedness parameter $\gamma = 2.5$ for wind sea, and $\gamma = 6.0$ for ocean swells.

For regular sea states, the *design wave approach* is applied, where the dimensioning wave height is assumed equal to:

$$H_{max} = 1.9 \times H_S \tag{9}$$

The regular wave period is set equal to the peak period, T_p (Standard Norway, 2009).

The preferred method is up to the supplier of the equipment, and regular wave analyses are most common in the industry today. For irregular wave analyses, the extreme load effects are determined from long-term extreme value distribution. This topic is described in chapter 8.

Determination of Current

The dimensioning current velocity can be determined by one of the following options:

- Measurements of current for one year and use of long-term statistics

- Measurement of current for one month and use of multiplication factors

- Use of previous current measurements

In the case of measurements for one month, the multiplication factors in table 5.4 is applied to determine current velocity for 10 and 50 year return period. If the calculated 50 year current velocity is lower than 50 cm/s, the dimensioning current should be set to 50 cm/s regardless of the measurements (Standard Norway, 2009).

Table 5.4: Multiplication factor for determination of current (Standard Norway, 2009)

Return period	Multiplication factor
10	1.65
50	1.85

6   Sea Loads

Aquaculture installations are exposed to both functional loads, such as operation of equipment, and environmental loads. The governing loads regarding design of these installations will be the load contributions from environmental forces, more specifically from wind, waves, and current. The intensity of these loads varies both in time and space, and it is important to address this variability when determining the characteristic loads that act on the aquaculture installation.

This chapter will focus on sea loads that influence the response of aquaculture cages. The effects of waves, current, and non-linearities will be presented, and modelling of sea loads on floater and net will be described at the end of this chapter.

6.1   Description of Environment

The sea loads that influence the behavior of aquaculture installations mainly consist of forces from wind, waves and current. *Wind loads* act on the parts of the fish farm that lie above the surface, and for aquaculture installations this will include components such as bird nets and hand rails. The response of the structure due to wind is usually small, since it only acts on a small area, and wind loads can be neglected when studying single cages. If an entire installation, including feeding barge and live fish carriers, is studied, the wind loads will have a greater impact on the response.

Wave loads act mainly on the floating collar and upper parts of the net structure, and the extent of the response depends on the location of the installation. For exposed sites, both wind-induced waves and ocean swells must be considered in response analyses.

Current loads act on the submerged parts of the structure, and current is often the governing environmental load when studying single cages, since they mostly consist of submerged components (Fredheim and Langan, 2009).

The flexibility of the net and floating collar allows the cage to change shape when it is exposed to waves and current. The permeability of the net let parts of the flow field stream through the net cage, while the rest of the fluid will flow around the cage. For a fish farm with multiple cages, the presence of downstream cages will alter the flow field, and this must be accounted for when analyzing an entire marine fish farm (Løland, 1993). This effect is illustrated in figure 6.1.
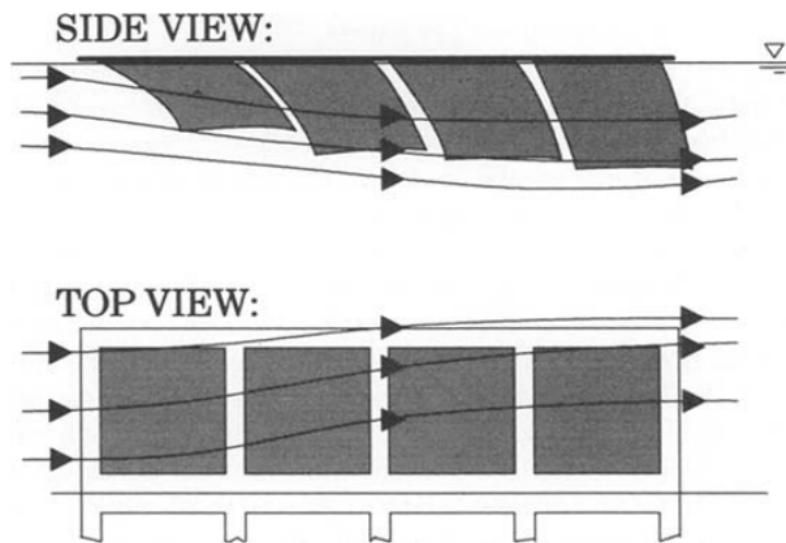
Figure 6.1: Flow through a system of net cages (illustration by Løland (1993))

6.2 Wave Loads

Aquaculture installations are affected by wave loads, which are dynamic of nature. The size and intensity of wave loads vary in time and space, and must be analyzed in terms of the size of the structure.

6.2.1 Classification of Wave Loads

When performing structural analyses of floating installations, it is beneficial to characterize the structural members by their size compared to wave height and wave length (Fredheim and Langan, 2009). For *large-volume structures*, diffraction loads are the governing loads. Diffraction loads refer to loads induced by incident waves and their modification due to the presence of the structure. *Small-volume structures*, on the other hand, does not affect the incident waves, thus long-wave approximation can be applied. The long-wave approximation implies that the wave loads can be modelled as if the body was not present in the fluid. Small-volume structures can be subdivided into drag dominated and inertia dominated structures (Faltinsen, 1990).

To classify the structure as either large– or small-volume, it is beneficial to study a cylinder with diameter D in regular waves, with wave length λ, and wave height H. If $\frac{\lambda}{D} < 5$, the structure is classified as large-volume, while if $\frac{\lambda}{D} > 5$, the structure is considered small-volume. The proposed limits between large– and small-volume structures only serve as guidelines, and the classification of the structure will also depend on environmental conditions

and the specific phenomenon that is studied (Pettersen, 2007).

Whether small-volume structures are drag dominated *or* inertia dominated depends on different factors. Drag dominated structures are influenced by viscous forces that arise from pressure forces due to separated flow. Drag loads can be hard to determine due to the uncertainties connected to viscous effects, but the structure can be considered to be drag dominated when $\frac{H}{D} > 4\pi$ (Pettersen, 2007). Classification of wave loads are summarized in figure 6.2.
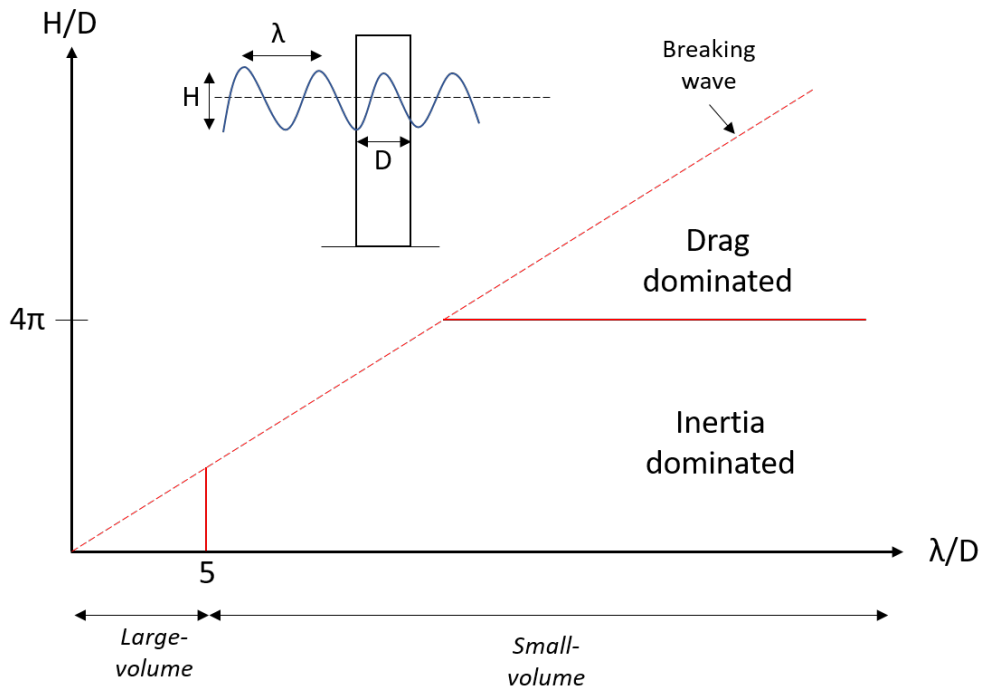
Figure 6.2: Classification of wave loads

6.2.2   Morison's Equation

Floating fish farms are complex systems since the differences in length scales makes these installations a combination of large – and small-volume bodies (Kristiansen and Faltinsen, 2015). For the components of the fish farm that are considered small-volume, Morison's equation can be applied to derive the wave loads. Morison's equation is used to calculate wave forces on components with circular cross-section. The horizontal force, dF, on a strip, dz, can be determined by (Morison et al., 1950):

$$dF = \underbrace{\rho\pi\frac{D^2}{4}C_M A_W \; dz}_{Inertia\,force} \; + \; \underbrace{\frac{1}{2}\rho C_D D |V_W| V_W \; dz}_{Drag\,force} \tag{10}$$

where

ρ	density of water
D	cylinder diameter
C_M	mass coefficient
C_D	drag coefficient
A_W	wave particle acceleration
V_W	wave particle velocity

The terms in Morison's equation are summarized in figure 6.3.
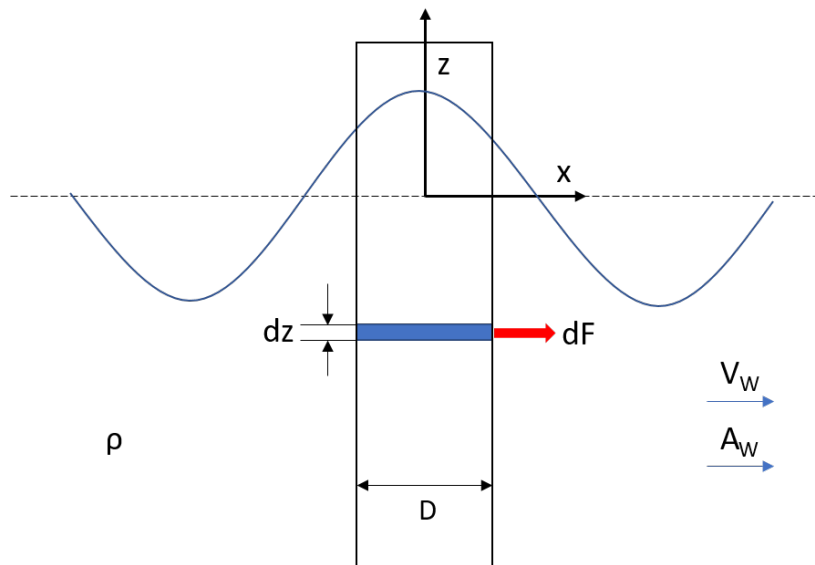
Figure 6.3: Horizontal force, dF, on a circular cylinder

For a single aquaculture cage, the contribution from inertia forces is small compared to the drag forces, due to low particle acceleration, and drag loads are thus the governing forces. The drag coefficient depends on several factors, and can be determined from empirical formulas. This will be described in section 6.5.2.

The drag term in Morison's equation is quadratic with respect to velocity. The velocity is not only influenced by the wave particle velocity, V_W, but also the current velocity, V_C, and velocity of the structure, V_S. *Relative velocity* can be defined as the relative velocity between the fluid and the structure. In general, increasing relative velocity gives an exponential increase in drag force. This is only true for structures that does not deform when exposed to environmental loads. However, for fish farms, the geometry of the net cage will change due to its flexibility, and thus the total drag load will be lower than for a rigid structure (Kristiansen and Faltinsen, 2012). It is therefore important to properly model the deformation of the structure and the relative velocity between the structure and the fluid, and not just account

for wave loads when calculating drag forces.

6.2.3   Diffraction Loads

For larger components of the fish farm, such as barges and live fish carriers, *diffraction theory* is applied to determine the resulting wave loads (Berstad et al., 2014). Diffraction theory is based on considering the forces, F_i, on a body that arise when the structure is restrained from oscillating. These forces are composed of Froude-Kriloff and diffraction forces. The two contributions are obtained by integrating the incident-wave dynamic pressure and the diffraction dynamic pressure along the mean wetted surface of the structure, respectively (Faltinsen, 1990):

$$F_i = \underbrace{-\iint_S pn_i \, ds}_{Froude-Kriloff} + \underbrace{A_{i1}a_1 + A_{i2}a_2 + A_{i3}a_3}_{Diffraction} \tag{11}$$

where

p	hydrodynamic pressure on the submerged structure
n_i	normal vector
A_{ij}	added mass coefficient
a_j	acceleration

The wave forces decrease rapidly with depth, and are therefore most critical with respect to the floater. For the net cage, current will have larger influence on the loads.

6.3   Current Loads

Current loads are static loads, which means they do not change with time, and the load contribution from currents are often dominating for small-volume structures with a large submerged area. Calculation of current loads is also based on the Morison equation presented in equation 10, and can be determined from:

$$F_C = \frac{1}{2}\rho \, C_D D V_C^2 \tag{12}$$

where V_C is the current velocity. Current will also influence the relative velocity, and must be seen in conjunction with wave loads and structure motions. For low current velocities, a quadratic increase in drag can be observed. For larger V_C, a linear increase is seen, and for high current velocities, the curve is expected to flatten out. This is a result of the flexibility of the net (Kristiansen, 2013).

Current loads act on the submerged parts of the structure, and thus affect the deformation of aquaculture cages, which are very elastic. The degree of deformation is highly influenced by the weight of the sinker tube or bottom weights. Figure 6.4a illustrates the deformation of the net cage under influence by "high exposure" current velocity of 1.38 m/s for a standard sinker tube with weight of 80 kg/m. Figure 6.4b illustrates the deformation of the net cage exposed to the same current velocity, but with a sinker tube with weight of 1000 kg/m. The illustrations are taken from the simulation software AquaSim.

(a) Standard sinker tube

(b) Heavy sinker tube
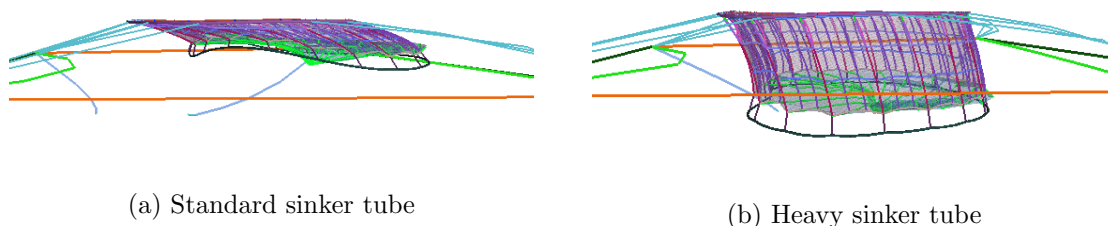
Figure 6.4: Deformation of net cage under influence by current

6.4   Second-order Effects

For irregular waves, the forces on the structure are irregular of nature, and can be split into two main contributions: (i) wave-frequency motions, which are first-order oscillatory forces with wave-frequency, and (ii) low-frequency motions, which are second-order slowly-varying forces with frequencies low compared to the wave frequency. Wave-frequency forces cause the structure motions, and the response frequencies will be equal to the frequencies in the wave spectrum. These first-order forces are proportional to the wave height. On the other hand, the low-frequency forces are proportional to the square of the wave height. They cause large-amplitude horizontal motions, which implies that low-frequency motions are important for moored structures (Pinkster, 1975).

The complex behavior of an aquaculture cage system placed in current and waves introduce non-linearities, and the system must therefore be treated as a second-order non-linear problem. Second-order effects are typically small relative to first-order load contributions, but can still have an important impact on the structural response. Second-order effects cause (Greco, 2012):

- Mean wave drift forces

- Slow drift motions

- Sum-frequency effects

Aquaculture installations are small-volume structures, and mean drift forces and slow drift motions are the most relevant second-order effects on these structures.

6.4.1   Viscous Drift

Both mean drift forces and slow drift motions on aquaculture structures arise from viscous effects which can give significant contributions to the low-frequency loads. Potential theory is not adequate to cover these effects, since viscous loads cause non-linear dependence of waves and current in combination (Lie and Kaasen, 2008).

The second order effects from mean drift forces is illustrated in figure 6.5. The mean offset of the structure due to current, waves, and structure motion is much larger than the summation of current only and waves only. This increased offset is a result of viscous effects, and the superposition principle is thus not valid when second order effects are of importance (Burns, 1983).
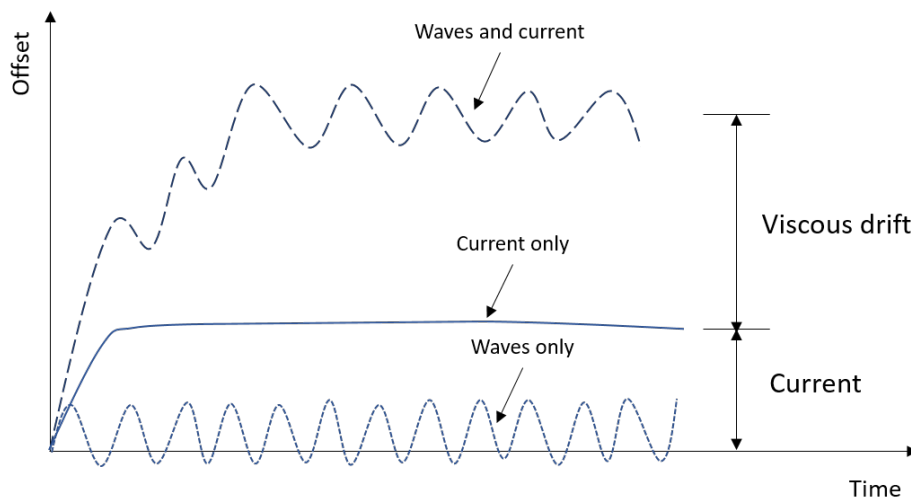
Figure 6.5: Structure offset due to viscous drift in regular waves

For irregular waves, the combination of waves with different frequencies and amplitudes cause viscous drift in terms of slow-drift motions. Slow-drift motions are resonance oscillations excited by non-linear effects that arise due to the interaction between the fluid and the motion of the structure. The resonance frequencies are excited at frequencies low compared to the frequency of the incoming wave (Greco, 2012). The total response of the structure will thus be affected by both low-frequency motions and wave-frequency motions.

Slow-drift motions are typically of importance for moored installations. The restoring force provided by the mooring lines for a moored structure will lead to large resonance periods in

the range of e.g. 1-2 minutes for horizontal motions. Slow-drift motions will thus occur in the horizontal plane corresponding to surge, sway, and yaw (Greco, 2012).

6.4.2 Predicting Viscous Drift

This following section presents equations for predicting viscous drift, and is based on Burns (1983).

Viscous drift may result from the relative velocity term in Morison's equation.. The relative velocity describes the velocity between the structure and fluid, which is affected by both current and wave induced water particle velocity. Total relative velocity can then be determined by:

$$V_R = V_C + V_W \cos(\theta + \psi) - V_S \cos(\theta) \qquad (13)$$

where V_C is the current velocity, V_W is the particle velocity of the wave, and V_S describe the motion of the structure. θ is the wave phase and ψ is the phase shift from wave phase. By simplifying the difference between the wave particle velocity and the structure motion, and introducing a phase shift, we can rewrite relative velocity as:

$$V_R = V_C + V_r \cos(\phi) \qquad (14)$$

where ϕ is the phase of the partial relative velocity, V_r. This simplification is derived in appendix A. The drag force can then be written using a Morison formulation as a function of relative velocity:

$$F_D = \frac{1}{2}\rho C_D D \left(V_C + V_r \cos(\phi)\right) |V_C + V_r \cos(\phi)| \qquad (15)$$

By dividing the drag force by the constant $R = \frac{1}{2}\rho C_D D$, equation 15 can be written as:

$$\frac{F_D}{R} = (V_C + V_r \cos(\phi)) |V_C + V_r \cos(\phi)|, \qquad (16)$$

which is a non-linear quadratic force. Equation 91 and 92 in appendix A is valid for the *mean* drift force. When free-surface effects are introduced, the equations must account for higher order, where second order forces predominate. Equation 16 can then be written on a similar form as equation 89 in appendix A:

$$\frac{F_D}{R} = V_C^2 + 2V_C V_r \cos\phi + V_r^2 \cos\phi^2 \qquad (17)$$

Only the first and third term contributes to viscous drift, and the equation can be rewritten in terms of second-order effects as:

$$\frac{\bar{F}}{R} = V_C^2 + \frac{1}{2}V_r^2 + \frac{1}{2}V_r^2 \cos(2\phi) \qquad (18)$$

Equation 18 illustrate three effects; the first term is related to the current force, the second term represent the mean viscous drift, while the third term produces the slow drift oscillations.

Mean Viscous Drift

Viscous drift force in regular waves can be calculated from

$$\bar{F} = \frac{1}{2}\rho g C_{FD}^2 A_a^2 = C_{VD} \; A_a^2 \tag{19}$$

where C_{VD} is the viscous drift coefficient, which can be determined experimentally, and A_a is the amplitude of the regular wave. The mean drift force in irregular waves can be determined from the wave energy density spectrum:

$$F_S = 2 \int_0^\infty S_0(f) C_{VD}^2(f) \; df \tag{20}$$

where $S_0(f)$ is the regular wave spectrum, given as $S_0(f)df = \frac{1}{2}A_a^2$. Equation 20 is derived by Pinkster (1975), and will not be derived here.

Oscillating Drift

The slowly-varying part of viscous drift is represented by the third term in equation 18. The low-frequency response is characterized by a load spectrum, $S_F(\mu)$, within a range of low frequencies, μ. This load spectrum must be determined to estimate the response to low-frequency loads (Greco, 2012). The following derivation is based on Pinkster's formula (Pinkster, 1975), described in Burns (1983).

Oscillating drift arise from the difference in frequency of two wave components, called beating effect, and the slowly-varying load spectrum, at beat frequency μ is defined as:

$$S_F(\mu) = 8 \int_0^\infty S_0(f) S_0(f + \mu) C_{VD}^4(f + \frac{\mu}{2}) \; df \tag{21}$$

where $S_F(\mu)$ is the mean value of the load spectrum for the beating frequency of two wave components. Equation 21 can be simplified by introducing an expression for the slow drift oscillation amplitude:

$$x^2 = \int_0^\infty S_F(\mu) N^2(\mu) \; d\mu \tag{22}$$

where x represents the root mean square (rms) amplitude of drift oscillation, and $N(\mu)$ represents the dynamic response function. By integrating the dynamic response function, and assuming $S_F(\mu)$ to be constant, equal to $S_F(f_n)$, we can write:

$$x_{rms} = \sqrt{\frac{S_F(f_n)\pi f_n}{4\zeta K^2}} \tag{23}$$

where ζ is the damping coefficient, K is the spring constant, and where

$$S_F(f_n) = 8 \int_0^\infty S_0^2(f) C_{VD}^4(f) \; df \tag{24}$$

which can be solved by numerical integration. This entails that the low-frequency loads can be determined from the slow-drift spectrum, $S_F(f_n)$, which can be obtained when the drift forces in regular waves are known.

Free-surface Effects

Also, viscous drift can arise from free-surface effects, due to the fact that the submerged area of surface-piercing structures changes with incoming waves. For wave crests, the area subjected to drag forces are larger than for a wave through. This will give a net force acting in the same direction as the wave. For a wave trough, the effect will be opposite, and a net force in the opposite direction of the wave will arise (Burns, 1983). This effect is illustrated for a circular cylinder in figure 6.6.
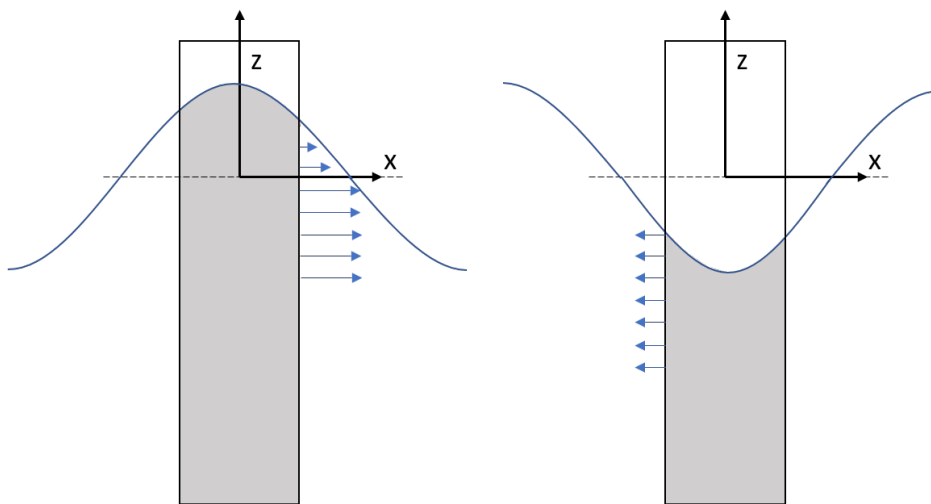
Figure 6.6: Viscous effects due to free surface penetration

6.5   Modelling of Sea Loads

Accurate numerical models are important to implement to be able to investigate the behavior of floating fish farms for design purposes. As aquaculture installations increase in size and on-site conditions become harsher, it is more difficult to perform full-scale experiments. Numerical mathematical models must therefore be applied to determine the hydrodynamic forces that act on the structure. The hydrodynamic effects on marine structures can generally be obtained by vector superposition of all the forces that act on the individual structural components of the fish farm (Enerhaug et al., 2012). The following sections will explain how wave and current loads can be numerically modelled for the floater and net. The numerical models presented here are mainly those implemented in the software FhSim, which will be introduced in chapter 9.

6.5.1 Wave Loads on Floater

Due to the flexibility of the floater, it will deform when exposed to waves. Its elasticity causes the collar to nearly follow the waves for long wave lengths, but for wave lengths in the range of floater diameter and long relative to cross-sectional diameter, free-surface effects are important (Li and Faltinsen, 2012).

Wave loads on the floater can be modelled by a Morison type model, where free surface and middle position of the floater is used as reference for submerged area. The force is calculated based on a linear model, where dynamic pressure, diffraction forces, and added mass is calculated with mean position as reference. The instantaneous position of the floater is only used for calculation of stiffness and forces in mooring lines (Endresen, 2017).

Due to the elasticity of the floater, asymmetric external loads and short-crested waves must be accounted for to determine deformation around the x- and y-axis. Modified expressions for vertical and horizontal radial displacement at a point on the ring could then be determined from (Endresen et al., 2014):

$$w(\beta, t) = a_0^v(t) + \sum_{n=1}^{N} [a_n^v(t) \cos n\beta + b_n^v(t) \sin n\beta] \tag{25}$$

$$v(\beta, t) = \sum_{n=2}^{N} [a_n^h(t) \cos n\beta + b_n^h(t) \sin n\beta], \tag{26}$$

respectively. a_n^v and b_n^v are the vertical response of the ring corresponding to mode n, while a_n^h and b_n^h are the corresponding modal response for horizontal movement. β denotes the polar angle of the ring. The cosine modes of equation 25 and 26 gives the symmetric deformations around the x-axis, while the sine modes corresponds to symmetric deformations around the y-axis. The combination of the two equations produce a model of the arbitrary non-symmetric motions (Endresen et al., 2014).

6.5.2 Current Loads on Net Structure

Current forces act on the submerged parts of the structure and are most often the governing sea loads contribution that affect the behavior of single cages. Since the net structure have large submerged area, the current will highly influence the behavior of the net.

Solidity

When a net cage is placed in current, it will alter the flow field. A part of the flow will go around the net, while the rest will flow through the net cage with increased velocity due to the presence of the net. The water will accelerate because of conservation of mass, and the

flow speed-up effect is highly dependent on the area covered by twines, which is expressed by the *solidity* of the net (Enerhaug et al., 2012). Solidity ratio, S_n, can be defined as the ratio between the area covered by twines and the total net area, and calculated by (Løland, 1993):

$$S_n = \frac{2 \times d}{\lambda} \tag{27}$$

where

d	twine diameter
λ	mesh length

and the increase in velocity of the water passing through the net elements, U_S, can be determined as a function of inflow velocity, U_∞, and solidity ratio, S_n (Enerhaug et al., 2012):

$$U_S = \frac{\sqrt{2 - S_n}}{\sqrt{2}(1 - S_n)} U_\infty \tag{28}$$

Figure 6.7a illustrates a simple knotless net structure, while figure 6.7b shows basic definitions used to determine the solidity ratio. The mesh is assumed to be rhombic, that is, all mesh sides are of equal length (Enerhaug et al., 2012).

(a) Typical net structure (Berstad et al., 2014)
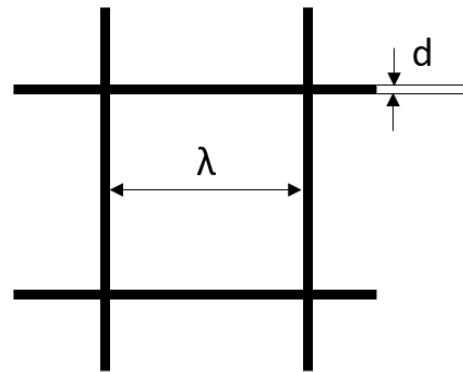
(b) Mesh definitions

Figure 6.7: Illustrations of net structure

Wake Effect

When a net structure is placed in current, both upstream and downstream effects will influence the velocity. The initial velocity of the water passing through the net will speed up due to the presence of the net, but the velocity behind each individual twine will be reduced. This reduction of velocity is called *wake effect* (Enerhaug et al., 2012).

The reduced velocity behind each twine in the net will have an impact on the forces that act on the net and the deformations of the structure. Due to the wake effect, net segments that

are located downstream will experience a lower inflow velocity than the upstream segments. To calculate the drag forces accurately, the wake effects must be properly modelled. Two levels of wake effects must be included in the hydrodynamic force model; (i) *Local* wake effects act between the mesh bars in a triangular element (Endresen et al., 2013). This is illustrated in figure 6.8.
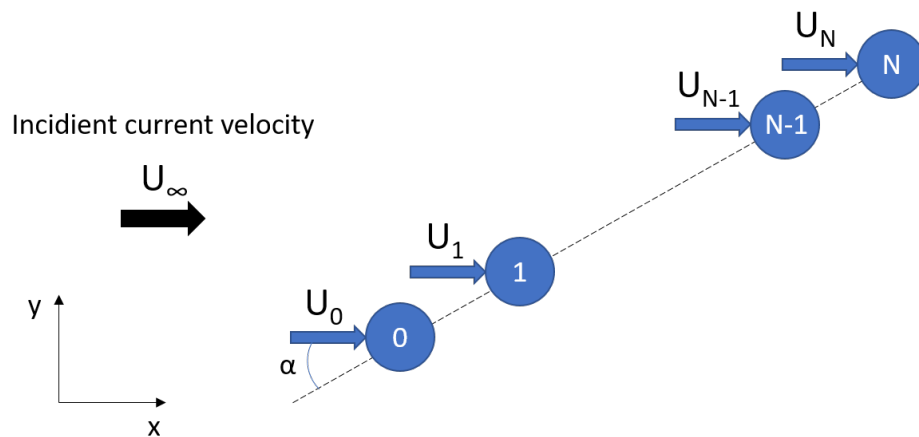
Figure 6.8: Local wake effect between mesh bars

(ii) *Global* wake effects act between separate net segments. The downstream net panel will experience lower inflow velocity compared to the upstream net segment (Endresen et al., 2013). This is illustrated in figure 6.9.
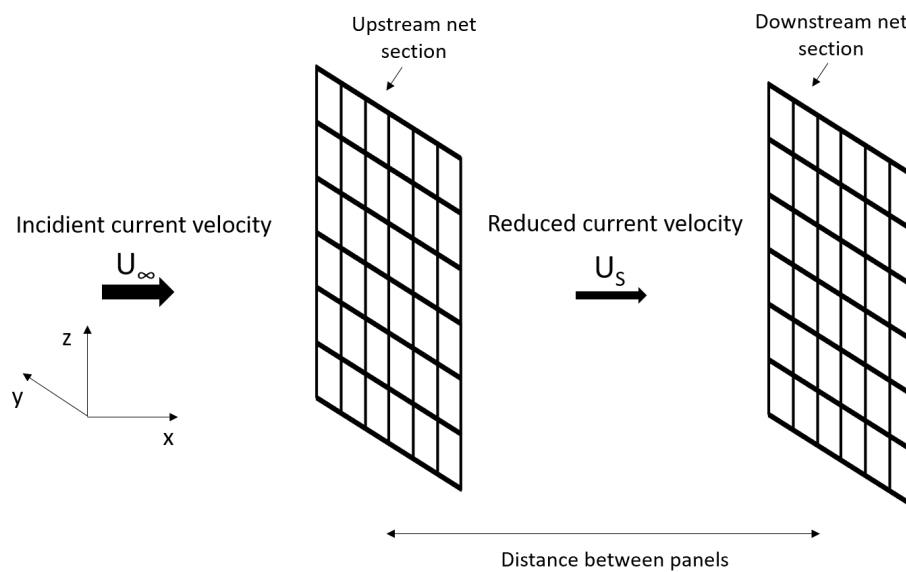
Figure 6.9: Global wake effect between net segments

Net Model

As previously noted, the drag loads are the governing contribution to the hydrodynamic loads that act on the net structure. Current and wave loads on the net structure can be modelled by a hydrodynamic force model based on the Morison equation introduced in section 6.2.2. A simplified approach for calculation of wave and current forces on the net is to apply the Morison equation to each twine in the net, by assuming cylindrical twines with constant diameter. However, this method overpredicts the drag force for large inflow angles and does not account for the interaction effects between the twines (Kristiansen and Faltinsen, 2012). The method is also both time consuming and require large computer capacity.

Another option for calculation of current loads on the net cage is to divide the net into a set of *panels*. These panels could be square or triangular elements, as illustrated in figure 6.10. The number of panels needed to determine hydrodynamic forces depends on the shape of the net cage (Kristiansen and Faltinsen, 2012).
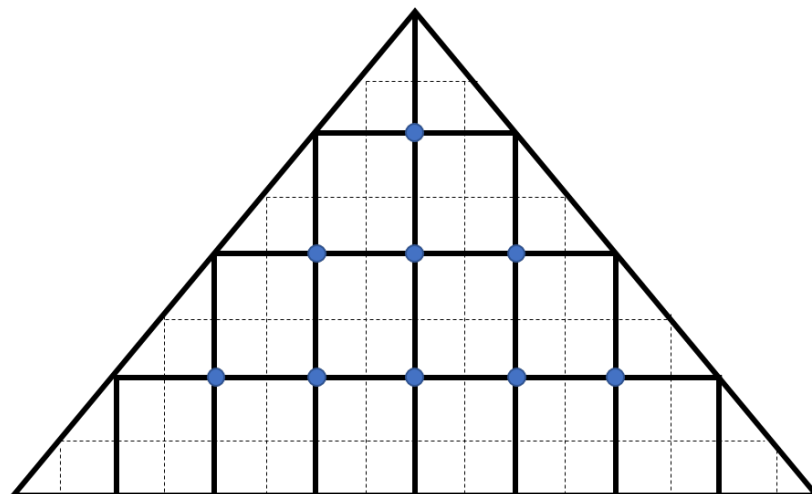
Figure 6.10: Triangular net panel used for calculation of wave and current forces

In addition to the complex behavior in current, net structures have intricate geometries. Even though nets intended for aquaculture usually consist of knotless netting, the intersections between meshes cover a larger area than single twines, and this intersection can be modelled as knots. Drag force on the knots can be calculated by assuming that each knot is spherical, with diameter twice the thickness of the twines (Enerhaug et al., 2012). Experiments show that this simplification does not impact the response significantly, since most of the loads will act on the twines and not the intersections (Føre, 2017).

Due to high number of knots and twines in a net structure, calculation of their equilibrium positions is time consuming. To make calculations more efficient, the net can be split into

an appropriate number of triangular elements, such that each element covers a large number of meshes (Priour and Germain, 2005). A net split into a number of triangular elements is illustrated in figure 6.11.
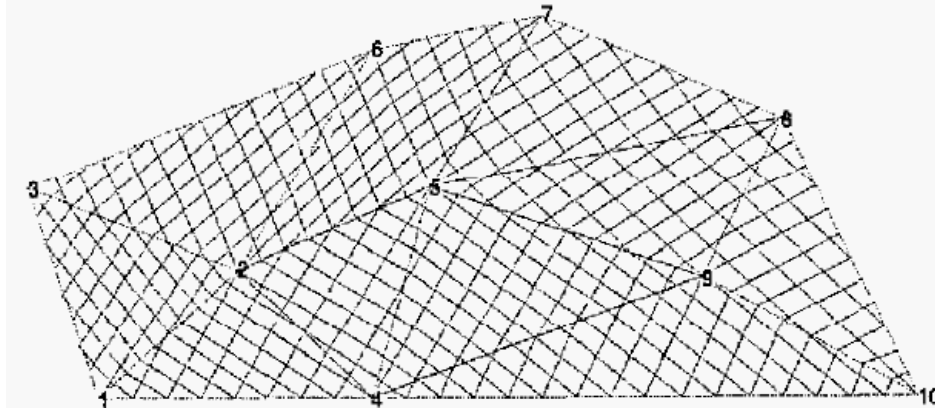
Figure 6.11: Net split into triangular elements (Priour and Germain, 2005)

Calculation of current loads on triangular elements is based on assuming that the net panels consist of a set of twines with a certain direction relative to the net panel. For rhombic mesh models, the net is modelled with two directions of twines. One assumes that these directions will not change with time, and that each direction of twine is kept parallel in each triangular net element. This entails constant deformation for each direction of twines. The forces can then be calculated for one twine per direction (two in this case), and multiplied with the number of twines in each direction (Priour and Germain, 2005).

The environmental loads that act on the net can then be calculated by summarizing the forces acting on each triangular element, by assuming constant inflow angle. The resulting force are decomposed into drag– and lift components for one twine in each direction and then summarized for each net element:

$$dF_D = \frac{\rho}{2} \; C_D(\alpha, S_n, Re) \; D \; |u|u \; dz \tag{29}$$

$$dF_L = \frac{\rho}{2} \; C_L(\alpha, S_n, Re) \; D \; |u|u \; dz \tag{30}$$

Decomposition of forces are shown in figure 6.12. F_N and F_T denotes normal – and tangential force, while F_R denotes the resultant force. F_D and F_L represents the drag – and lift forces calculated by equation 29 and 30, respectively.
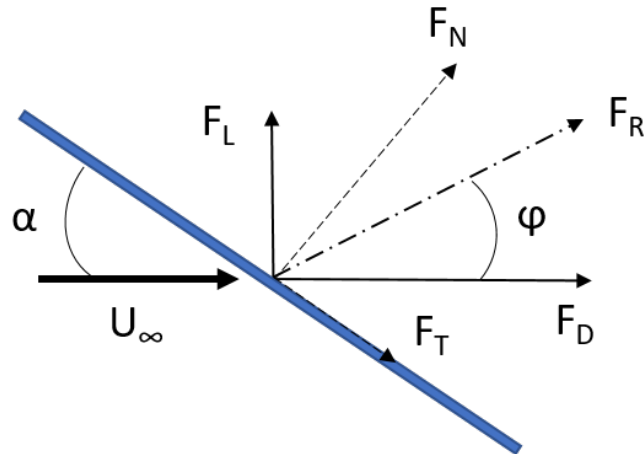
Figure 6.12: Hydrodynamic forces on a two-dimensional net panel

The drag – and lift coefficients in equation 29 and 30 depends on the flow pattern around the mesh bars and knots, and can be calculated based on a polynomial expressed as a function of the logarithm of the Reynolds number. The flow pattern is influenced by the solidity of the net, the flow speed (Reynolds number), dimensions and structure of the material, as well as inflow angle, α (Kristiansen and Faltinsen, 2012). When the orientation of the net panel change, the resultant hydrodynamic force and deflection angle (denoted ϕ in figure 6.12) will change with the angle of attack (denoted α in figure 6.12) (Enerhaug et al., 2012). This effect is important to capture in order to model the hydrodynamic drag forces that act on the net structure.

7 Dynamic Response Analysis

Structural analyses are conducted to determine the response of the structure, and aims to document that the structural reliability of the installation is sufficient for its purpose and location. The first step in conducting such analyses is to determine whether the system can be described by a static or dynamic model. Dynamic analyses are generally necessary for describing response due to transient loads. Also, if the inspected load process contain energy within the same range as the eigenfrequency of the system, dynamic analyses must be conducted to capture this effect (Naess and Moan, 2012).

Aquaculture installations and their components are subject to ocean waves and current, which are transient of nature. The intensity of environmental loads varies in both space and time, and the description of the loads needs to address this variability. Response analyses therefore have to account for the dynamics of the system (Naess and Moan, 2012).

This chapter will introduce the general requirements and purpose of dynamic mooring analyses, how the system motion can be described as a function of time, and how the equation of motion can be solved in time-domain.

7.1 Analysis of Mooring Systems

To perform analyses of the mooring system, the floating fish farm must be examined as a global system. The excitation loads that act on the fish farm will affect the tension and forces imposed on the mooring lines, such that the interaction effects between the different parts of the installation must also be assessed in a complete mooring analysis.

7.1.1 Requirements

The supplier of the mooring system must provide sufficient documentation to prove that the system is suitable for the specific site. The documentation describes the specifications of each mooring line, the expected limit states, design working life, etc., and the documentation must be supported by calculations and tests (Standard Norway, 2009).

A certified mooring analysis is required by NYTEK for all fish farming sites. To perform an analysis of a complete mooring system, it is essential to have prior knowledge about the specific site where the system is going to be deployed. The site survey includes information about water depth, bottom type and topography, providing the basis for the mooring analyses. NS9415 requires that a sketch of the facility including the mooring system is contained

in the documentation of the system. The documentation must include the intended laying pattern, attachment points, line lengths and depths. An example of a mooring lay-out is shown in figure 7.1.
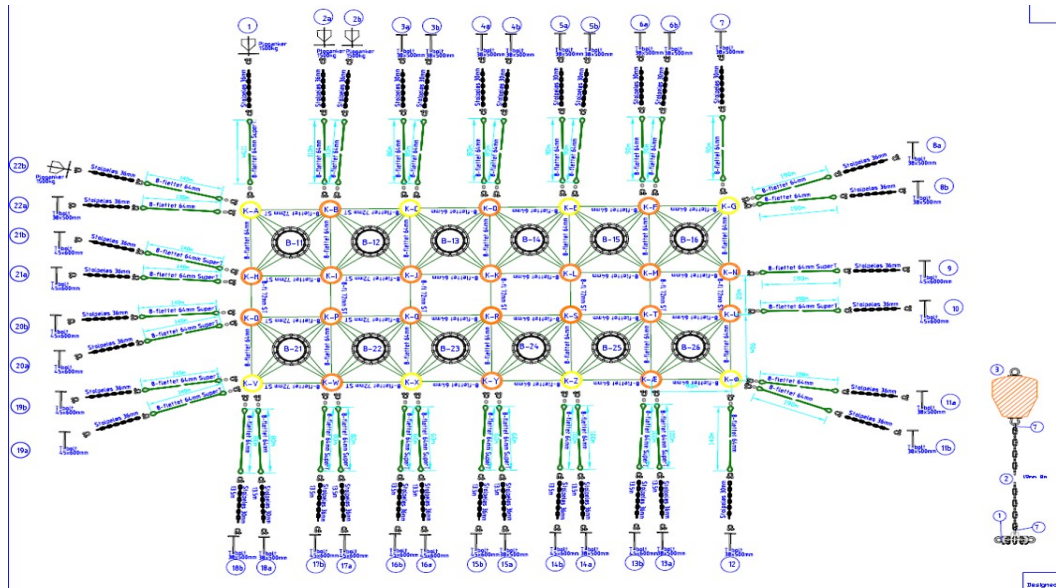
Figure 7.1: Mooring lay-out (illustration by Aqualine)

7.1.2   Mooring Analysis

Mooring analyses aim to determine the characteristic loads that act on the system to ensure that the system has sufficiently low probability of failure, that is, that the design load don't exceed the design strength of the component. The dynamic response of the mooring system that induce the characteristic loads are determined from simulations and calculations by exposing the system to environmental loads. In standard mooring analyses, the *tension* in the mooring lines are of particular interest, since this variable is directly comparable to the strength of the component. If the characteristic tension exceeds the minimum breaking strength of the component after applying safety factors, the mooring line can fail. The response of the structure must be assessed for eight different load directions (Standard Norway, 2009). Windward mooring lines are most prone to bad weather, but the slack in the leeward lines must also be assessed to ensure that bottom contact is avoided.

Mooring line tension is related to the horizontal movement of the aquaculture installation when exposed to sea loads, which are transient of nature. The response of the mooring lines will have a static contribution from current loads, and a dynamic contribution from wind and wave loads. Since most of the structure is submerged, the current loads will be the

dominating load for response calculations. Figure 7.2 illustrates an aquaculture net cage exposed to wind, waves, and current. T illustrates the tension in the mooring lines, and x show the direction of motion of the system.
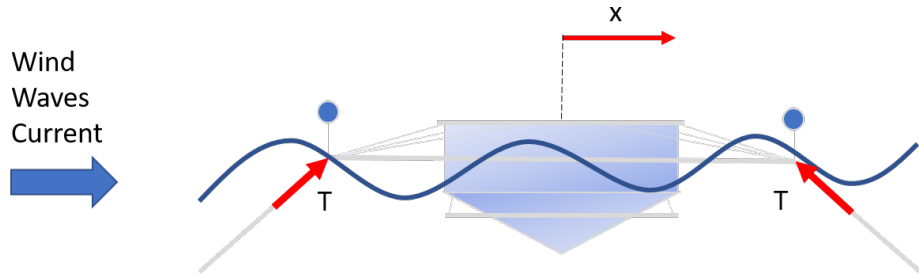
Figure 7.2: Aquaculture net cage exposed to sea loads

7.2   Equations of Motion

Aquaculture net cages are highly flexible structures that experience large deformations when exposed to waves and current, and fish farms will behave differently in their environment compared to rigid installations. The different loads that affect the behavior of a marine fish farm must be analyzed such that the effect of interaction between the different components of the farm is accounted for. The combination of stiff and soft parts imposes a challenge for analyzing the fish farm as an integrated coupled system. All components will move and behave under mutual influence, and hydroelastic analyses is required to account for structural deflection. Hydroelastic analyses capture the time-dependent interaction of the hydrodynamic forces from the fluid and the elastic structural forces (Kristiansen and Faltinsen, 2012).

The equation of motion is used to describe the system motion as a function of time, and can generally be expressed as:

$$(M + A)\, \ddot{\mathbf{x}} + C\, \dot{\mathbf{x}} + K\, \mathbf{x} = Q(x) \tag{31}$$

where

M	mass
A	added mass
x	position vector
C	damping
K	stiffness
Q	excitation force

For an aquaculture net cage, the equation of motion can be used to describe its horizontal

movement, i.e. movement in x-direction. The excitation forces correspond to the environmental forces; wind, waves, and ocean current. The mass term includes the mass of the structure, as well as hydrodynamic mass. Damping is mainly provided by the net. Stiffness for a single cage, as well as an entire fish farm, is provided by the mooring system.

7.2.1   Mass

The mass term in the equation of motion includes the mass of the floating structure and the hydrodynamic mass (added mass). The net cage itself has low weight in water, thus the mass will mainly be provided by the weight of the collar and sinker tube. The installation will have an added mass contribution from the effect of fluid inside the net (Kristiansen and Faltinsen, 2012).

7.2.2   Damping

Damping denotes the structure's ability to dissipate kinetic energy, that is, its ability to transform kinetic energy into other types of energy (Langen and Sigbjörnsson, 1999). Submerged structures have larger damping forces than those in air, mainly due to viscous forces (Larsen, 2014). The damping forces on fish farms are provided primarily by drag forces on the net cage, and viscous effects are the most important contribution to damping. Different damping scenarios are presented in figure 7.3. For an overdamped system, the installation returns to equilibrium without oscillating, while underdamped systems oscillate with gradually decreasing amplitude. Critically damped systems return to equilibrium as quickly as possible without oscillating. An aquaculture net cage will be overdamped in heave, surge and sway, due to the viscous damping from the net (Søreide, 2016).
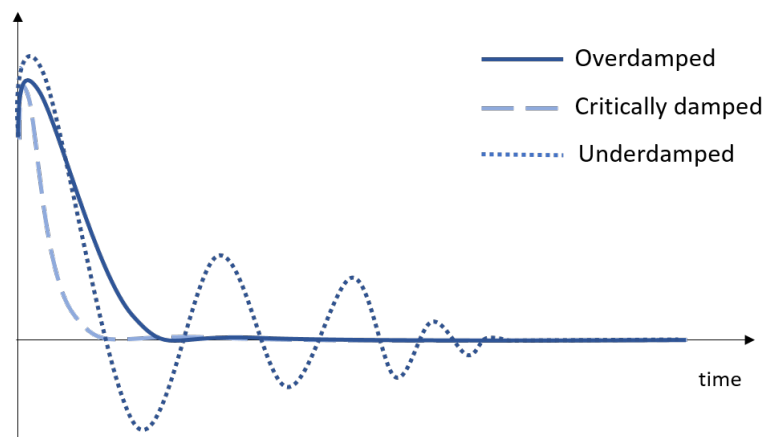
Figure 7.3: Damping scenarios for damped free vibration

7.2.3   Stiffness

Stiffness of the aquaculture installation is provided by the mooring system. The effective stiffness is composed of *geometric* and *elastic* stiffness. Geometric stiffness is provided by line weight, and is the governing stiffness contribution from chains. Elastic stiffness is provided by line axial elongation, due to material characteristics and cross section properties of the mooring lines. For synthetic mooring lines, elastic stiffness is the dominating contribution (Faltinsen, 1990).

A floating fish farm is moored by pretensioned mooring lines, which implies that there is a certain tension in the lines when the farm is in its equilibrium position. Pretension is applied to ensure that the mooring lines don't go slack to avoid wear due to bottom contact. When the structure moves in response to environmental forces, the geometry of the mooring lines change, which, in turn affects the tension. The offset of the structure will not be constant, but rather oscillate around a mean position, due to the installation's motion in waves. Mooring lines will thus impose a spring effect on the fish farm that depends on the stiffness of the system (Faltinsen, 1990).

For spread mooring systems, several pretensioned mooring lines are anchored around the fish farm to keep it at its desired position. The tension that restrains the farm from moving is provided by weight and/or elastic properties of the mooring lines. Segmented mooring lines that consist of both chain and polyethylene provides stiffness by both weight and elasticity (Faltinsen, 1990).

Total stiffness, k_{tot}, can be calculated by summarizing the inverse of the geometric and elastic stiffness:

$$\frac{1}{k_{tot}} = \frac{1}{k_G} + \frac{1}{k_E} \tag{32}$$

where

k_G	geometric stiffness
k_E	elastic stiffness

The horizontal stiffness contribution from one mooring line is determined by the mooring line characteristics. The horizontal distance between the anchor and the floater can be plotted against horizontal tension in the mooring line to examine the displacement of the structure due to static loads. Figure 7.4 illustrates the line characteristics for one elastic line and one inelastic line, with the same pretension and length. Line characteristics of the synthetic mooring line, with high elasticity and low weight in water, is linear. For the inelastic line, the horizontal tension also increases for increasing displacement, but as the offset gets larger, the tension increase more rapidly.
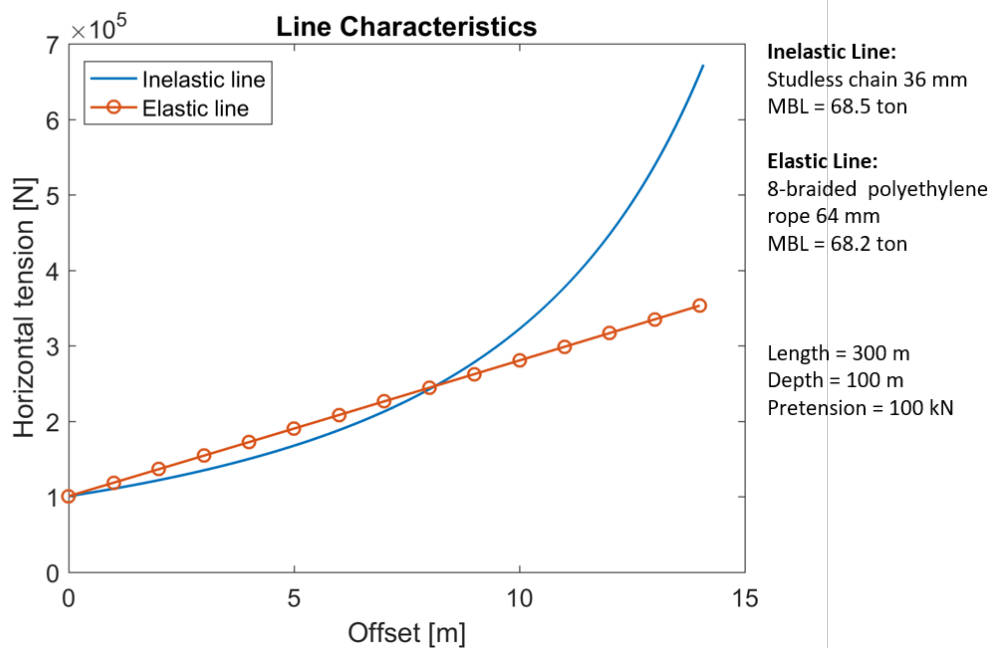
Figure 7.4: Line characteristics for elastic and inelastic mooring lines

7.2.4   Excitation Forces

The excitation forces that act on a floating aquaculture installation are mainly sea loads, which corresponds to waves, wind, and current. Wind act on the parts of the fish farm that lies above surface. Wave forces act on the floating collar and the upper parts of the net cage. Current forces act mainly on the net cage, but mooring lines, the floating collar and floatation is also influenced by current (Fredheim and Langan, 2009). Sea loads were described in detail in chapter 6.

7.3   Solution of Equations of Motion

The equation of motion is solved to determine the motion of the structure. This can be done in numerous ways. The following sections will describe solutions in time-domain by numerical integration of the equations of motion, and the methods implemented in FhSim.

7.3.1   Frequency– and Time-domain

The equation of motion can be solved in two ways, either in frequency-domain or time-domain. The choice of formulation depends on several factors, such as (Naess and Moan, 2012):

- Nature of the loading, i.e., whether the load change with time

- Frequency dependence of mass, damping and stiffness

- Non-linear features of the response

Non-linearities in structural analyses can arise from geometric non-linearities, non-linear material properties or non-linear effects due to interaction between the structure and its environment (Langen and Sigbjörnsson, 1999).

Time-domain methods are suitable for solving non-linear equations of motion for complex systems. Aquaculture installations are complex due to the combination of stiff and soft components, elastic material properties, and the transient nature of the loading (Haver, 2011). This makes time-domain analyses suitable.

7.3.2   Numerical Integration

The differential equations for an aquaculture cage structure can be solved by numerical integration. Numerical integration is beneficial for solving non-linear ordinary differential equations that are difficult to solve analytically, and is performed by subdividing the time interval into sub-intervals of length h. If starting values such as displacement, velocity and/or acceleration are known, the solution at the end of a time series can be determined by assuming variations in the motion pattern throughout the interval. The computed results from the previous time increment is then used as starting values for the next interval. This procedure gives approximate solutions at each interval of the time series, and the accuracy depends on the length of the time steps. Smaller time step gives a more accurate solution, but also increase computing time (Langen and Sigbjörnsson, 1999).

Several numerical integration methods are available, but all methods are generally based on finding the velocity and displacement at each new time step by integrating the acceleration twice (Langen and Sigbjörnsson, 1999):

$$\dot{x}_{n+1} = \dot{x}_n + \int_0^h \ddot{x}(t)dt \tag{33}$$

$$x_{n+1} = x_n + \int_0^h \dot{x}(t)dt \tag{34}$$

where

$$\ddot{x}(t) = \frac{1}{M}\left(Q(t) - C\dot{x}(t) - Kx(t)\right) \tag{35}$$

7.3.3   Runge-Kutta Methods

The difference between the different numerical integration methods lie in the assumptions concerning how the acceleration will vary over the inspected time interval. *Runge-Kutta methods* are a collection of methods that are based on approximating equation 33 and 34 by expressions on the form (Langen and Sigbjörnsson, 1999):

$$\dot{x}_{n+1} = \dot{x}_n + h\phi_1(t_n, x_n, \dot{x}_n, h) \tag{36}$$

$$x_{n+1} = x_n + h\phi_2(t_n, n_k, \dot{x}_n, h), \tag{37}$$

where ϕ_1 and ϕ_2 represent average values in each time interval, for $\ddot{x}(t)$ and $\dot{x}(t)$, respectively. ϕ_1 and ϕ_2 are obtained as weighted averages of several approximations to acceleration and velocity within the interval.

The Runge-Kutta methods can then be formulated as (Hairer et al., 1993):

$$x_{n+1} = x_n + h\sum_{i=1}^{s} b_i k_i \tag{38}$$

Let s be an integer equal to the number of stages in the method, and a_{21}, a_{21}, a_{21},...,$a_{s,s-1}$, b_1,...,b_s,c_2...,c_s be real coefficients. Then

$$\begin{aligned}
k_1 &= f(t_n, x_n) \\
k_2 &= f(t_n + c_2 h, x_n + h(a_{21}k_1)) \\
k_3 &= f(t_n + c_3 h, x_n + h(a_{31}k_1 + a_{32}k_2)) \\
&\ldots \\
k_s &= f(t_n + c_s h, x_n + h(a_{s1}k_1 + a_{s2}k_2 + \ldots + a_{s,s-1}k_{s-1}))
\end{aligned} \tag{39}$$

Various methods of the Runge-Kutta family are distinguished by their *Butcher tableau*, which is a mnemonic device that present the integer s, coefficients a_{ij}, b_i and c_i (Hairer et al., 1993). A general Butcher tableau is presented in table 7.1.

Table 7.1: Butcher tableau for Runge-Kutta integration methods

0					
c_2	a_{21}				
c_3	a_{31}	a_{32}			
...	...	...	...		
c_s	a_{s1}	a_{s2}	...	$a_{s,s-1}$	
	b_1	b_2	...	b_{s-1}	b_s

Embedded variations of the Runge-Kutta methods are available to estimate the local truncation error of each step of the method. This is performed by having two methods in the Butcher tableau; one of order p and one of order $p-1$. The lower step is then determined from:

$$x^*_{n+1} = x_k + h \sum_{i=1}^{s} b^*_i k_i \tag{40}$$

where k_i is the same as for the higher order method (see equations 39). The corresponding extended Butchers tableau will have an extra line, as shown in table 7.2

Table 7.2: Butcher tableau for embedded Runge-Kutta integration methods

0					
c_2	a_{21}				
c_3	a_{31}	a_{32}			
...	...	...	...		
c_s	a_{s1}	a_{s2}	...	$a_{s,s-1}$	
	b_1	b_2	...	b_{s-1}	b_s
	b^*_1	b^*_2	...	b^*_{s-1}	b^*_s

One variation of the Runge-Kutta methods is the embedded *Runge–Kutta–Fehlberg method*, or RFK45 method, which is a method of order $O(h^4)$ with an error estimator of order $O(h^5)$ (Hairer et al., 1993). The corresponding Butchers tableau with numerical values is shown in table 7.3.

Table 7.3: Butcher tableau for the Runge-Kutta-Fehlberg (RKF45) integration method

0					
$\frac{1}{4}$	$\frac{1}{4}$				
$\frac{3}{8}$	$\frac{3}{32}$	$\frac{9}{32}$			
$\frac{12}{13}$	$\frac{1932}{2197}$	$-\frac{7200}{2197}$	$\frac{7296}{2197}$		
1	$\frac{439}{216}$	-8	$\frac{3680}{513}$	$-\frac{845}{4104}$	
$\frac{1}{2}$	$-\frac{8}{27}$	2	$-\frac{3544}{2565}$	$\frac{1859}{4104}$	$-\frac{11}{40}$
	$\frac{16}{135}$	0	$\frac{6656}{12825}$	$\frac{28561}{56430}$	$-\frac{9}{50}$	$\frac{2}{55}$
	$\frac{25}{216}$	0	$\frac{1408}{2565}$	$\frac{2197}{4104}$	$-\frac{1}{5}$	0

8   Stochastic Analysis

Aquaculture installations and their components are subject to constantly changing loads in the ocean environment, and dynamic analyses are carried out to account for time-varying external forces, damping, inertia forces, reaction forces, and corresponding responses. Dynamic analyses can be performed in two ways, either by deterministic or stochastic analyses. In *deterministic* analyses, known load history implies that all future states are also known. *Stochastic* analyses, on the other hand, describe random phenomenons, which implies that load history cannot be used to describe future conditions. Thus, statistical concepts are used to assume future states instead. Ocean waves and wind are examples of random loads, i.e. stochastic load processes (Naess and Moan, 2012). Due to the randomness of the excitation loads, the wave induced loads and responses will also be stochastic load processes (Haver, 2011).

This chapter describes the statistical concepts applied to determine the short- and long-term distribution of extreme response. The extreme value distribution will be introduced, and two methods for developing this distribution will be presented.

8.1   Statistical Description of Waves

The ocean environment is described by regular incident waves, that is, waves oscillating in time with period T, and in space with wavelength λ. Regular waves are far from being similar to how the ocean waves appear in reality, but they are useful to describe more general waves. By assuming linearity, the output is considered to be proportional to the input, and the linear superposition principle is valid (Greco, 2012). The concept of linear theory allows for simulation of irregular waves as a sum of regular waves with different amplitudes, frequencies and phase angles, and thus statistical estimates can be obtained (Faltinsen, 1990).

8.1.1   Stochastic Wave Process

The ocean environment change with time and prediction of future states must be done in accordance with statistics. Consider three recorded timeseries of surface elevation as shown in figure 8.1 from laboratory experiments. The three plots represent waves from the same wave condition, but each plot show differences on a local level. However, the three time series are distributed around a certain value, zero in this case, which is similar to the outcome of random variables. The surface elevation can be considered a random function, or *stochastic process*, $X(t)$, with time, t, as the variable argument. By definition, $X(t)$ is considered a

stochastic process if $X(t)$ equals a random variable for all values t in the interval (a, b). A sample space, N, of the stochastic process is obtained by repeating the experiment or measurement, and collecting all possible surface elevation time series at the same predefined conditions (Naess and Moan, 2012).
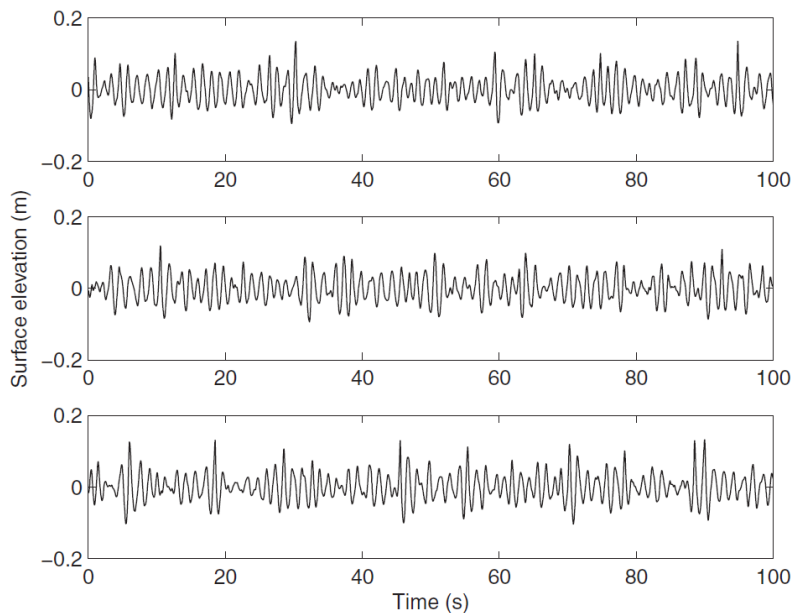
Figure 8.1: time series of wave elevation (Naess and Moan, 2012)

8.1.2   Modelling of Irregular Waves

Ocean waves can be modelled by assuming that the surface constitutes a stochastic wave field. Due to the irregularity of ocean waves, it is difficult to achieve a correct description of the wave field, and some assumptions has to be introduced. The wave process is assumed to be (Myrhaug and Lian, 2009):

- Stationary

- Ergodic

- Normally distributed

The standard approach when modelling irregular waves is to assume that the wave field is *stationary* in time and homogeneous in space. A stationary wave process is characterized by constant standard deviation and mean value, i.e. they do not change with time. However, the wave process is only assumed stationary for limited time periods, usually of duration from 20 minutes to 3 hours, such that the wave process is idealized as "piecewise" stationary (Naess and Moan, 2012). This is referred to as the short-term description of the wave field,

and will be further discussed in section 8.2.

To be able to use one single time series as representative for the entire wave process, the process is assumed to be *ergodic*. This enables that the expected value and variance can be calculated by time averaging one single time series (Myrhaug and Lian, 2009). An ergodic wave process is automatically stationary (Naess and Moan, 2012).

The wave elevation is assumed to be normally distributed, or *Gaussian* distributed, which implies zero mean value and constant variance (Myrhaug and Lian, 2009). Gaussian distributed surface elevation implies that the elevation at a given point in time and space at sea surface can be represented by a Gaussian random variable. The Gaussian probability distribution can be used to assess the response of marine installations, and can be determined from (Naess and Moan, 2012):

$$f_X(x) = \frac{1}{\sqrt{2\sigma_x^2 \pi}} \, exp\Big(- \frac{(x - \mu)^2}{2\sigma_x^2} \Big) \tag{41}$$

where σ_x is the standard deviation and μ is the mean value. Probability distribution will also be discussed in detail in section 8.2.

By applying the assumptions of a stationary, ergodic, and Gaussian distributed wave process, the wave elevation of a long-crested irregular wave can be written as a sum of a large number of regular wave components (Faltinsen, 1990):

$$X(t) = \sum_{j=1}^{N} A_j \cos(w_j t - k_j x + \varepsilon_j) \tag{42}$$

where

A_j	wave amplitude
w_j	circular frequency
k_j	wave number
ε_j	random phase angle

The wave amplitude, A_j, can be expressed by a wave spectrum, $S(w)$. The wave spectrum describes the distribution of energy for different wave frequencies and wave lengths on the surface, and we can write (Faltinsen, 1990):

$$\frac{1}{2} A_j^2 = S(w_j) \Delta w_j \tag{43}$$

or

$$A_j = \sqrt{2S(w_j)\Delta w_j} \tag{44}$$

where Δw_j is a small frequency interval. By introducing equation 44 in equation 42, the wave elevation at a particular location in space ($x = 0$) can be approximately represented

as:

$$X(t) = \sum_{j=1}^{N} \sqrt{2S(w_j)\Delta w_j} \cos(w_j t + \varepsilon_j) \tag{45}$$

Equation 45 can then be used to model irregular sea states.

8.1.3   Wave Spectrum

Random ocean waves can be described by an energy density spectrum, or *wave spectrum*, $S(w)$. The wave spectrum has all the necessary information about the statistical properties of the wave amplitude, A_j. Since the wave spectrum and weather information of specific locations are not usually known, several standardized wave spectra are available. The standardized formulas are empirical, which means they are based on observed properties of ocean waves (Chakrabarti, 2005).

Wave spectra are based on one or more parameters that represents statistical quantities for the storm represented by the spectrum. These parameters describe the total energy content of the storm and the frequency distribution, which are important factors for determining the response of the structure. Different spectrum models differ from each other in the way that the energy is distributed across the frequency band. This will in turn affect the response of the structure (Chakrabarti, 2005).

Choice of spectrum depends on (i) which frequency range that is studied, (ii) if the spectrum has the required integrability, and (iii) that the spectrum have a reasonable number of parameters (Myrhaug and Lian, 2009). The basic form of wave spectra, called Pierson-Moskowitz spectrum, and the JONSWAP spectrum will be presented in the following.

Pierson-Moskowitz Spectrum

The basic form of wave spectrum is referred to as a Pierson-Moskowitz (PM) type of spectrum, and have the form of

$$S(w) = \frac{A}{w^5} \, exp\left(-\frac{B}{w^4}\right) \tag{46}$$

where A and B are constants that vary for the different variations of the PM spectrum. The PM model is valid for fully developed sea states and have one peak (Myrhaug and Lian, 2009). The following three PM spectrum models are commonly used to describe the wave process (Naess and Moan, 2012):

- The *standard PM spectrum* is a one-parameter spectrum, and written in terms of the peak frequency w_p, which corresponds to the frequency at which the wave spectrum reach its maximum value. It can also be described by the mean wind speed, U_w.

- The *modified PM spectrum* is a two-parameter spectrum, which, in addition to peak frequency, require significant wave height, H_S, as input.

- The *ISSC spectrum* is also a two-parameter spectrum which is based on the significant wave height and mean frequency of the individual waves, $\bar{w}$.

Formulas for the most common spectrum models are summarized in table 8.1.

Table 8.1: Formulas for standardized wave spectra

Wave spectrum	Parameters	Formula
Pierson-Moskowitz	w_p	$S(w) = \frac{\alpha g^2}{w^5}\ exp(-1.25\frac{w_p^4}{w^4})$
Modified PM	H_s, w_p	$S(w) = 0.3125\ H_S\ \frac{w_p^5}{w^5}\ exp(-1.25\frac{w_p^4}{w^4})$
ISSC	$H_s, \bar{w}$	$S(w) = 0.1107\ H_S\ \frac{\bar{w}^4}{w^5}\ exp(-0.4427\frac{\bar{w}^4}{w^4})$
JONSWAP	$H_s, w_p, \gamma, \sigma_A, \sigma_B$	$S(w) = \frac{\bar{\alpha} g^2}{w^5}\ exp(-1.25\frac{w_p^4}{w^4})\ \gamma^{a(w)}$

JONSWAP Spectrum

The JONSWAP spectrum is a five-parameter spectrum, and is also a version of the PM model. It is constructed by multiplying the PM spectrum with a factor $\gamma^{a(w)}$:

$$S(w) = \frac{\bar{\alpha} g^2}{w^5}\ exp\Big(-1.25\frac{w_p^4}{w^4}\Big)\ \gamma^{a(w)} \tag{47}$$

where

$$a(w) = exp\Big(-\frac{(w - w_p)^2}{2\sigma^2 w_p^2}\Big) \tag{48}$$

and

$$\sigma = \begin{cases} \sigma_A = 0.07, & \text{for} & w \leq w_p \\ \sigma_B = 0.09, & \text{for} & w > w_p \end{cases} \tag{49}$$

γ represents the peakedness parameter, and typically range between 1 and 7. For typical storm conditions in the North Sea, the γ-values lies around 3, and $\gamma = 3.3$ is commonly applied (Naess and Moan, 2012). For fully developed sea, that is, for $\gamma = 1.0$, the JONSWAP spectrum reduces to the modified PM spectrum (Chakrabarti, 2005).

$\bar{\alpha}$ determines the shape of the spectrum in the high frequency range. For North Sea applications, the following formula is usually applied (Naess and Moan, 2012):

$$\bar{\alpha} = 5.058\ \frac{H_S^2}{T_p^4}\ (1 - 0.287\ \ln\gamma) \tag{50}$$

Figure 8.2 shows the JONSWAP spectrum with two different peakedness parameters, $\gamma = 1$ and $\gamma = 3$.
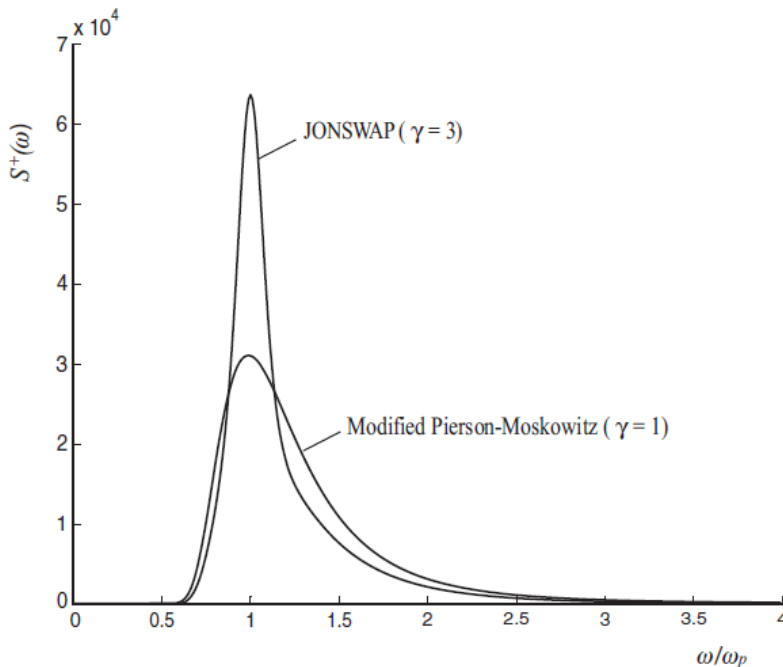
Figure 8.2: JONSWAP spectra for $\gamma = 1$ and $\gamma = 3$ (Naess and Moan, 2012)

8.1.4 Response Spectrum

For a given load frequency, the response of the structure will be a linear function of the load amplitude, and have the same frequency as the load. The load is described as a function of time, but the transfer between the load and the structural response can be modeled as a time-invariant system described by the transfer function, $H_{FX}(w)$. The response spectrum can then be determined by (Naess and Moan, 2012):

$$S_X(w) = |H_{FX}^2(w)| \times S_F(w) \tag{51}$$

where $S_F(w)$ is a variance spectrum of the stochastic load process $X(t)$. The relation between load and response is shown in figure 8.3.
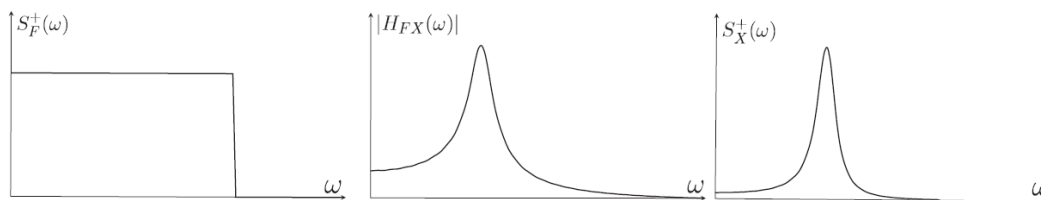
Figure 8.3: Relation between load and response (Naess and Moan, 2012)

A response spectrum describes the energy intensity of the response as a function of frequency. If a time series describing the load process is known, the response spectrum can be determined by Fourier Transformation (Larsen, 2014). This topic will not be discussed here.

8.2   Short-term Statistics

The statistical description of waves are also applicable for response calculations. For design purposes, it is beneficial to get an idea of how the structure is affected by the environmental conditions over longer time periods. To predict the characteristic loads that affect the structure, the response in short time periods can first be examined and then generalized for longer periods.

The short-term distribution is used to inspect the distribution of *individual maxima* of the wave process, that is, the maximum values between each zero-upcrossing (Larsen, 2014). This is illustrated in figure 8.4.
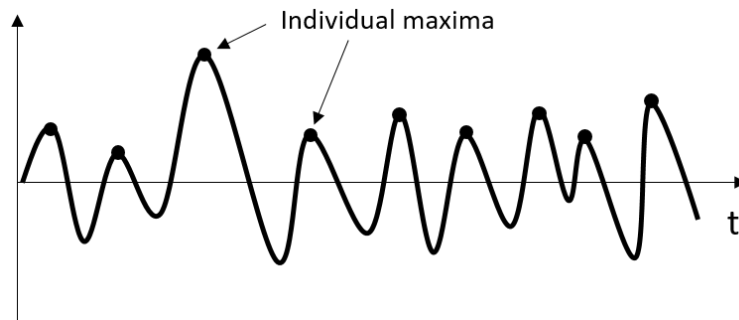
Figure 8.4: Illustration of the individual maxima in a wave process

The short-term distribution describes the probability of a random response value, x_a, being less than a given response level in specific environmental conditions, X_a, and can be expressed by:

$$P(X_a \leq x_a) = F_{X_a}(x_a) = \int_{-\infty}^{x_a} f_{X_a}(y)dy \tag{52}$$

where $F_{X_a}(x_a)$ is the cumulative distribution function (CDF) and $f_{X_a}(x_a)$ is the probability density function (PDF). CDF express the probability of X_a being less than or equal to the random variable x_a. The PDF, on the other hand, is used to express the probability of the random variable being greater than x_a, which implies the relationship (Naess and Moan, 2012):

$$f_{X_a}(x_a) = \frac{dF_{X_a}(x_a)}{dx} \tag{53}$$

The relation between the CDF and PDF is illustrated in figure 8.5. The total area under the PDF curve always equal one.
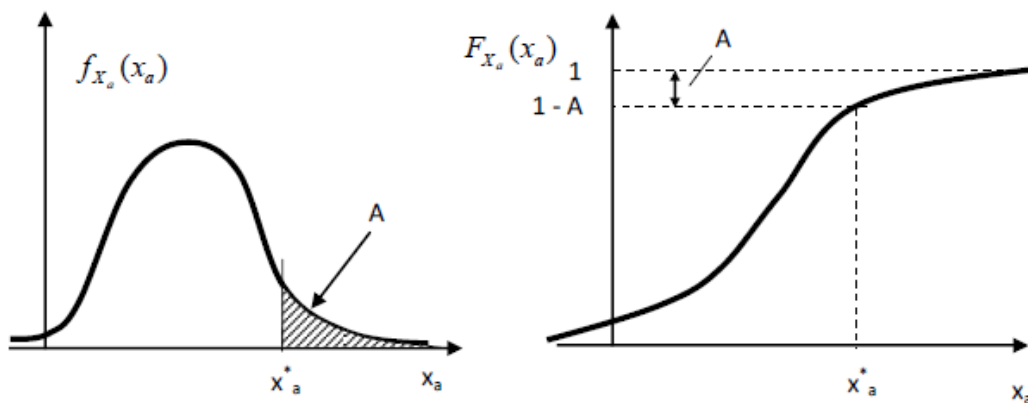
Figure 8.5: Left: PDF, right: CDF (Larsen, 2014)

If we assume that the stochastic process is Gaussian distributed, and that all individual maxima for each stochastic process are statistically independent from each other, the short-term distribution can be described by the Rayleigh distribution (Larsen, 2014):

$$F_{X_a}(x_a) = P(X_a \leq x_a) = 1 - exp\left(-\frac{x_a^2}{2\sigma_x^2}\right) \tag{54}$$

The corresponding PDF is determined from equation 53:

$$f_{X_a}(x_a) = P(X_a > x_a) = \frac{dF_{X_a}(x_a)}{dx_a} = \frac{x_a}{\sigma_x^2} exp\left(-\frac{x_a^2}{2\sigma_x^2}\right) \tag{55}$$

where X_a is an arbitrary maximum response value drawn from a stationary stochastic process, $X(t)$, with variance σ_x^2. The shape of the Rayleigh distribution for a variable x is shown in figure 8.6. The solid line represents the PDF, while the dashed line represents the CDF.
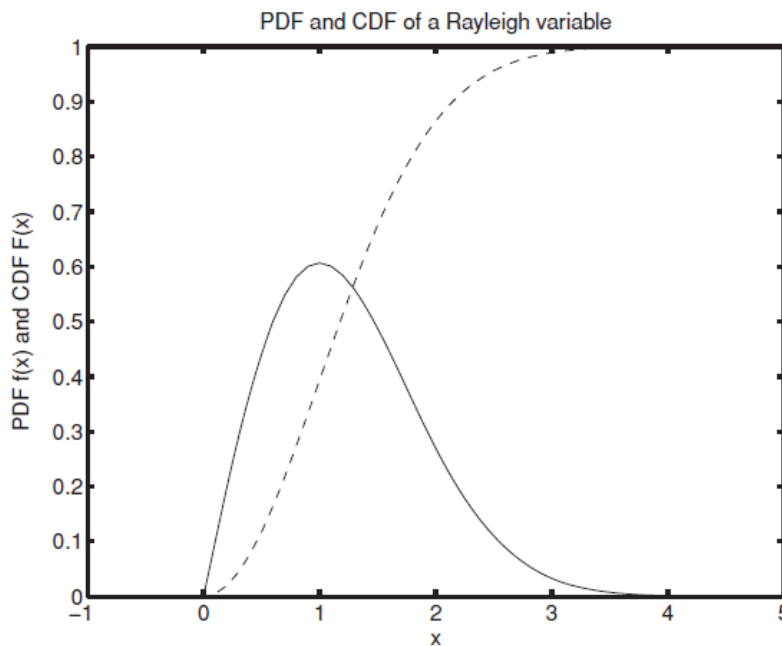
Figure 8.6: Rayleigh distribution of a variable x (Naess and Moan, 2012)

The Rayleigh distribution is valid for narrow-banded processes, that is, stochastic processes with a narrow frequency spectrum, no negative maxima, and only one maximum value between each zero up-crossing. Contrary, a broad banded process can have negative maxima and several maximum values between each zero-upcrossing (Larsen, 2014). Such processes are described by the Rice distribution, but this will not be treated here. The concept of narrow banded and broad banded processes are shown in figure 8.7.
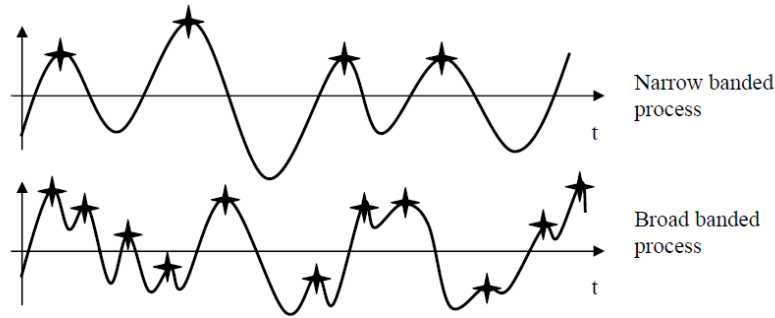
Figure 8.7: Illustration of narrow – and broad banded processes (Larsen, 2014)

8.3 Extreme Value Distribution

When designing marine installations, the *extreme* response in design storm conditions are of particular interest. Design storm conditions are based on parameters that describe the short-term environmental conditions, such as significant wave height, H_S, and spectral peak period, T_p, as well as duration of the storm (Larsen, 2014). In the aquaculture industry, the design conditions represent environmental conditions with 10 and 50 year return period.

The extreme value from a process can, as for the individual maxima, be described as a stochastic variable, since the largest maximum response will vary independently for each short-term time series. Extreme value theory is also based on a sequence of independent and identically distributed random variables $\{X_1, X_2, ..., X_N\}$ which are Rayleigh distributed. The extreme value of this sequence is found as $X_{max} = max\{X_1, X_2, ..., X_N\}$, and the extreme value distribution is determined by identifying the largest maxima, x_{max}, from N storm samples, that is

$$F_{X_{max}}(x_{max}) = P(X_{max} < x_{max}) = \left[F_{X_a}(x_{max}) \right]^N \tag{56}$$

where X_{max} is then the largest response achieved among all maxima during N storm samples. The extreme value distribution of maximum response from four different storm samples is illustrated in figure 8.8.
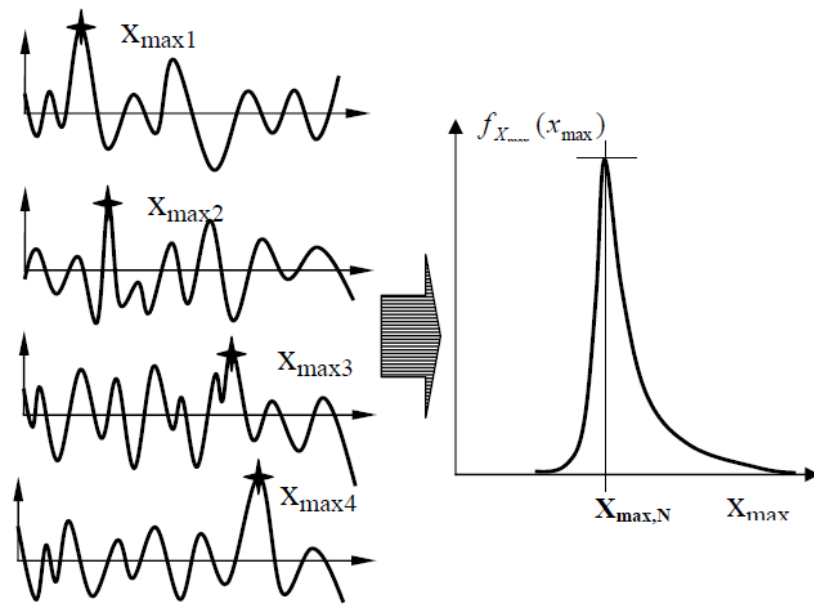
Figure 8.8: Extreme value distribution (Larsen, 2014)

The extreme value distribution of response processes relevant for marine installations usually follow the extreme value distribution type 1, or *Gumbel distribution*, expressed by (Naess and Moan, 2012):

$$f_{X_{max}}(x_{max}) = \frac{1}{\beta} \; \exp\left\{ - \left(\frac{x_{max} - \alpha}{\beta} + \exp\left[- \left(\frac{x_{max} - \alpha}{\beta}\right)\right]\right)\right\} \tag{57}$$

and the corresponding CDF:

$$F_{X_{max}}(x_{max}) = \exp\left\{ - \exp\left[- \left(\frac{x_{max} - \alpha}{\beta}\right)\right]\right\} \tag{58}$$

which is described by the parameters α and β. α represents the location parameter of the distribution, while β represents the scale parameter. The Gumbel parameters are illustrated in figure 8.9.
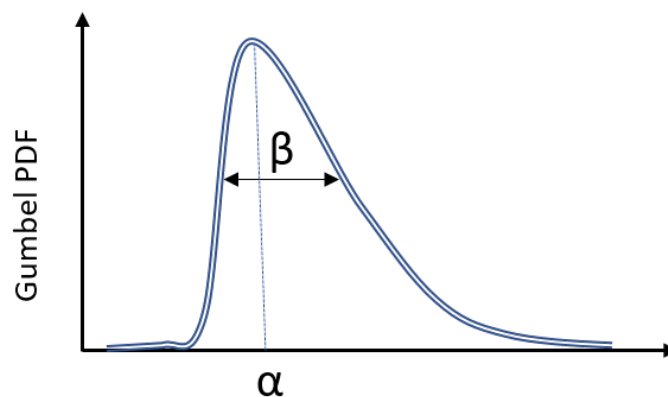
Figure 8.9: Illustration of Gumbel parameters

As α decrease, the distribution shifts to the left, and similarly, if α increase, it shifts to the right. β illustrates the width of the distribution, and as β increase, the PDF spread out and becomes wider. As β decrease, the PDF becomes taller and narrower (Naess and Moan, 2012).

If the stochastic process is assumed to be Gaussian distributed, and the individual maxima follow the Rayleigh distribution, the Gumbel parameters can be determined from the *method of moments*. The parameters α and β are related to the mean value, μ, and standard deviation, σ_x, of the extreme value sample space, as:

$$\mu = \alpha + 0.5772 \times \beta \tag{59}$$

$$\sigma_x = \frac{\pi}{\sqrt{6}} \times \beta \tag{60}$$

The estimates of μ and σ_x obtained from the available extreme value sample space will therefore provide estimates of the Gumbel parameters, α and β, which leads to the fitted Gumbel distribution by the moment method (Naess and Moan, 2012).

When inspecting extreme response, a specified quantile value of the fitted Gumbel distribution can be extracted and used for design considerations. This fractile is described by $100(1 - \eta)\%$, where η is usually a small number, typically $\eta = 0.1$. The quantile function of the Gumbel distribution is given by (Naess and Moan, 2012):

$$Q(p) = \alpha - \beta \times \ln(-\ln(p)) \tag{61}$$

where p is the probability level, equal to $1 - \eta$. The 90% quantile is determined from:

$$Q(0.9) = \alpha - \beta \times \ln(-\ln(0.9)) \tag{62}$$

8.4   Overview of the Distributions

Figure 8.10 illustrates the different probability density distributions presented. $\underline{A}$ shows a stationary Gaussian distributed process, $X(t)$, with zero mean value and constant variance. $\underline{B}$ shows the Rayleigh distributed individual maxima of $X(t)$ for a narrow-banded process. $\underline{C}$ represents the extreme value distribution for various number of storm samples, N. It can be seen from the figure that the extreme value distribution, $f_{X_{max}}$, will have higher PDF values and become narrower for increasing number of storm samples, N (Naess and Moan, 2012).
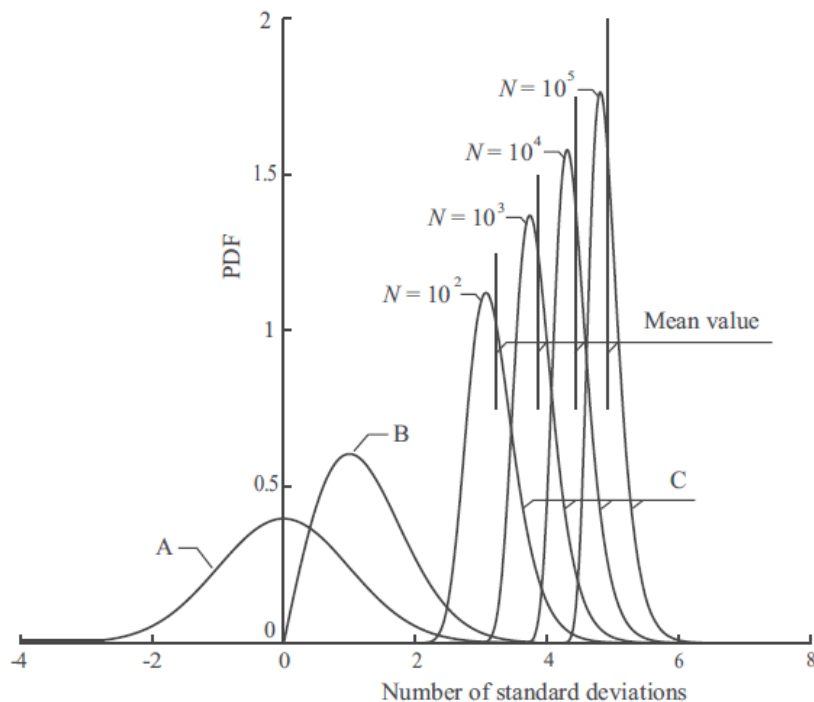
Figure 8.10: Overview of distributions (Naess and Moan, 2012)

8.5   Long-term Distribution

The short-term distribution is only valid for the specific sea state that is inspected. The structural response of a marine installation depends on factors such as sea severity and previous history of the wave process, such that the structural response over longer time periods must be investigated when designing marine structures (Naess and Moan, 2005). The most accurate ULS design approach is to use *long-term statistics* of response when determining the extreme load effects that act on the structure over its lifetime. This way, the changing environmental conditions is accounted for when the characteristic loads are estimated (Naess and Moan, 2012).

8.5.1   Structure of the Long-term Distribution

The long-term distribution is based on the short-term distribution, and is valid at any point in time for a specified location. The long-term distribution is described by the probability of exceeding the specific maximum value, denoted $Q_{X_a}(x_a)$, rather than using the CDF that describe the probability of being smaller than a random value x_a. This is to avoid numerical problems, and the long-term distribution is usually expressed as (Larsen, 2014):

$$Q_{X_a}(x_a) = P(X_a \geq x_a) = 1 - P(X_a \leq x_a) = 1 - F_{X_a}(x_a) \tag{63}$$

Let $X(t)$ denote a zero-mean stochastic process, such as response, that reflect the changing environmental conditions. This implies that $X(t)$ is *not* a stationary process, but this problem is solved by considering the long-term response as a sequence of N short-term stationary conditions (Naess and Moan, 2012). Let X_a be defined as the maximum value of the stochastic process $X(t)$ between two consecutive zero-upcrossings. The long-term distribution is found by combining the short-term distribution with the statistics of the parameters describing the sea states at the actual location, typically significant wave height and peak period. The short-term contributions are then summarized for all the inspected sea states, and the long-term distribution of the response X_a is calculated by (Larsen, 2014):

$$Q_{X_a}(x_a) = \sum_{H_S} \sum_{T_p} Q_{X_a|H_S,T_p}(x_a|H_S, T_p) \ P(H_S, T_p) \ W(H_S, T_p) \tag{64}$$

where

$Q_{X_a|H_S,T_p}(x_a|H_S, T_p)$ Short-term Rayleigh distribution

$P(H_S, T_p)$ Probability of an actual sea state

$W(H_S, T_p)$ Weight factor for the actual sea state

The weight factor accounts for variations of the relative frequency of the response for each sea state. The probability of an actual sea state, $P(H_S, T_p)$, is determined from measured data or simulations (Myrhaug and Lian, 2009).

8.5.2   Extreme Response

When dimensioning structures, the worst imaginable situation is often of particular interest. The long-term distribution can be used to estimate the long-term extreme values of response. NS9415 require that the structure must resist load effects from sea states with 10 and 50 years return period, and long-term response statistics is used to document that the structure will meet these design criteria. Regarding prediction of extreme values, it is the upper tail of the distribution that is of particular interest. The amount of data available therefore have to be sufficient to describe the tail region properly (Haver, 2012).

The extreme environmental conditions are often unknown due to lack of sufficient measured data. If wave data from e.g. one year is available, 10 and 50 year return period of significant wave height can be determined from probability analyses. The *Weibull distribution* is a continuous probability distribution that can be used for several purposes due to its simplicity and flexibility. The Weibull PDF is expressed by (McCool, 2012):

$$f_X(x) = \frac{\beta}{\lambda}\left(\frac{x}{\lambda}\right)^{\beta-1} \exp\left\{ -\left(\frac{x}{\lambda}\right)^{\beta}\right\} \tag{65}$$

and the corresponding CDF:

$$F_X(x) = 1 - \exp\left\{ -\left(\frac{x}{\lambda}\right)^{\beta}\right\} \tag{66}$$

To ensure that the data follow the Weibull distribution, a quantile-quantile (Q-Q) plot can be computed, with the vertical scale ruled proportionally to the values of $ln(-ln(1-CDF))$ and with a logarithmic horizontal scale. If the data plot form approximately a straight line, the data can be assumed to follow the Weibull distribution (Naess and Moan, 2012). An example of a Q-Q plot for the Weibull distribution is shown in figure 8.11. Q-Q plots are also applicable for extreme value probability analyses, by plotting the extreme values and CDF of the Gumbel distribution to ensure the data set follow the Gumbel distribution.
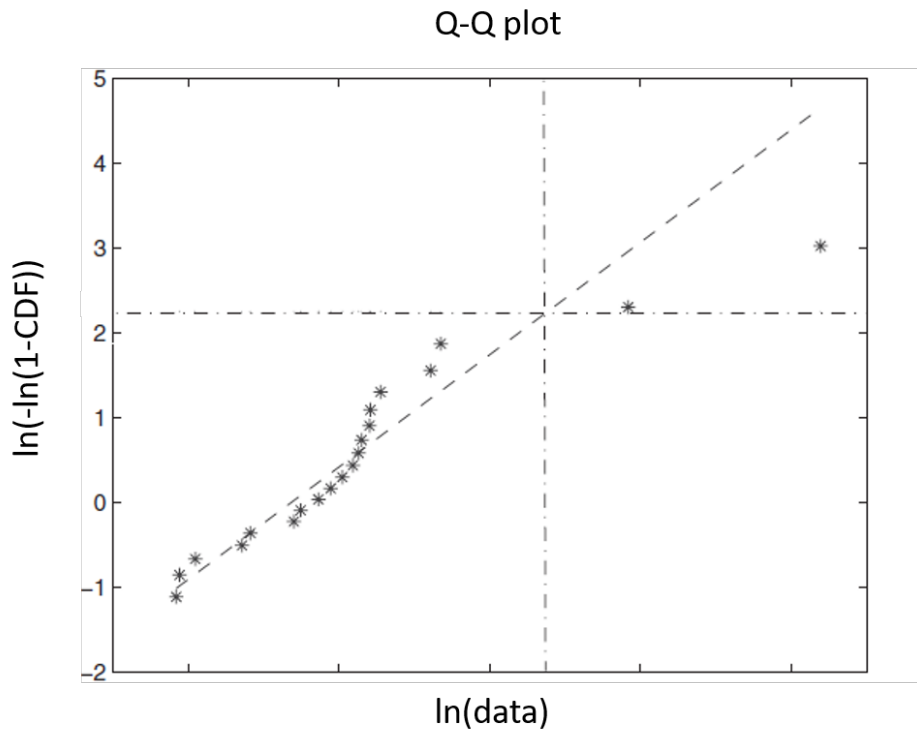
Figure 8.11: Q-Q plot with trend line

The Weibull distribution can then be used to determine $F_X(x)$ within graphical accuracy for the values of interest by inspecting the linear trend in a Weibull probability plot. In case of a data set that is representative for one year, 10 and 50 year values, corresponding to $F_X(x) = 0.90$ and $F_X(x) = 0.98$, respectively, are of particular interest. These can be determined graphically by looking at the intersection with the linear trend line and reading the values of the horizontal axis (McCool, 2012). An illustration of a Weibull probability plot is shown in figure 8.12. The points correspond to the data points, while the red line illustrates the linear trend.
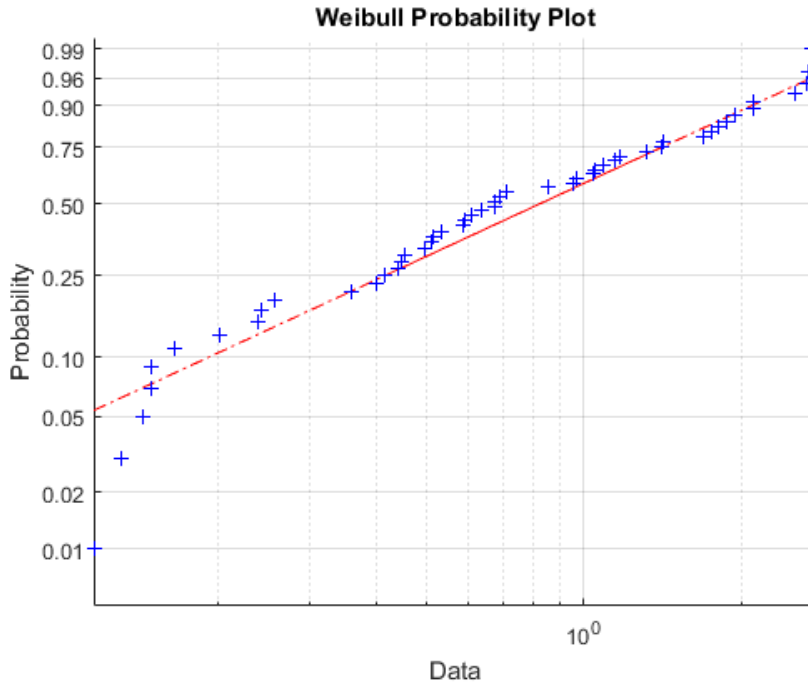
Figure 8.12: Weibull probability plot

8.5.3   Establishing the Long-Term Extreme Value Distribution

The long-term extreme response can be determined in two different ways, based on the amount of available data. The *All sea states approach* is applied when a wide range of sea states can be inspected and the probability of an actual sea state can be determined from measured data. The *Two sea states approach* is applied when there is lack of simultaneous environmental data. The method use two known sea states to determine the corresponding extrema and then fit the Gumbel distribution from the two known maxima. Both methods will be presented in detail in the following.

Method 1: All Sea States Approach

The All Sea States Approach consider both the short-term and the long-term variability. If there is sufficient amount of measured data available to estimate the distribution in the tail regions, the long-term distribution can be determined directly from equation 64. For extreme response design purposes, the weight factor $W(H_S, T_p)$ in equation 64 is not relevant, since only the maximum response of each long-term distribution is of interest. The extreme value distribution can then be written as:

$$Q_{X_a}(x_{max}) = \sum_{H_S} \sum_{T_p} Q_{X_a|H_S,T_p}(x_{max}|H_S,T_p) \ P(H_S,T_p) \tag{67}$$

where $Q_{X_a|H_S,T_p}(x_{max}|H_S,T_p)$ is the short-term Gumbel distribution with parameters α and

β. These parameters are determined by inspecting the mean and standard deviation of the extreme value distribution. This distribution accounts for the randomness of extreme values within the short-term duration of the sea state, which usually range from 20 minutes to 3 hours (Puente and Lian, 2017).

The joint probability of an actual sea state, $P(H_S, T_p)$, express the long-term description of the sea state, and can be determined from a frequency table, often denoted *scatter diagram*. A scatter diagram presents the number of observations of sea states for any environmental combination, usually H_S and T_p. An example of a frequency table is shown in table 8.2.

Table 8.2: Example of frequency table for significant wave height and peak period

Significant wave height [m]	Peak period [s]										
	2-3	3-4	4-5	5-6	6-7	7-8	8-9	9-10	10-11	11-12	12-13
$0.0 - 0.5$	0	219	245	63	69	88	68	77	0	1	0
$0.5 - 1.0$	0	0	244	120	58	64	12	55	6	0	0
$1.0 - 1.5$	0	1	0	22	98	554	5	5	2	5	0
$1.5 - 2.0$	0	0	66	97	78	55	2	3	1	0	0
$2.0 - 2.5$	0	0	0	0	65	87	4	2	1	0	0
$2.5 - 3.0$	0	0	0	0	0	0	0	14	2	0	0
> 3.0	0	0	0	0	0	0	0	0	1	0	1

The probability for an actual sea state can then be found directly from this table by the ratio between the number of observations of a specific sea state and total number of observed sea states, N (Larsen, 2014).

If the long-term distribution of the individual response maxima, X_a, is known, then the response level for any return period can be determined directly from the long-term distribution. The probability of exceeding the individual response level X_a once every year, is calculated from (Puente and Lian, 2017):

$$Q_{X_a}(x_{max,d}) = \frac{q}{m_d} \tag{68}$$

where q is the target annual exceedance probability, and m_d is the annual number of events of duration d.

Equation 68 cannot be solved analytically, and the solution is thus obtained by iteration.

Method 2: Two Sea States Approach

If the scatter diagram is too coarse, that is, if the available simultaneous data is not sufficient, it will give poor resolution in the tail regions of the extreme distribution. This will in turn lead to inaccurate long-term extreme value estimates (Naess and Moan, 2012). The Two

Sea States Approach can be applied when there is not enough available data to estimate the probability of an actual sea state, $P(H_S, T_p)$.

Consider two known sea states, 10 and 50 year conditions, where H_S and T_p are known. Each sea state is simulated N times, and each simulation run will generate an extreme response value. The selection of extreme responses in 50 year conditions, $\{x_{max,50}^1, x_{max,50}^2, ..., x_{max,50}^N\}$ from N storm samples are then used to estimate the mean and the standard deviation, which provide estimates of α and β in the Gumbel distribution. When the Gumbel parameters are estimated, a fitted Gumbel distribution can be established for the 50 year sea state. The 90% quantile value, x_{50}, of this fitted distribution is then extracted and used to fit the Gumbel distribution of the maximum *annual* response.

The same procedure is applied with the other known sea state, i.e. the 10 year environmental conditions. Similarly, the 90% quantile of the fitted 10 year extreme value distribution is extracted. The procedure is summarized in figure 8.13.
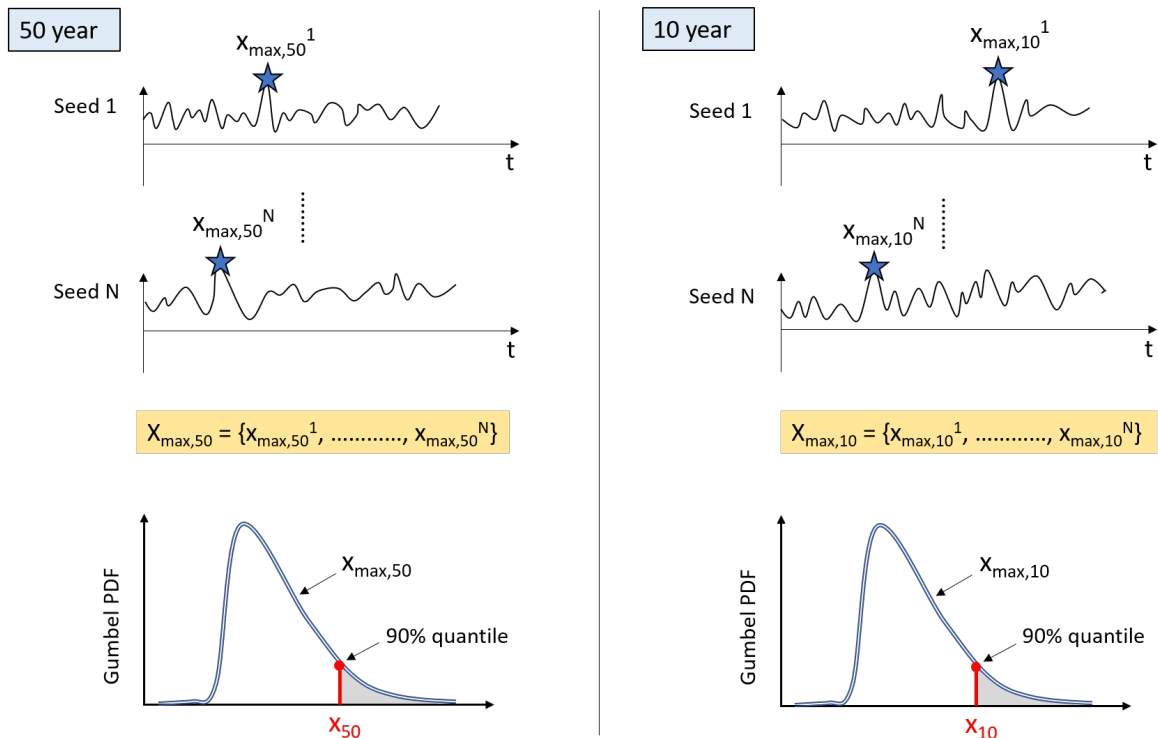
Figure 8.13: Illustration of the Two Sea States Approach

With these two extreme values, x_{50} and x_{10}, known, the Gumbel distribution of the largest annual response can be estimated by determining the Gumbel parameters from the equation for cumulative probability distribution, for each of the two sea states:

$$F_{X_{max}}(x_{50}) = \exp\left\{ -\exp\left[-\left(\frac{x_{50} - \alpha}{\beta}\right)\right]\right\} = 1 - \frac{1}{50} = 0.98 \tag{69}$$

and

$$F_{X_{max}}(x_{10}) = \exp\left\{ -\exp\left[-\left(\frac{x_{10} - \alpha}{\beta}\right)\right]\right\} = 1 - \frac{1}{10} = 0.90 \tag{70}$$

for 50 and 10 year conditions, respectively. $F_{X_{max}}(x_{50})$, $F_{X_{max}}(x_{10})$, x_{50} and x_{10} is known, which gives two equations with two unknowns; α and β. The distribution of the maximum annual response can then be obtained from only two known sea states. This is illustrated in figure 8.14.
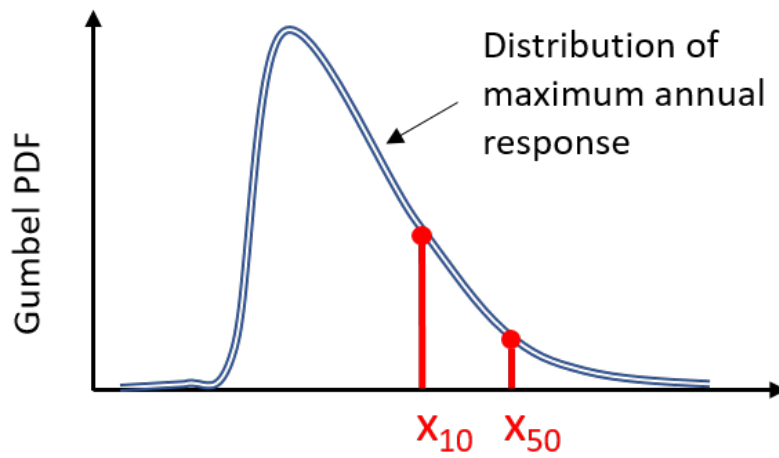
Figure 8.14: Distribution of maximum response from two known sea states

9   Time Domain Simulation of Marine Systems

Marine systems within aquaculture are often complex. Fish cages are highly flexible and must be modelled by non-linear differential equations. *FhSim* is a software framework developed by SINTEF Ocean, used to simulate marine systems and operations in time domain. Time-domain integration is applied to ensure that the system behavior is simulated realistically by including non-linear effects (Reite et al., 2014). The following chapter is mainly based on Reite et al. (2014), and will describe the architecture and core functionality of FhSim.

9.1   FhSim Architecture

In FhSim, complex marine systems are designed by modelling the components of a system as a combination of sub-models. The sub-models are interconnected by input/output ports facilitating the necessary information and properties to conduct a simulation (Endresen et al., 2014). The modularity of the software platform makes it easy to adapt the simulation studies to specific purposes.

9.1.1   Key Components

Figure 9.1 illustrates an overview of the FhSim architecture.
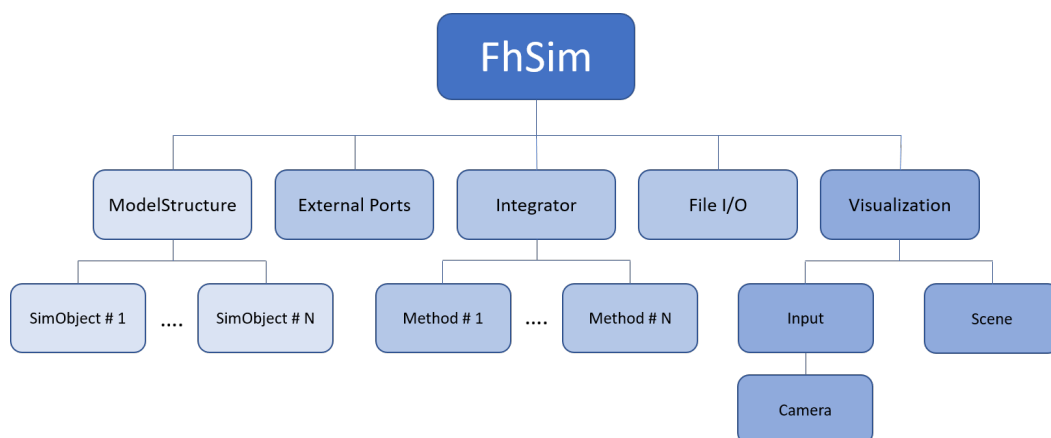
Figure 9.1: FhSim Architecture

The software consists of five key components, where FhSim represents the overarching main component where the user interaction occur. FhSim interconnects the system model described in ModelStructure with the Integrator, File I/O, External ports and Visualization

components. Input to the software is provided by the user from textual input files, while outputs are provided from the FhSim component as either text files, screen shots or messages to console.

SimObjects can be seen as the building blocks of an FhSim simulation. These objects implement the different sub-models and each SimObject computes its own state derivatives, visualization and output ports. The *ModelStructure* implement all SimObjects to a total system model. This will represent the simulation model, and can for instance be a fish farm interacting with live fish carriers and feeding barges. The ModelStructure contain an overview of the interconnections between the SimObjects defined in the input file. The *Integrator* keeps track of the states of the total system model and reads and writes initial conditions. Several integration methods are available in FhSim. *File I/O* handles the interaction (input and output) between the model system and files, which includes interpretation of input, message logging, and writing the resulting data to output files. Output is given as .csv-files which includes element forces in x, y, and z-direction. The coordinate system in FhSim is not an ordinary right-hand system, but rather a north-east-down system, where north = x, east = y, and down = z.

The *External ports* component enables integration between FhSim and external systems. *Visualization* manages visualization of the simulations, which makes real-time 3D visualization and recording of simulations possible.

9.1.2   System Setup

The FhSim setup is facilitated through XML input files specified by the user. The XML file specifies which objects to include in the simulation and how they are connected to each other, the initial states of the SimObjects, as well as integrator options and output options. The input file consists of four sections (SINTEF Ocean, 2017):

- Objects – specifies which SimObjects to include in the simulation and the necessary input parameters.

- Interconnections – specifies how the SimObjects are connected. They could either be connected to each other or assigned constant values by the user.

- Initialization – specifies the initial conditions of the SimObjects.

- Integration – specifies which integration method to use and details regarding step length and intervals, i.e. how the simulation is run.

9.2   Simulation

The actual simulation procedure in FhSim consist of numerical integration of differential equations in combination with visualisation.

9.2.1   Numerical Integration

Various methods based on numerical integration is available in FhSim, including Forward Euler methods, Heun's method, as well as Runge-Kutta methods, which was presented in section 7.3.3. The preferred integration method must be specified under the integration section in the input file, together with time step length and total duration of the simulation. The simulation can be conducted with either fixed or variable time steps - the latter can be beneficial for highly non-linear problems.

9.2.2   Visualization

Visualization in 3D is available in FhSim through an open source rendering engine. The geometry of the structures in FhSim can be realized as either static or dynamic meshes. Static meshes often represent rigid bodies such as ship hulls, buoys and feeding barges. Dynamic meshes change for each visualization frame, and represent flexible structures such as nets and floating collars. Figure 9.2 show illustrations from simulations of irregular waves and current.
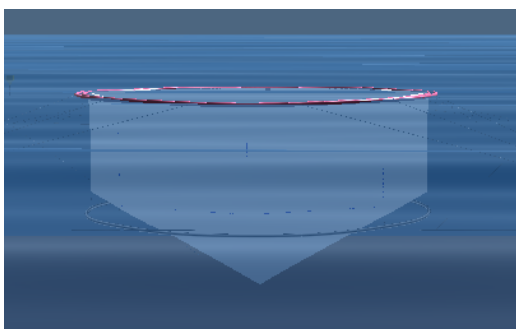
(a) Side view
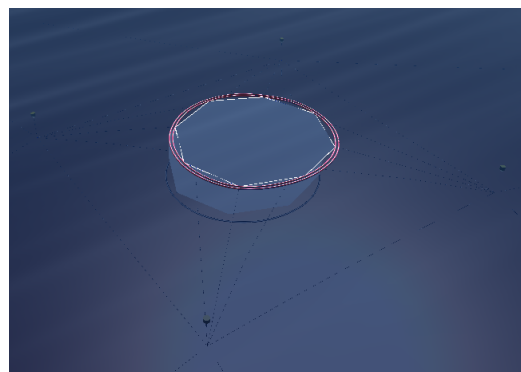
(b) Top view

Figure 9.2: Visualization of simulations in FhSim

9.3   Generic Models

FhSim can implement several sub-models to create the total system model. A selection of generic sub-models is available in the software, such that the user only needs to know the interface of the SimObjects (SINTEF Ocean, 2017).

9.3.1   Floating Collar

The floating collar is modelled by a circular 6 degrees of freedom (DOF) ring element. The mode superposition principle is used to model the structural response of the ring, which is based on summarizing the response for the natural modes to determine the total response. This model accounts for elastic deformations, while the effects of axial force, shear forces and torsion are not included (Endresen et al., 2014).

9.3.2   Net Structure

The net structure itself is modelled by a collection of triangular net elements, and the ropes embedded in the net structure are modelled by basic cable elements. The net is assumed to be knotted, with spherical knots of twice the twine diameter, even though aquaculture nets are usually knotless. All parts of the net structure are interconnected through nodes and the mass of the elements are distributed to the closest node. The hydrodynamic, as well as structural forces that act on each element is also distributed to the nodes. The acceleration of the node is found by summarizing all the forces acting in one node, and applying Newton's second law with known node mass and added mass. This enables calculations of velocity and position of the node, which is used to simulate the deformations and movement of the net structure in response to the external and internal forces (Endresen et al., 2014).

The net model is initialized by its own sub-model which contain an overview of all net and cable elements comprising the desired net structure, and information on how these are interconnected. Parameters such as twine diameter (mm), mesh bar length (mm), and density (kg/m^3) are specified for each element (Endresen et al., 2014).

The net model can account for wake effects between twines, as well as wake effects between elements. This is especially beneficial for fish farms that consist of several cages.

9.3.3   Cables, Ropes and Chains

Cables, ropes and chains are modelled by a generic cable model in FhSim. The cable model consists of interconnected rigid bar elements, and the hydrodynamic forces that act on the bar elements are computed by a Morison type expression (Reite et al., 2014). By applying constraint equations to the bar elements, structural properties such as bending stiffness, axial forces etc. can be provided. When implementing the cable model, parameters such as cable length (m), weight per unit (kg/m), number of elements, diameter (m), as well as E-modulus (N/m^2), must be specified in the input-file.

9.3.4   Environment

FhSim can be used to model both regular and irregular sea states. For irregular sea states, realizations of JONSWAP and ISSC spectra are available in the software, and the preferred spectra must be specified in the input-file.

10   Stochastic Analysis of Mooring Line Tension

The aim of this Master Thesis was to inspect whether the technical standard and design procedures are good enough to cover the new challenges the industry face. This was done by performing numerical simulations of mooring line tension for different environmental conditions, and develop an extreme value distribution of mooring line tension based on stochastic mooring analyses. The effects of irregular environmental conditions were studied and compared with the response of the structure in regular waves, to see if the irregular effects had prominent influence on the characteristic loads.

This chapter presents the simulation study conducted to examine the long-term mooring line tension. First, the procedure that was applied to determine extreme response of the system, and how to develop the annual extreme value distribution of mooring line tension, will be presented. Then, the results from the stochastic mooring analyses will be presented, and a discussion of the results will follow at the end of this chapter.

10.1   Method

Long-term stochastic analysis of extreme mooring line tension were performed by the *Two Sea States Approach*, presented in chapter 8, section 8.5.3. Simulations of 10 and 50 year environmental conditions were conducted in FhSim, and the extreme response of the structure was used to develop an extreme value distribution for each sea state. The two sea states were then used as basis for determining the *annual* extreme value distribution of mooring line tension.

Distribution of the extreme load was compared with distribution of strength of the component, to inspect the significance of the load and material factor in the partial coefficient method. The following sections will describe the procedure in detail.

10.1.1   Environmental Data

Environmental parameters for the different sea states were based on a site survey for the locality Salatskjæra from 2015. The site survey was conducted by Havbrukstjenesten AS, and provided by Aqualine with permission from SalMar, who owns the report. Also, environmental data recorded from an ocean buoy at Salatskjæra from March 9th, 2016, to March 14th, 2017, was provided by SINTEF Ocean in conjunction with the Exposed Aquaculture project. The site survey was used as basis for the simulations, while the data from the

ocean buoy was used to study the environmental conditions in detail. The following sections will highlight the environmental data used in the simulation study and summarize how the parameters in the site survey were determined.

Location

The inspected area is located in Frøyhavet, off the coast of Sør-Trøndelag county in Norway. Salatskjæra is exposed to open sea, with some islets and small islands north-west, west and south of the locality (Havbrukstjenesten AS, 2015). The locality is highlighted in figure 10.1.

Figure 10.1: Location Salatskjæra (map from the Directorate of Fisheries map service)

Current

Measurements of current velocity for the site survey were performed on an empty locality in 2013/2014. The measurement period was set to minimum one month and logging occurred every 10th minute at two levels; 5 meter and 15 meter. Current velocity was measured from December 5th to January 21st for 5 meter depth, and from July 25th to September 3rd for 15 meter depth. The 10 and 50 year conditions were then determined by multiplying the maximum measured value for each depth with the multiplication factors presented in table 5.4. Maximum measured current speed was 49.9 cm/s at 5 meter depth, which resulted in 10 and 50 year conditions of 82 cm/s and 91 cm/s, respectively (Havbrukstjenesten AS, 2015).

Wind-induced Waves

The exposed location of Salatskjæra entails both wind-induced waves and ocean swells. NS9415 states that wind-induced waves should be determined by (i) wave measurements, or (ii) calculations based on effective fetch length. For this location, calculations based on effective fetch length were used to determine 10 and 50 year significant wave height and corresponding peak period (Havbrukstjenesten AS, 2015).

Equation 6 was applied to determine the adjusted wind velocity, and the wind conditions on site, U_{10}, were determined in accordance with NS-EN 1991-1-4, based on the reference wind velocity for Frøyhavet. H_S and T_p were calculated from equation 7 and 8, respectively. Results from calculations of wind-induced waves based on effective fetch length are presented in table 10.1 (Havbrukstjenesten AS, 2015). Wind from north-east resulted in the highest wind-induced waves.

Table 10.1: Calculation of wave height based on effective fetch length

Return period	Wind direction	U_A [cm/s]	H_S [m]	T_p [s]	Direction (°)
10 year	NE	23	2.8	5.4	59
50 year	NE	25	3.0	5.7	60

Ocean Swells

Ocean swells also have an impact on the locality, due to the exposed location of Salatskjæra. These wave conditions were calculated based on extreme value analyses of NCEP (National Centers for Environmental Prediction) model data at reference points along the Norwegian coast. NCEP is a free weather database which can be used to model ocean waves. 10 and 50 year conditions were determined from a Weibull analysis (described in section 8.5.2) of the model data (Havbrukstjenesten AS, 2015).

The results of the analyses showed that ocean swells from north, north-west and west, with wave height of $0.7 - 1.3$ m and peak period of $14.0 - 16.0$ s propagates at the location with direction $61 - 65°$ (Havbrukstjenesten AS, 2015).

Combination Waves

The combination of wind-induced waves from north-east, and ocean swells from north-west, increased the wave height with $0.4 - 0.5$ m. This resulted in maximum significant wave height of 3.3 m and peak period of 6.3 s for a 10 year return period, and wave height of 3.5 m and period of 6.5 s for a 50 year return period (Havbrukstjenesten AS, 2015).

10 and 50 Year Environmental Conditions

For practical reasons, the maximum wave conditions and current velocity were assumed to arise from the same direction in the simulations. The 10 and 50 year environmental conditions used for the simulation study are summarized in table 10.2. A more detailed overview of the results from the site survey are presented in appendix B.

Table 10.2: 10 and 50 year environmental conditions from site survey

Return period	V_C at 5m/15m [cm/s]	H_S [m]	T_p [s]
10 year	82/73	3.3	6.3
50 year	91/82	3.5	6.5

Weibull Analysis

The 10 and 50 year significant wave height in the site survey were based on calculations of wind-induced waves and NCEP model data of offshore swells, and not actual measurements on site such as the dimensioning current. The data from the ocean buoy located at Salatskjæra was used to perform a Weibull analysis of the significant wave height. The data set contained measurements for one year, and this was used to estimate the Weibull parameters and develop a fitted Weibull distribution. A linear fit of the data was extracted to estimate 10 and 50 year significant wave height. The dimensioning significant wave height from the Weibull analysis was then compared to those provided in the site survey.

10.1.2   Simulation Model

The model used for simulations in FhSim was based on the Aqualine Midgard® system, presented in figure 10.2.
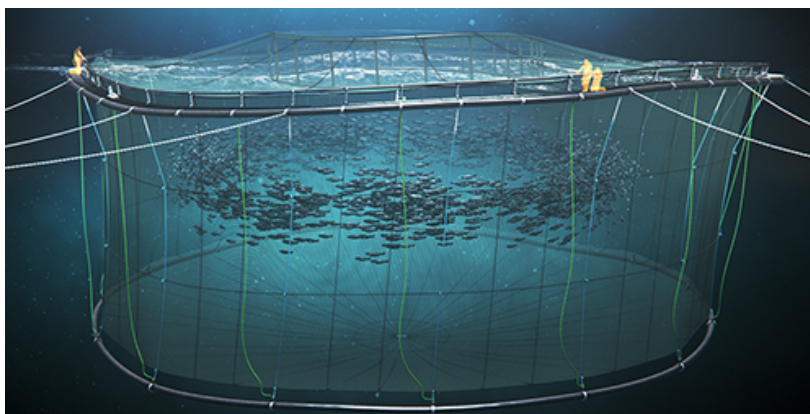
Figure 10.2: Aqualine Midgard® system (illustration by Aqualine)

The Aqualine Midgard® system is an integrated net cage and distension system that consist of double circular collar floaters, a net cage with cone-shaped bottom, and a submerged sinker tube to maintain the shape of the cage.

The circular cage itself is connected to a mooring frame by three bridles in each corner, and the total system is moored to the seabed by eight mooring lines. The main components of the Midgard® model are illustrated in figure 10.3
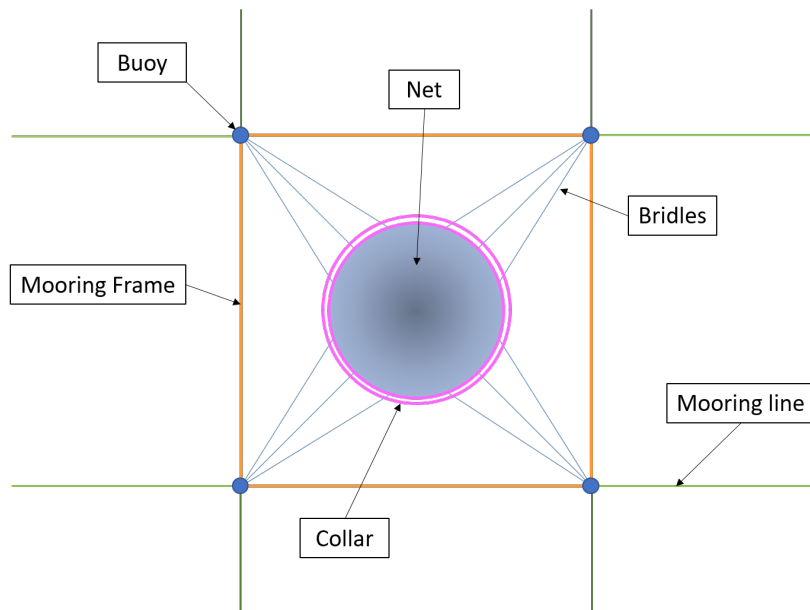
Figure 10.3: Simplified cage model with main components

Aquaculture cages comes in various sizes, but the simulation model was chosen with ring circumference of 157 meter, and diameter of 50 m. The cage model had a total depth of 28 meter, including cone depth. The mooring frame was laid at a depth of 8 meter to avoid interaction with live fish carriers and operational vessels, and the whole system was moored at 100 meter depth. Model dimensions are summarized in figure 10.4 and figure 10.5.
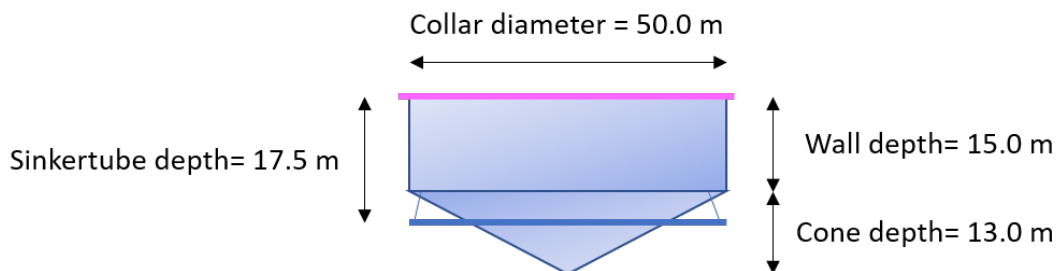
Figure 10.4: Cage dimensions
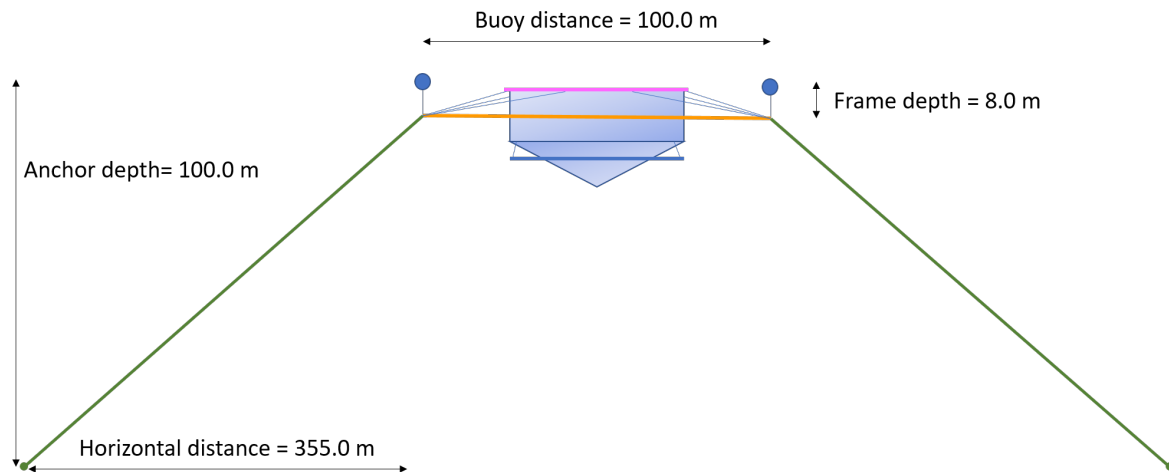
Figure 10.5: Mooring system dimensions

The floater was modelled by two polyethylene pipes of cross-sectional diameter 0.5 meter. The net model consisted of 80 triangular elements, with mesh thread diameter of 1.7 mm and solidity of 22.3%. For practical purposes, the mooring lines were modelled only by polyethylene ropes, without any chain segments. The same rope dimensions were used for the anchor lines and mooring frame, while the 12 bridle ropes were given a smaller cross-sectional area. All relevant data of the simulation model is provided in appendix C.

The mooring system was pretensioned according to the industry's "best practise". Pretensioning is applied to ensure that the leeward mooring lines does not go slack and wear out from contact with the sea bed. The pretension usually ranges from 1 to 10 tonnes, and depends on depth, length, neighboring mooring lines, amount of anchor chain, as well as type of bottom attachment (Hval, 2017). To achieve the desired pretension for the model, the position of the anchors and the weight of the mooring lines were altered.

10.1.3 Simulation in FhSim

The simulation study was performed in the simulation software FhSim, which was introduced in chapter 9. FhSim was selected for this purpose due to well proven numerical models for simulations in irregular environmental conditions. The following sections explain how the simulations were performed and important specifications applied to FhSim.

Environment

FhSim was applied to simulate 10 and 50 year environmental conditions and inspect the extreme response of the mooring lines. A JONSWAP spectrum, with peakedness parameter $\gamma = 3.3$, was used to simulate long-crested irregular waves. The resulting JONSWAP spec-

trum for 50 year conditions is presented in figure 10.6. The dashed line indicates the peak frequency, w_p.
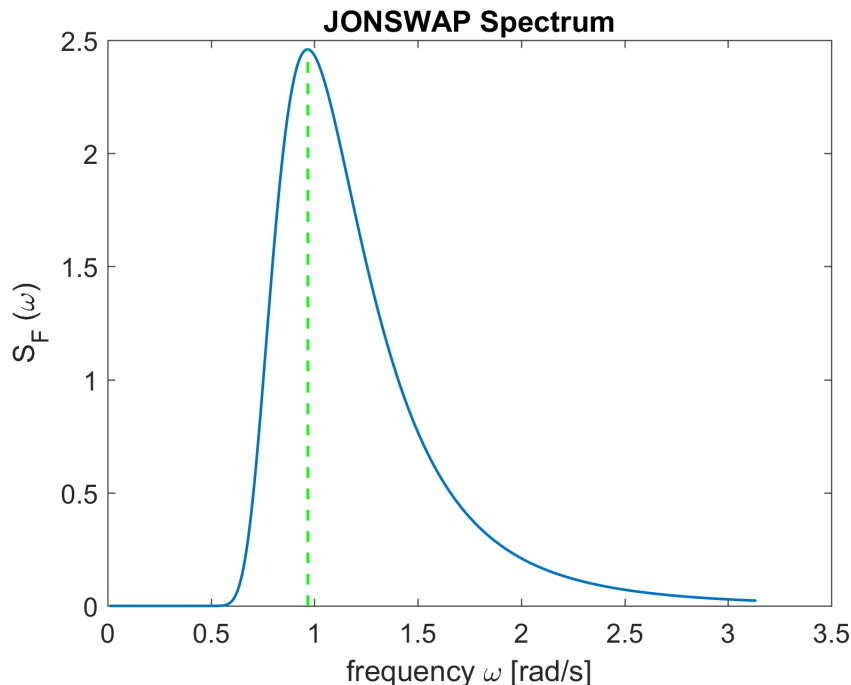
Figure 10.6: JONSWAP spectrum for 50 year conditions

When simulating irregular sea states, each sea state should vary from another while still having the same predefined conditions. This is done by varying the *seed number*. The wave seed number is a random value, which will give different maximum wave rise and wave fall, as well as vary the time window for when the peak response will occur, during the simulation (Suwarno and Lee, 2016). In FhSim, the seed number updates automatically for each simulation run. This can also be done manually if preferable.

Regular sea states were simulated by specifying wave frequency and wave amplitude in the input-file.

Length of Time Series

Several short-term wave processes are required to develop a long-term description of the wave field. These short-term processes usually have duration of 20 minutes to 3 hours (Naess and Moan, 2012). The length of the time series for this simulation study was determined by simulating several different lengths and examine at which time the response converge, as well as the length of the actual simulation. The FhSim model consist of many small elements and has complex net structure, and simulation turned out to be a time-consuming process. Simulation time thus became the critical factor for determining the length of the

time series. Simulation of time series from 500 seconds to 3000 seconds were performed, and 1000 seconds turned out to be enough to capture the extreme response, without having too time-consuming simulations. The length of time series was thus set to 1000 seconds, with logging interval of 1.0 second.

Input

The simulation model itself was kept identical for all simulation purposes, but the input in terms of environmental conditions were adjusted based on which environment to study. First, pretension was determined by simulation without environmental forces. Then, 10 and 50 year irregular and regular environmental conditions were simulated by altering the input-values in the SimObject called "Deep sea gravity waves". Also, simulations with current only, as well as waves only, were performed to inspect the static and dynamic contribution to the mooring line response. The SimObjects corresponding to the different environments used in this simulation study is included in appendix D.

The preferred numerical integration method is also specified by the user in the input-file. For all simulations performed in this simulation study, the Runge-Kutta-Fehlberg method (RKF45) was applied. This method was described in detail in section 7.3.3.

Output

FhSim generates the output in .csv-files. For this simulation study, the tension in the mooring lines were of particular interest, and thus the output was specified to only cover the cable forces. "Cable force" includes the force in all bridles, mooring frame, and mooring lines, and the force in both the upper and lower element. For each element end, the force in x-direction (north), y-direction (east), and z-direction (down) was given, and mooring line tension was calculated from:

$$T = \sqrt{F_x^2 + F_y^2 + F_z^2} \tag{71}$$

The output-files were transferred to MATLAB for further processing. The MATLAB codes programmed for this simulation study are included in appendix F.

Simulation Runs

FhSim was used to simulate different environmental conditions, both regular and irregular environments, and these are presented in table 10.3.

Table 10.3: Simulation runs

Simulation	V_C [cm/s]	H_S [m]	T_p [s]	# of seeds
Irregular				
50 year conditions	91/82	3.5	6.5	45
10 year conditions	82/73	3.3	6.3	45
Load combination 1	91/82	3.3	6.3	1
Load combination 2	82/73	3.5	6.5	1
Current only	91/82	-	-	1
Waves only	-	3.5	6.5	1
Regular				
50 year conditions	91/82	3.5	6.5	-
Design wave - combination 1	91/82	6.27	6.5	-
Design wave - combination 2	82/73	6.56	6.5	-

10.1.4   Mooring Line Tension

The mooring line tension was of specific interest for this stochastic analysis. FhSim provided output values for all eight mooring lines, and the tension in the upper element connected to the mooring plate was selected as reference to inspect the mooring line response. Numbering of the mooring lines in the simulation model is shown in figure 10.7.
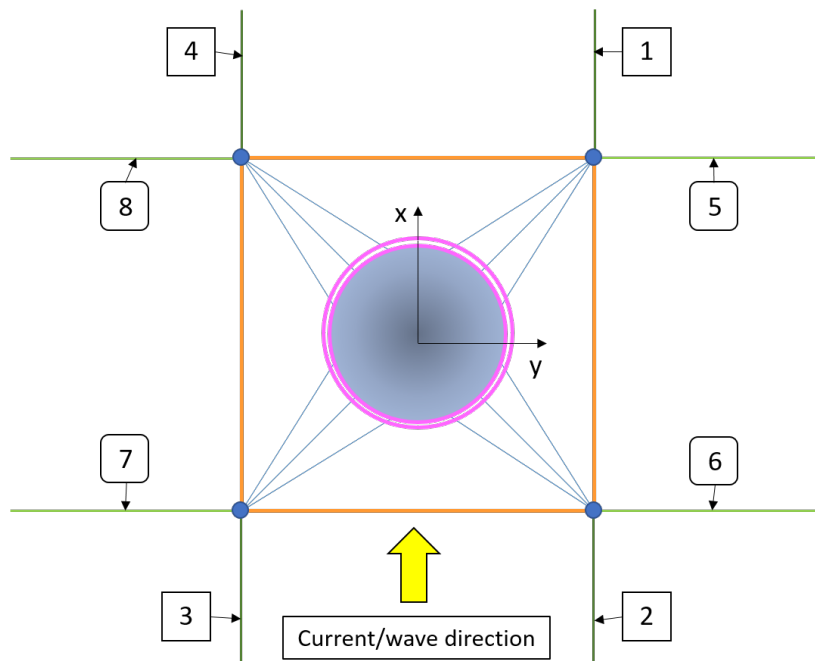
Figure 10.7: Numbering of mooring lines

Tension in all mooring lines were inspected to determine which mooring line that was most vulnerable to the environmental loads. The mooring line with the largest response was then selected as reference for the extreme value analysis.

10.1.5   Response

The range of the mooring line tension were examined by plotting the time series from several seed numbers together, and the interaction between the sea loads was inspected by isolating the response from current and waves. A response spectrum, as described in section 8.1.4, was established to examine the frequency range of the response from the waves and the combination of waves and current.

10.1.6   Load Combinations

NS9415 states that characteristic load should be determined from analyses of the two load combinations presented in table 5.1. Load combinations in both regular and irregular conditions were simulated, and the most unfavorable of the two were chosen as reference for characteristic load.

10.1.7   Static and Dynamic Response

The static and dynamic response were isolated by simulating only current and only waves, respectively, as well as a combination of current and waves. Also, the combination of current and waves was compared to the theoretical superposition of current only and waves only, to examine the linearity of the response.

Simple hand calculations were performed to estimate the drag force on the net structure, and the resulting force was compared with the results of the static simulation to validate the results. Drag forces on the cage were estimated by assuming a square cage and neglecting drag forces on the net sides and bottom. The drag load on the floating collar was also neglected. A simplified procedure for calculating drag force on a series of net panels is presented in appendix E.

10.1.8   Regular and Irregular Response

Simulation of regular environmental conditions was also conducted in FhSim. First, 50 year conditions were simulated to compare the frequency motions of the response with irregular

environmental conditions. Then, the design wave approach was simulated to compare the characteristic load resulting from the design wave approach to the characteristic load from irregular environmental conditions.

10.1.9   Extreme Value Distribution

The mooring line response was assumed to be a piecewise stationary Gaussian process with zero mean value, and the maxima was assumed to be Gumbel distributed. A Q-Q plot of the extreme values for each sea state was established to validate the latter assumption.

Number of storm samples needed to describe the extreme value distribution is dependent on the Gumbel parameters. It is important to ensure that the Gumbel parameters converges, and the number of storm samples needed are thus dependent on the mean and standard deviation of the extreme value distribution. The chosen number of storm samples, N, was verified by plotting the Gumbel parameters against N. This is illustrated in figure 10.8.
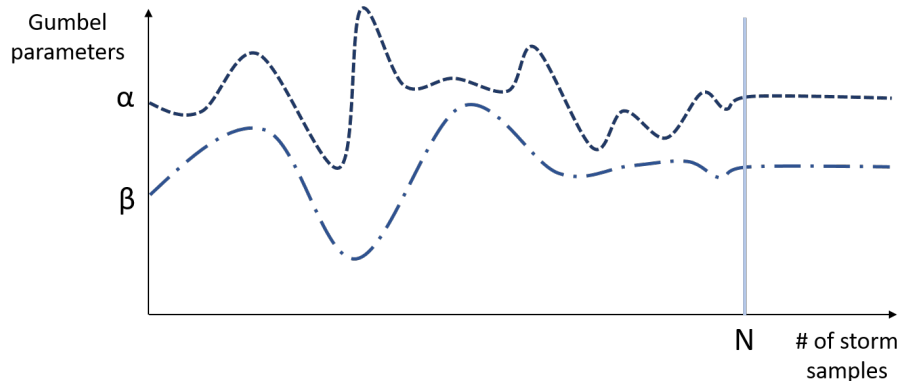
Figure 10.8: Convergence test of Gumbel parameters

In addition, the 90% quantile of the mooring line tension had to converge, since this was of particular interest for this simulation study. Equation 61 was applied to calculate the 90% quantile for each sea state, and plotted against N to ensure convergence of the extreme values.

The extreme value distribution of the mooring line tension was estimated by the *Two Sea States Approach* described in chapter 8, section 8.5.3. Simulations in 10 and 50 year environmental conditions were performed, and the maximum mooring line tension from each simulation was used to estimate the extreme value distribution for both sea states. This was done by estimating the Gumbel parameters according to equation 59 and 60, which is based

on the mean and standard deviation of the sample space. The Gumbel PDF and CDF for each sea state were then calculated from equation 57 and 58, respectively.

The 90% quantiles for each condition were extracted and used to estimate new Gumbel parameters from equation 69 and 70. The new Gumbel parameters were then used to fit an annual extreme value distribution of the mooring line tension based on only two known sea states.

For design purposes, the extreme values in the tail region of the distribution are of particular interest. The probability of exceedance for the tail region was plotted for a large tension range.

10.1.10   Partial Coefficient Method

The fitted Gumbel distribution obtained from the Two Sea States Approach was plotted together with distribution of strength of the component, to inspect the significance of the load and material factors in the partial coefficient method.

Characteristic strength was assumed equal to minimum breaking load of 68.2 ton. Due to lack of test data, the component strength was assumed to be normal distributed with mean and standard deviation corresponding to equation 3 and 4. Distribution of load and strength did not have similar PDF scales, but were plotted together for illustrative purposes.

Which load factor to apply in the partial coefficient method depends on the type of analysis conducted. Both dynamic and static analyses were carried out to inspect the effects of the selected type of analysis. The most unfavorable of the two load combinations were used as characteristic load for the dynamic approach, while for the static approach, the characteristic load was determined from analyses of 50 year current.

Also, whether analyses in regular wave conditions or irregular conditions are conducted is up to the certification company, and the same load factor is applied regardless of analysis procedure. Analyses in both conditions based on the procedures explained in NS9415 were conducted to compare the outcome of the two analyses. Characteristic load for both conditions was determined from the most unfavorable load combination.

10.2   Results

The results from this simulation study were used to inspect the long-term extreme tension in one windward mooring line. The following sections will present key results from the simulation study, including mooring line tension for all mooring lines, the static and dynamic effect on response, as well as regular and irregular effect on response. The simulation results were used to develop an extreme value distribution of mooring line tension, and the resulting load distribution is presented and compared to the distribution of strength for the mooring line at the end of the result section.

10.2.1   Environment

The environmental parameters used for the simulations were based on the site survey. In addition, data from an ocean buoy placed at Salatskjæra was used to inspect the environmental parameters on site more closely. Figure 10.9 show the relation between significant wave height, H_S, and peak period, T_p. The scatter diagram show that most waves were in the range of 0.3 to 1.0 meter with a period of 2.0 to 7.0 seconds.
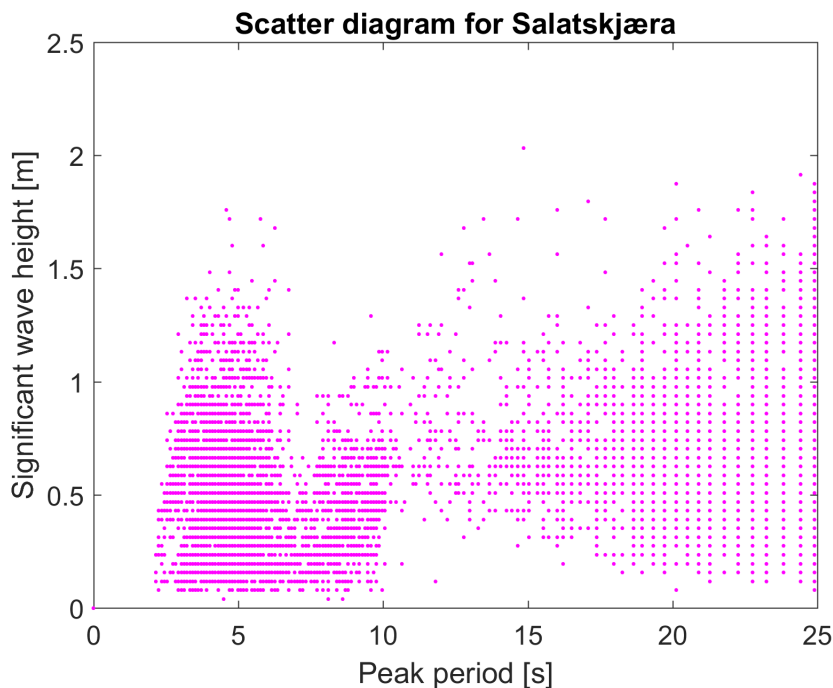
Figure 10.9: Scatter diagram for peak period and significant wave height

Figure 10.10 show a scatter diagram for current direction and wave direction. Current direction was measured at a depth of 4 meters, and presented in degrees *towards* inflow direction in the data set. Wave and wind direction, on the other hand, were presented by degrees at inflow direction. This means that waves from west equals 270 degrees, while current towards east equals 90 degrees in the data set. In figure 10.10, the current direction was fitted to the same direction description as the waves.
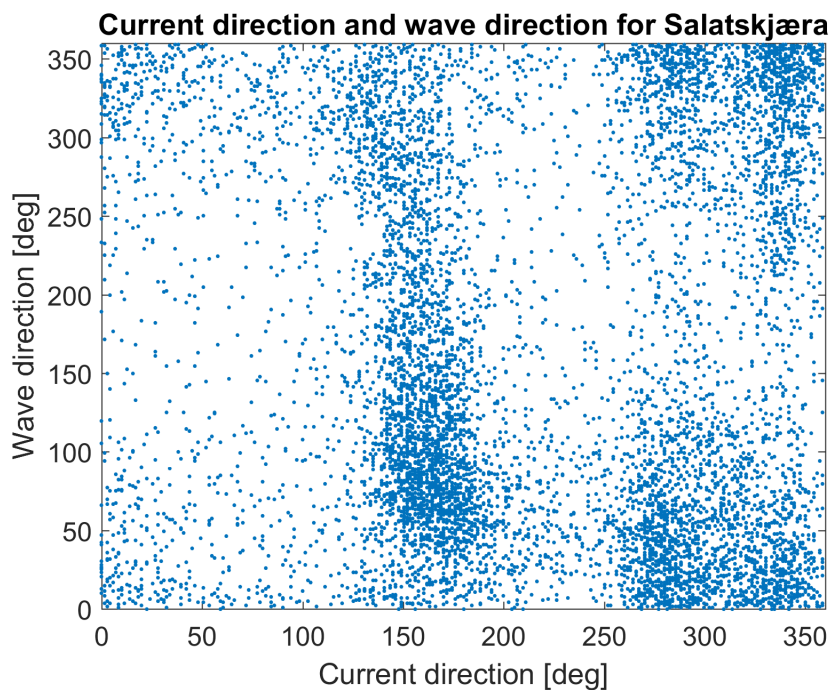
Figure 10.10: Inflow direction of waves and current

Figure 10.10 show some correlation between current and wave direction. Most of the sea states came with inflow angle around 180 degrees and 300 degrees, corresponding to east and north-west, respectively. The assumption of current and waves arising from the same direction for the simulations was therefore considered good enough.

To inspect whether the 10 and 50 year values from NCEP model data provided in the site survey were suitable for the Salatskjæra location, the significant wave height data from the ocean buoy was plotted in a Q-Q Weibull plot. The resulting plot is presented in figure 10.11. The linear trend line is indicated in red and the data from the ocean buoy seem to follow the Weibull distribution well for the upper region.
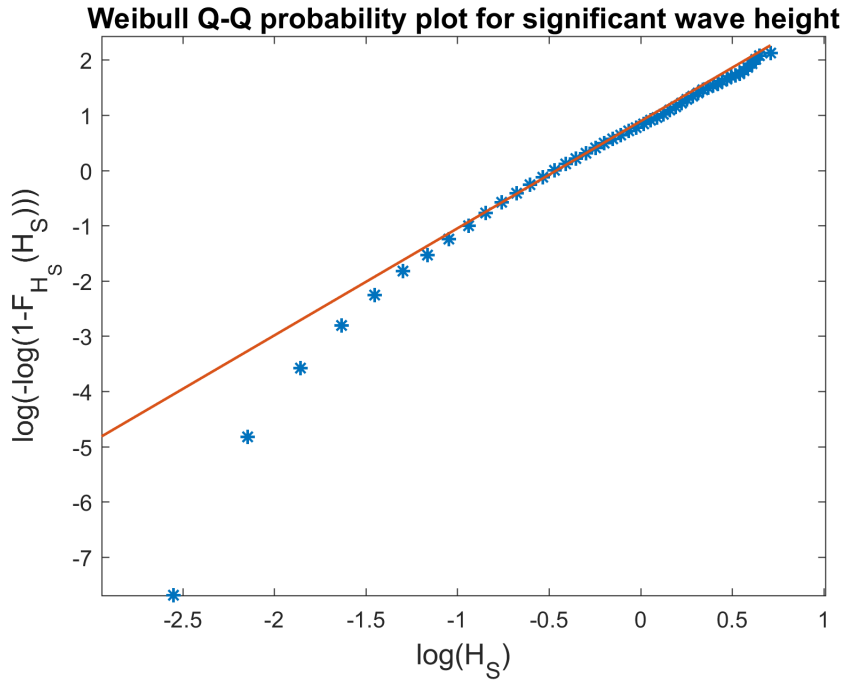
Figure 10.11: Weibull Q-Q probability plot of significant wave height

Figure 10.12 show an estimation of the upper tail region of the Weibull distribution, and this was used for prediction of 10 and 50 year values. The Weibull analysis gave 10 and 50 year significant wave height of $H_S^{10} = 2.217\ m$ and $H_S^{50} = 2.374\ m$, respectively.
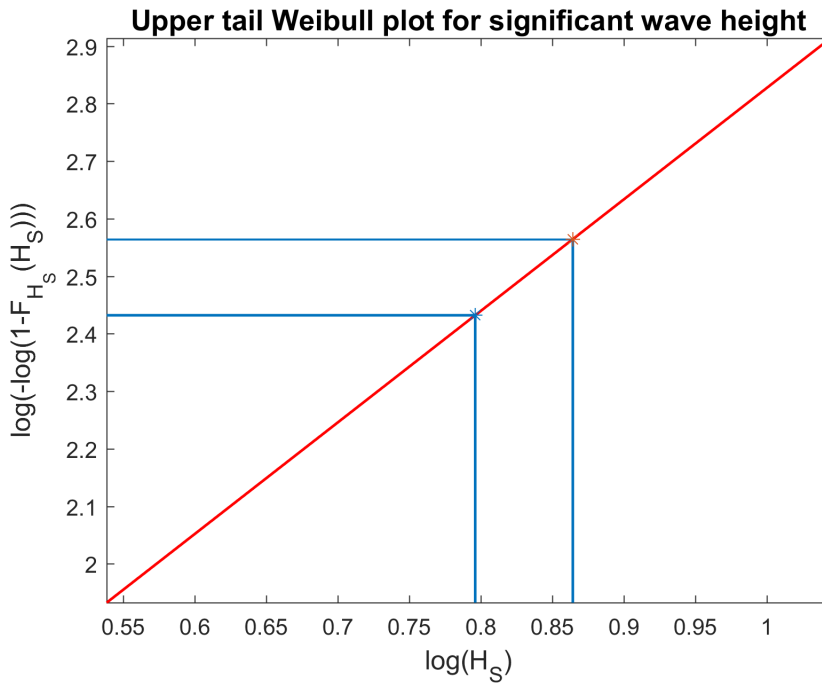
Figure 10.12: Upper tail Weibull fit

10.2.2 Pretension

Pretensioning of the system was performed by altering the weight of the mooring lines and position of the anchor. Due to lack of anchor chain, the weight of the mooring line was too low to contribute with significant geometrical stiffness. The system was therefore tightened by increasing line weight and by moving the anchors outwards. Figure 10.13 shows the result of pretensioning with two different placements of the anchors. An anchor distance of 355 meters was selected, and this gave pretension of about 55 kN, which is according to the industry's best practice.
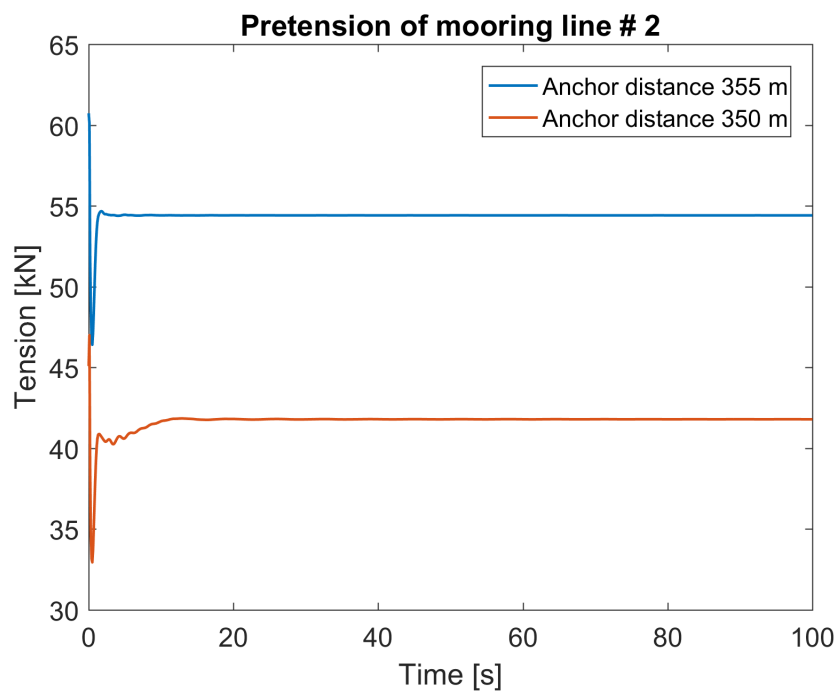
Figure 10.13: Pretension of mooring lines with different distance to anchors

10.2.3 Mooring Line Tension

The results from the simulations were used to plot time series of the mooring line tension. Tension in all 8 mooring lines due to response in 50 year irregular environmental conditions are shown in figure 10.14, and the tension in the windward and leeward mooring lines are outlined in figure 10.15.
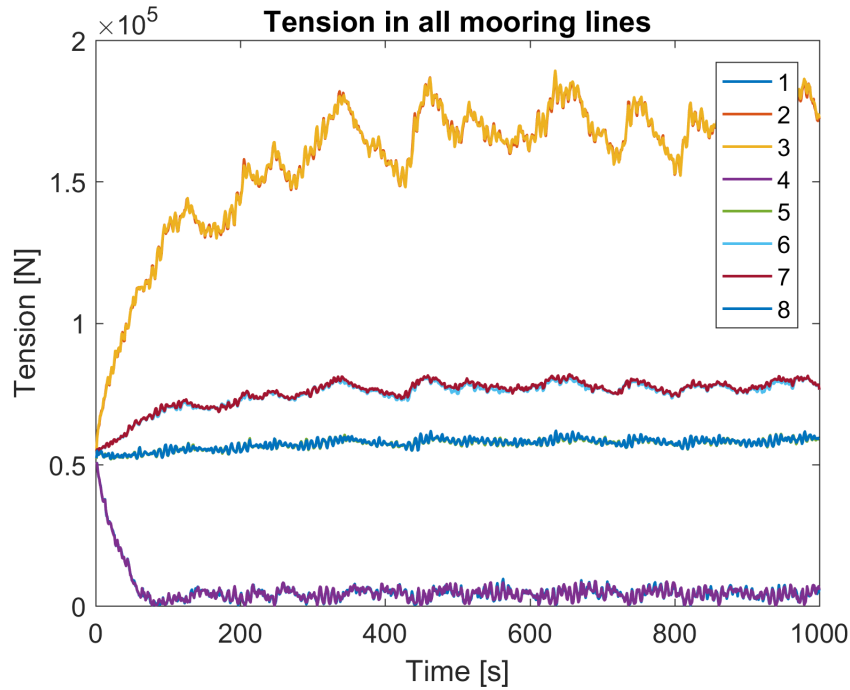
Figure 10.14: Tension in all eight mooring lines for one simulation
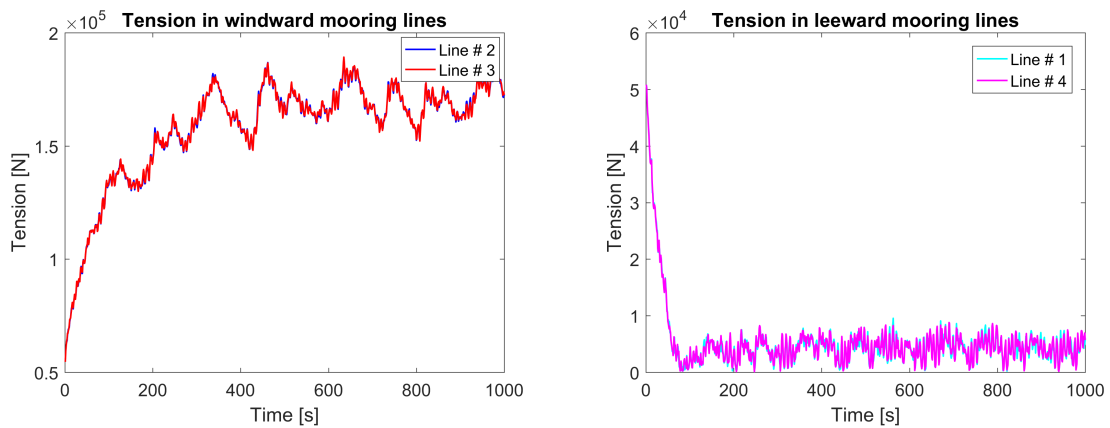
(a) Tension in windward mooring lines

(b) Tension in leeward mooring lines

Figure 10.15: Mooring line tension

Figure 10.14 show that mooring line number 2 and 3, which corresponds to the windward mooring lines in figure 10.15a, had the highest resulting tension. Mooring line number 2 was therefore chosen as reference for the extreme value study. The inspected line and element is highlighted in figure 10.16.
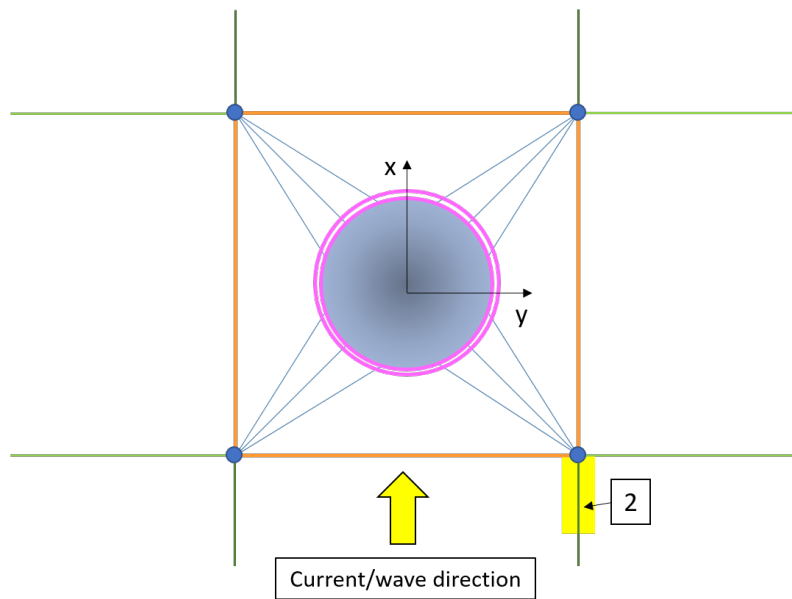
Figure 10.16: Reference mooring line

10.2.4   Response

Tension in mooring line number 2 for ten different seed numbers are shown in figure 10.17. All simulations show similar trends, without any outliers. The response converge around 300 seconds, and range from about 145 to 200 kN.
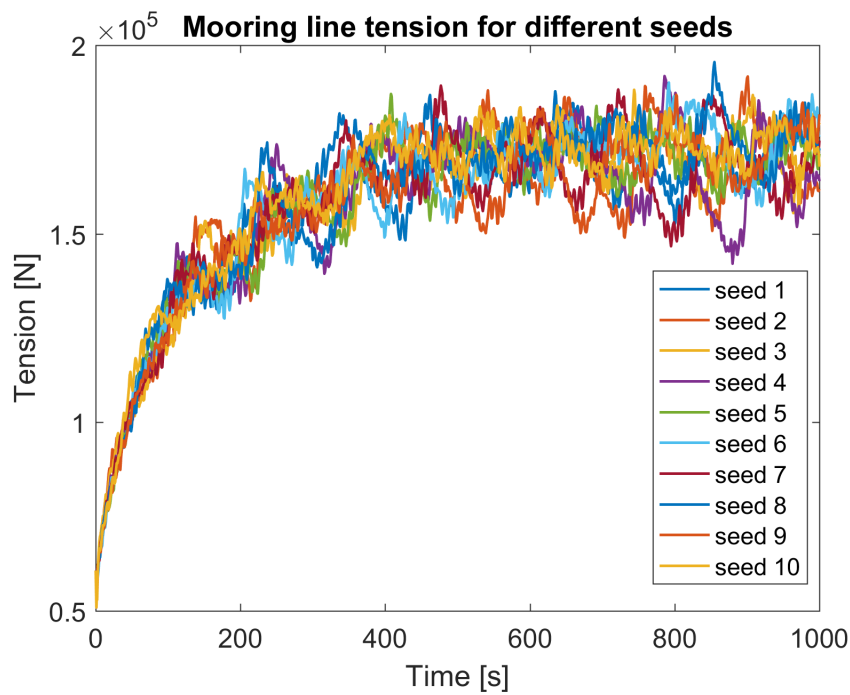
Figure 10.17: Tension in mooring line number 2 for ten different seed numbers

Figure 10.18 show the tension in mooring line number two after 300 seconds for one irregular simulation. The response oscillates around a mean tension of about 170 kN, as indicated on the figure, and seem to be influenced by both low-frequency motions and wave-frequency motions.
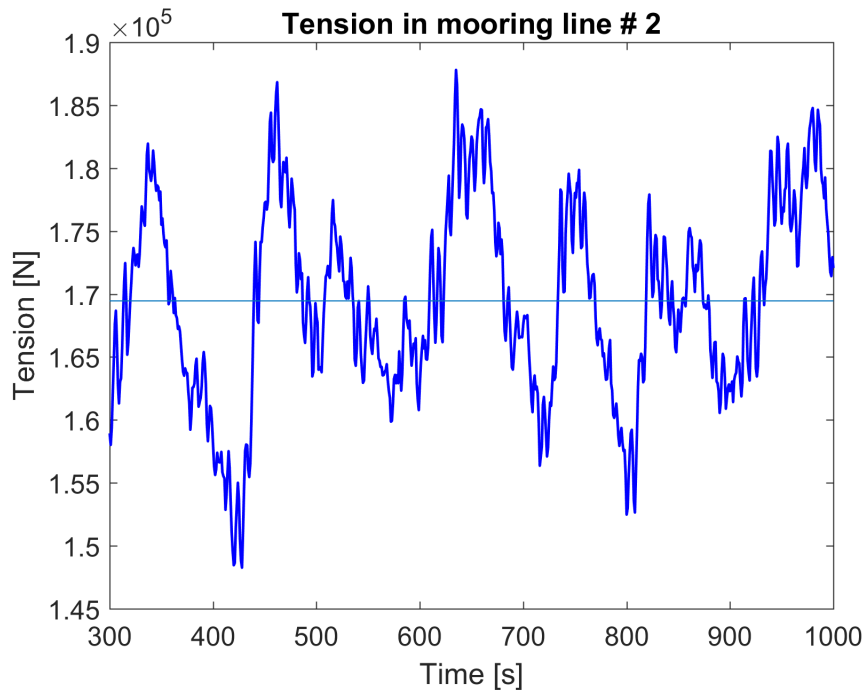
Figure 10.18: Tension in mooring line number 2 after 300 seconds

A response spectrum of the mooring line tension was established in frequency domain, and the result for combined waves and current in 50 year conditions, as well as 50 year waves only, is presented in figure 10.19. The response showed a peak near 0 rad/s, which represent the low-frequency motions, and a peak at 0.8 rad/s, which represent the wave-frequency motions.

The response in waves only was low compared to the combination of waves and current. The wave-frequency motions was relatively small and showed a peak at frequency 1.3 rad/s.
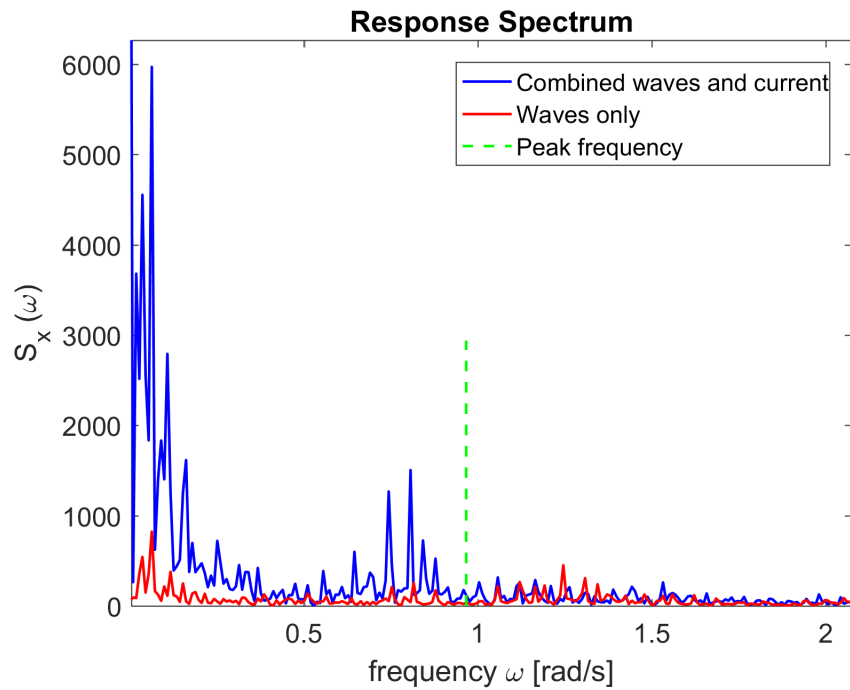
Figure 10.19: Response spectrum

10.2.5   Load Combinations

Results from irregular analyses of the two combinations is presented in figure 10.20.
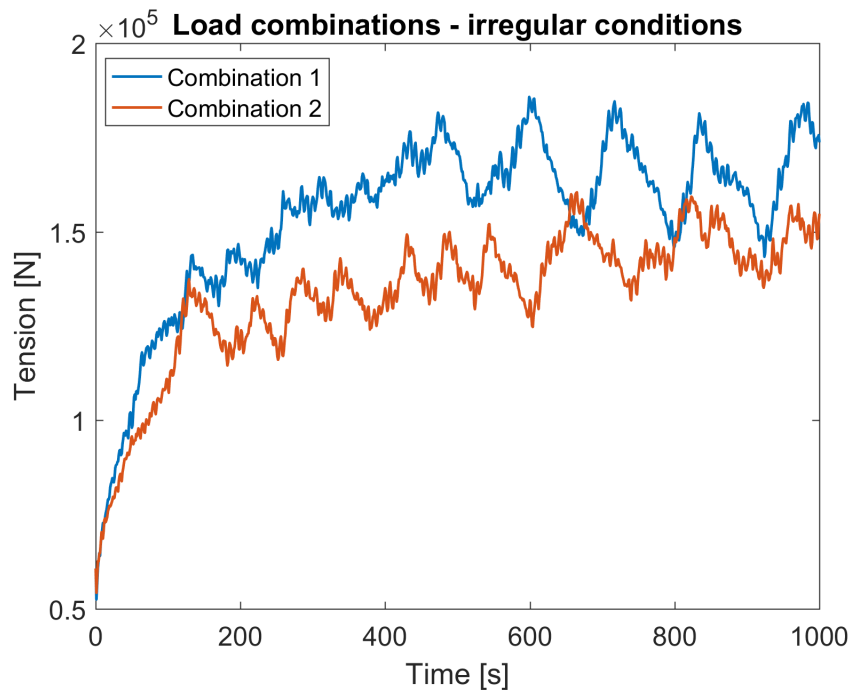
Figure 10.20: Resulting mooring line tension from the two load combinations

Load combination 1 with 50 year current and 10 year waves gave the highest response in the inspected mooring line, and characteristic load was set equal to the maximum response due to load combination 1; $S_C^{irreg} = 186\ kN$.

Also, regular analyses with design wave equal to $H_{max} = 1.9 \times H_S$, were conducted for the two different load combinations. Combination 2, with 10 year current and 50 year waves, gave the highest maximum response, equal to $S_C^{reg} = 495\ kN$

10.2.6   Static and Dynamic Response

The resulting mooring line response in static and dynamic conditions, as well as a combination of waves and current are shown in figure 10.21. Current only and waves only corresponds to 50 year environmental conditions, while the combination of waves and current corresponds to 50 year conditions for both current and waves.
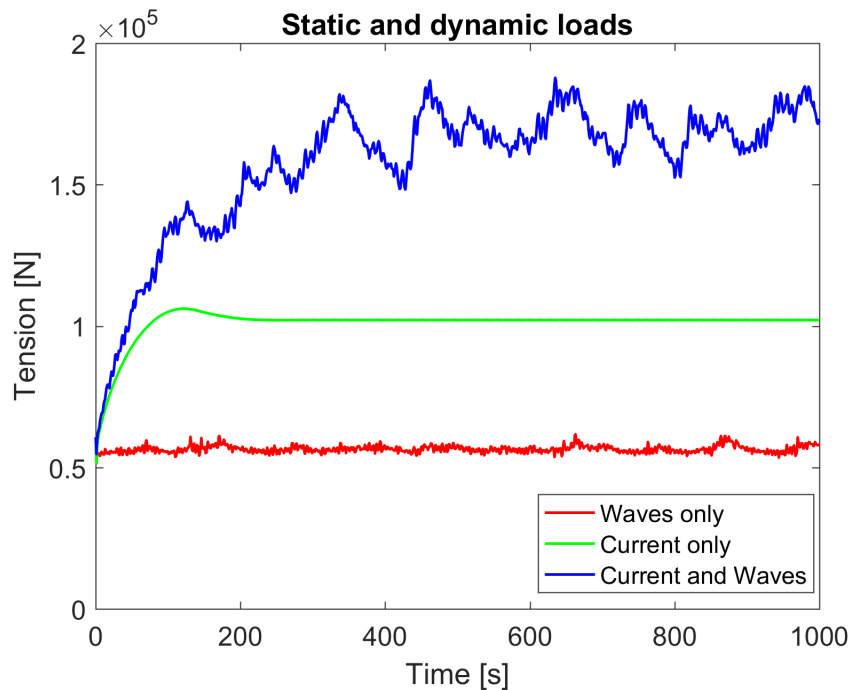
Figure 10.21: Static and dynamic response

Figure 10.22 show the response due to the combination of waves and current, together with summation of the response due to waves only and current only.
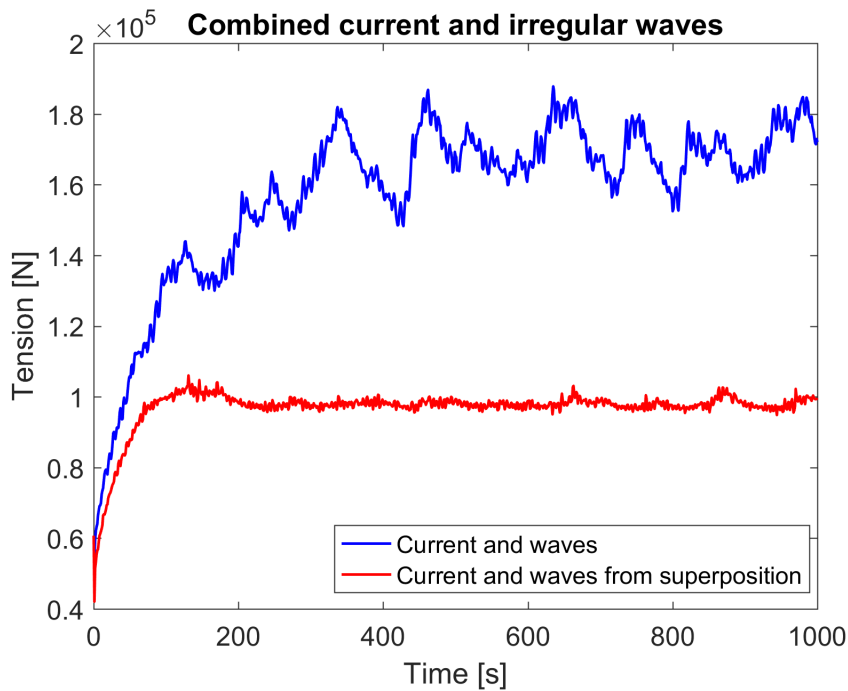
Figure 10.22: Combination of current and waves

The resulting characteristic load from static and dynamic simulations in the most unfavorable environmental conditions are presented in table 10.4. The dynamic characteristic load corresponds to load combination 1. Static characteristic load was determined from simulations of 50 year current velocity. Hand-calculations were performed to estimate the total drag force on the system due to static forces (current), and the procedure and results are included in appendix E.

Table 10.4: Characteristic load from static and dynamic analysis

Type of analysis	Characteristic load, S_C
Static - current only	1.0621×10^5 [N]
Dynamic - load combination 1	1.8578×10^5 [N]

10.2.7   Regular and Irregular Conditions

Figure 10.23 show the response in 50 year regular and irregular conditions, for a combination of waves and current. The regular simulations gave higher response in the inspected mooring line than the irregular environment, as expected. Regular conditions gave maximum tension of 250 kN, while this particular irregular environment gave maximum tension of 187 kN.
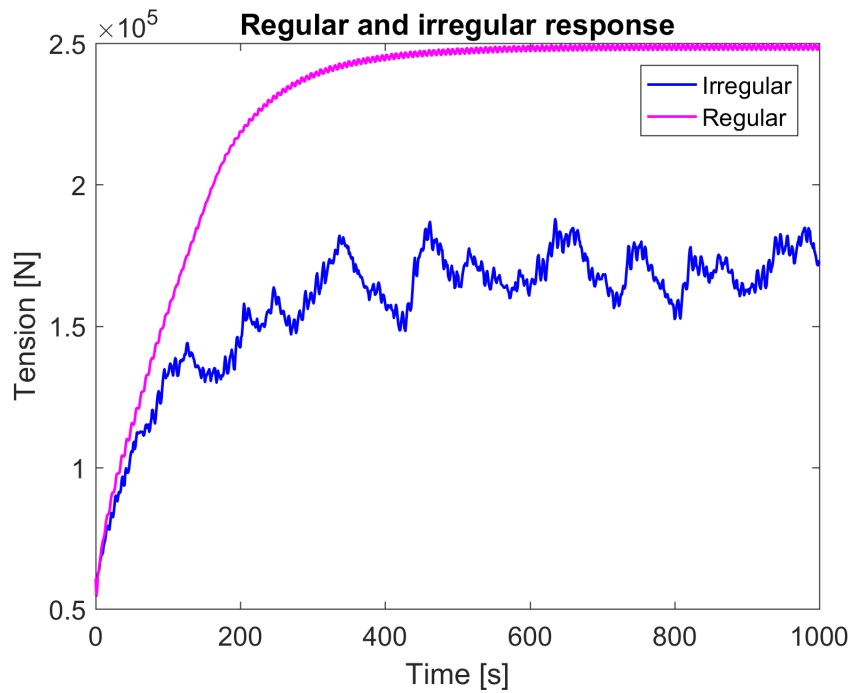
Figure 10.23: Response in regular and irregular conditions

Figure 10.24 show the converged response due to a combination of current and waves for regular and irregular conditions, plotted with the mean tension for both conditions.
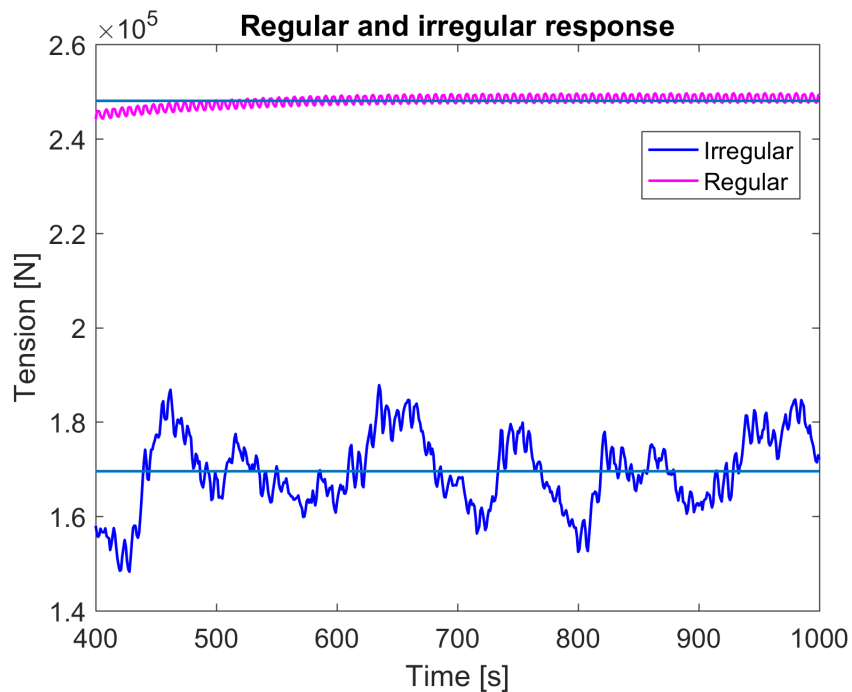
Figure 10.24: Converged response in regular and irregular conditions

The design wave method with $H_{max} = 1.9 \times H_S$ was applied to inspect the characteristic load, and this approach gave maximum mooring line tension of $495 \ kN$ for load combination 2. Characteristic load for irregular and regular environmental conditions from the most unfavorable load combination are summarized in table 10.5.

Table 10.5: Characteristic load from regular and irregular analysis

Type of analysis	Characteristic load, S_C
Irregular	1.8578×10^5 [N]
Regular - design wave	4.9458×10^5 [N]

10.2.8   Extreme Value Distribution

The maximum mooring line tension from all simulations was assumed to follow the Gumbel distribution. This was validated by plotting a Q-Q Weibull plot and inspect whether the data formed an approximate straight line. The resulting plots are shown in figure 10.25. The red line indicates the linear fit, and the stapled lines and intersection point indicate the 90% quantiles. The plots show good correlation with the Gumbel distribution.

(a) 10 year conditions

(b) 50 year conditions
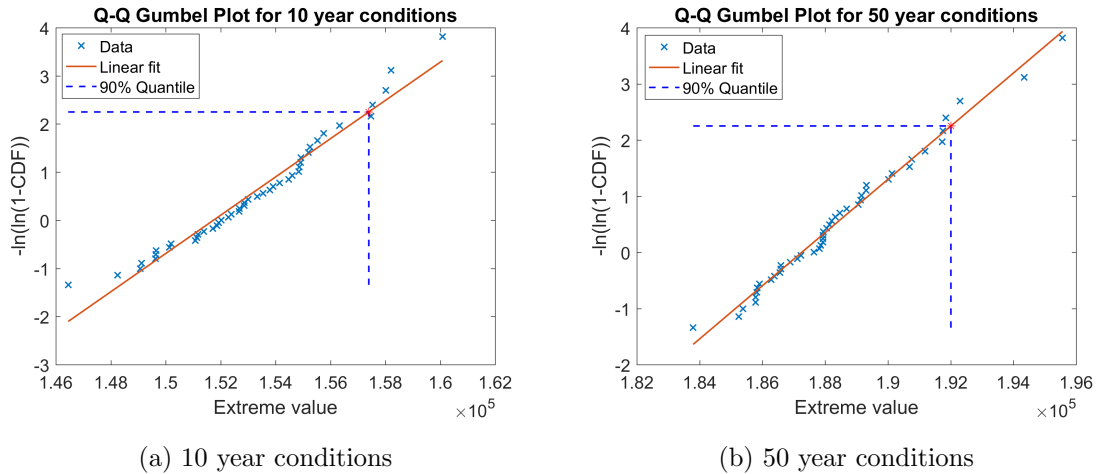
Figure 10.25: Q-Q Gumbel plots

To ensure that the sufficient number of storm samples needed to describe the extreme value distribution was included in the analyses, the Gumbel parameters, α and β, were plotted against number of storm samples, N. The result is shown in figure 10.26.
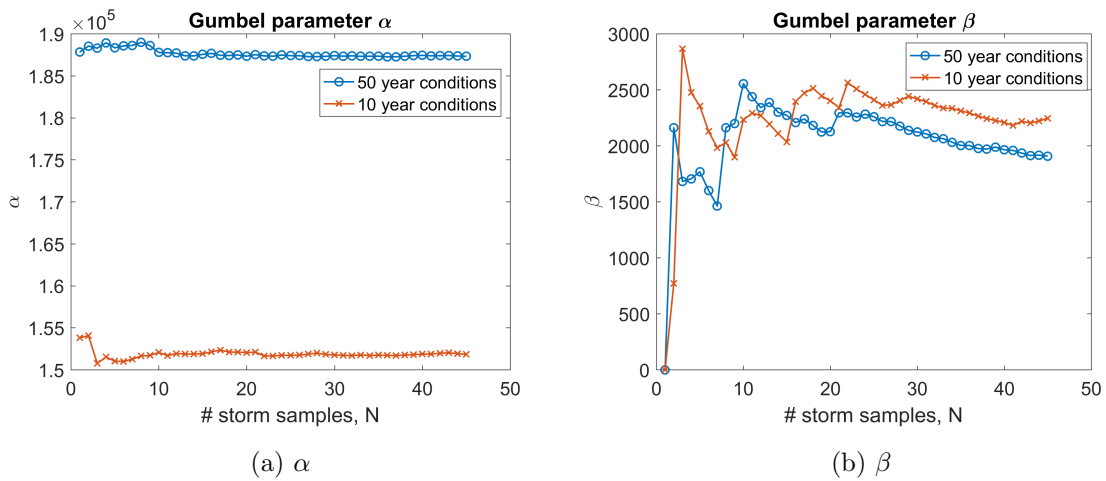
Figure 10.26: Convergence test of Gumbel parameters

Also, the 90% quantiles for 10 and 50 year environmental conditions were plotted against number of storm samples, N. The results are shown in figure 10.27. The calculated curve corresponds to the quantiles calculated from equation 61, while the fitted plot corresponds to the built-in function $evfit$ in MATLAB.
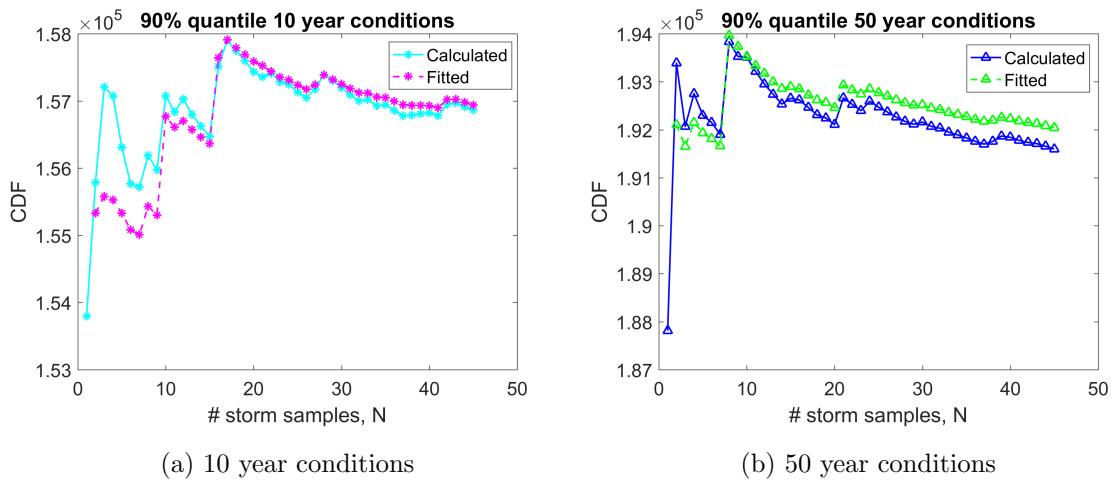
Figure 10.27: Convergence test of 90% quantile

The results of the convergence tests show that the scale parameter, β, which converge after about 25 simulation runs, turned out to be the critical factor. On the other hand, the 90% quantiles, shown in figure 10.27, converge very rapidly (notice the small scale on the y-axis). This was due to small variations in extreme response for each new seed number, which can be observed in figure 10.17. Since the extreme response was of particular interest for this purpose, 45 storm samples were considered sufficient to capture the maximum load effects.

10.2.9   Two Sea States Approach

For the Two Sea States Approach, 10 and 50 year environmental conditions were simulated for 45 different seed numbers to develop an extreme value distribution for each sea state. This resulted in Gumbel parameters and 90% quantiles (x_N) presented in table 10.6.

Table 10.6: Parameters for the 10 and 50 year Gumbel distributions

Parameter	10 year	50 year
α	1.4643×10^5	1.8104×10^5
β	2.1970×10^3	1.9045×10^3
x_N	1.5137×10^5	1.8533×10^5

The calculated Gumbel PDF and CDF are shown in figure 10.28 and 10.29, respectively. Also, the built-in function $evfit$ was applied in MATLAB to compare with the calculations. The 90% quantiles are indicated in both the PDF and CDF plots. The calculated PDF and CDF for 10 year conditions deviates from the fitted one's due to deviations in calculated and fitted β value.

(a) 10 year conditions

(b) 50 year conditions

Figure 10.28: Gumbel PDF

(a) 10 year conditions

(b) 50 year conditions
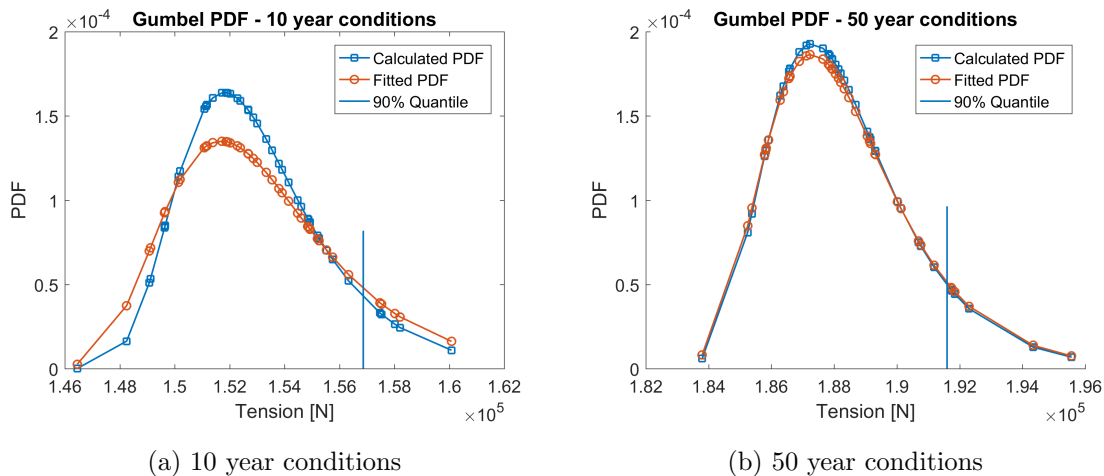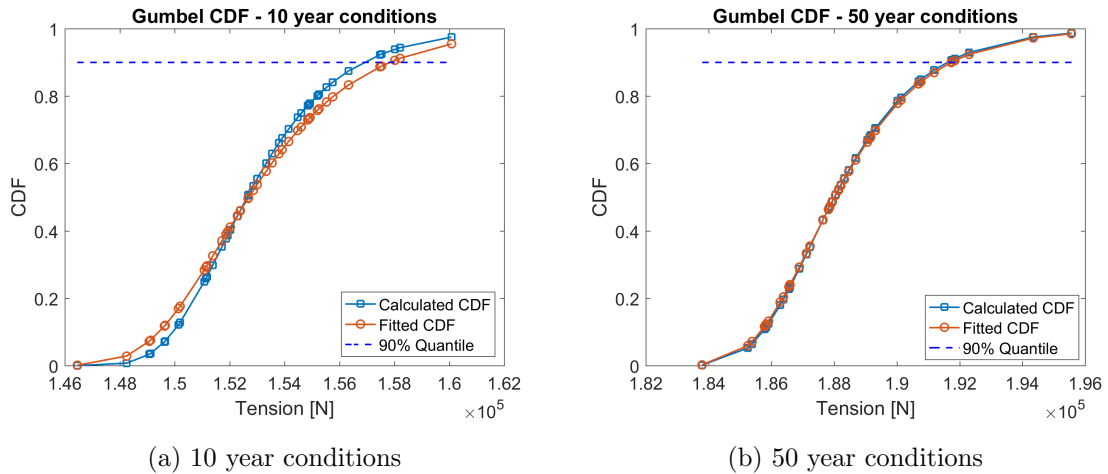
Figure 10.29: Gumbel CDF

The 90% quantile values x_{50} and x_{10} in table 10.6 were used to estimate the new Gumbel parameters. The resulting parameters are presented in table 10.7. The fitted Gumbel distribution of annual mooring line tension based on the estimated parameters are presented in figure 10.30.

Table 10.7: Gumbel parameters estimated from the Two Sea States Approach

Parameter	Value
α	1.0954×10^5 [N]
β	2.1029×10^4 [N]

(a) PDF

(b) CDF
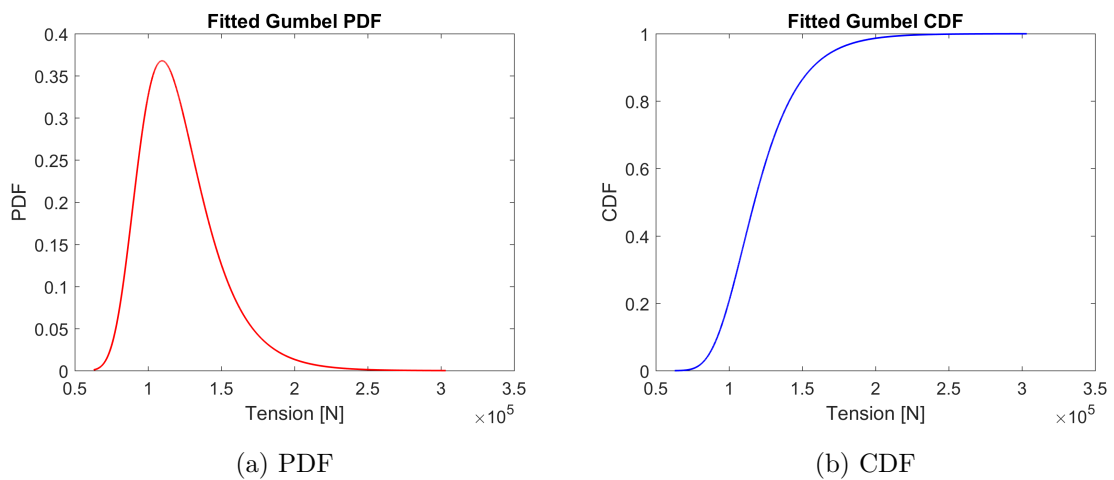
Figure 10.30: Fitted Gumbel distribution for annual response

For extreme response analyses, the tail of the Gumbel distribution is of particular interest. The probability of load exceedance for the tail region is presented in figure 10.31.
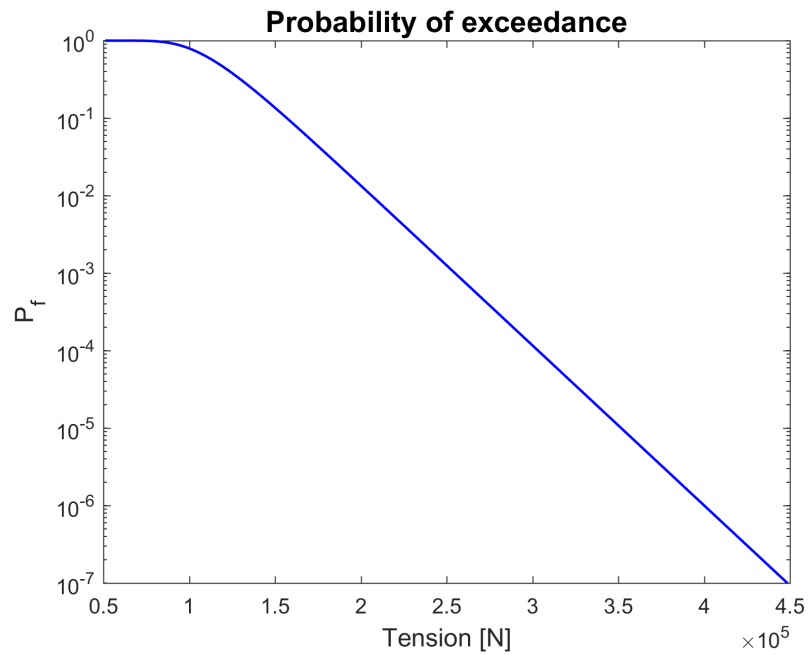
Figure 10.31: Probability of load exceedance

10.2.10   Partial Coefficient Method

Figure 10.32 show distribution of load for the mooring line tension with characteristic load and design load. Characteristic load from load combination 1 in irregular conditions and the design load, $S_D = S_C \times \gamma_f$, are indicated on the figure.
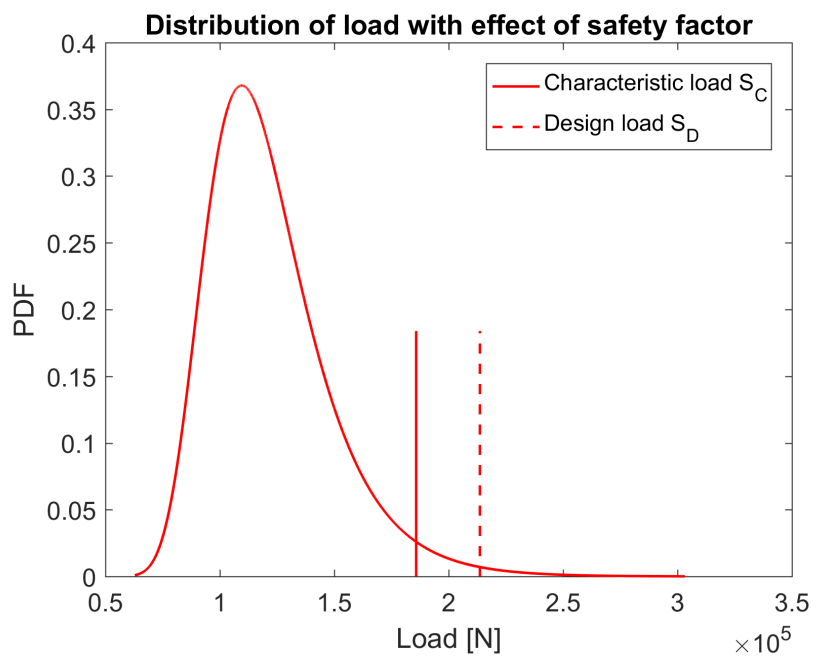
Figure 10.32: Distribution of load with characteristic load and design load

Figure 10.33 show distribution of strength with assumed mean value, $\mu = 70.2\ kN$ and standard deviation, $\sigma_x = 21.1\ kN$. Characteristic strength, R_C, and design strength equal to $R_D = \frac{R_C}{\gamma_m}$ are indicated on the figure.
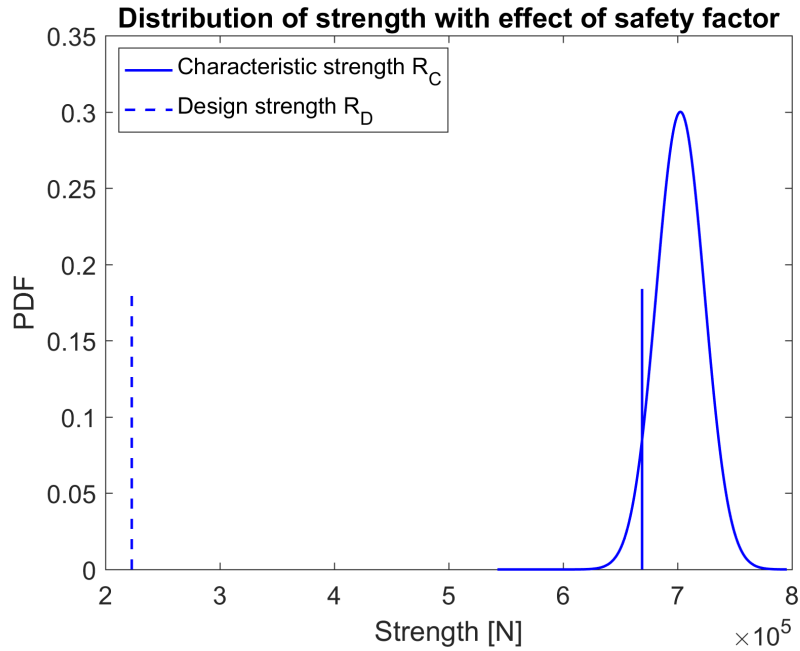
Figure 10.33: Distribution of strength with characteristic strength and design strength

Figure 10.34 show distribution of load and strength, together with characteristic and design values.
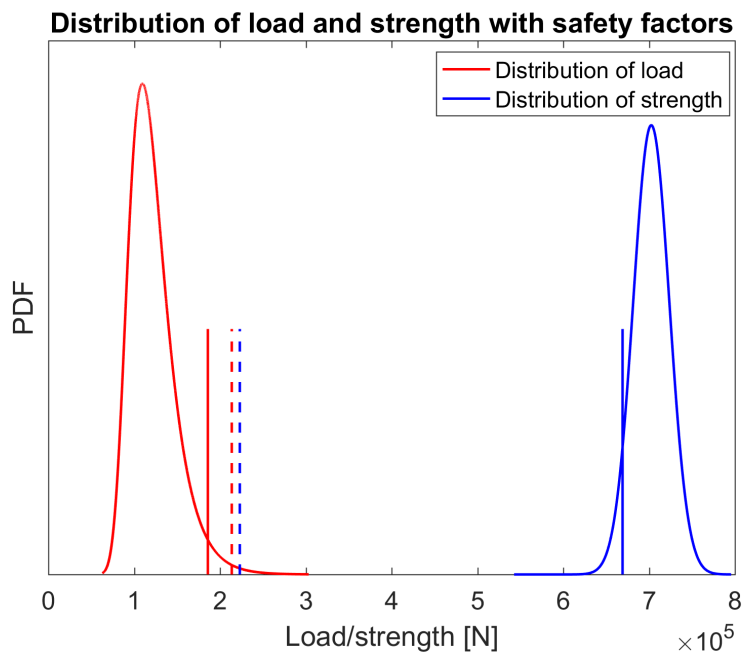
Figure 10.34: Load and strength distributions with effect of load factors

The two distributions did not have similar PDF scale, but was plotted together for illustrative purposes. The red solid line represents the characteristic load and the dashed red line corresponds to the design load after application of the load factor. The solid blue line represent the breaking strength of the mooring line, while the dashed blue line corresponds to the design strength after application of the material factor.

10.3   Discussion

The following sections will include a general discussion of the results obtained in this simulation study. The simulation study is only considered valid for the specific sea states inspected, and the specific simulation model, and the discussion is based on this particular study.

10.3.1   Extreme Sea States

The extreme value distribution obtained by the *Two Sea States Approach* was based on simulations in 10 and 50 year environmental conditions obtained from the site survey conducted by Havbrukstjenesten. 10 and 50 year current provided in the site survey were obtained from measurements at the actual location, where current velocity were measured from December 5th to January 21st for 5 meter depth, and from July 25th to September 3rd for 15 meter depth. The 10 and 50 year dimensioning current were then determined by the multiplication factors presented in table 5.4. Significant wave height and peak period were obtained from calculations based on effective fetch length and model data from NCEP.

In addition to the site survey, data from the SINTEF ocean buoy on the fish farm location was used to inspect the environmental conditions more closely. The data set contained measurements from March 9th 2016, to March 12th 2017, and logging took place every hour. The maximum measured values from the ocean buoy are summarized in table 10.8.

Table 10.8: Maximum measured parameters at Salatskjæra

Parameter	Extreme value	Unit
Current velocity	58.5938	cm/s
Significant wave height	2.0313	m
Maximum wave height	2.9688	m
Peak period	24.9023	s

Maximum current velocity from these measurements would result in 10 and 50 year values of 97 *cm/s* and 108 *cm/s* by multiplication with the factors in table 5.4. This gave higher dimensioning current velocity than the extreme values determined in the site survey. Maximum current velocity was measured in January, which was also used as measurement month for 5 meter depth in the site survey. On the other hand, for 15 meter depth, measurements were conducted during July to September, which had lower current velocity than in January. The standard does not specify which month to use for measurements, which implies that variations of dimensioning current can be significant due to selection of measurement month.

Dimensioning wave height in the site survey was determined from calculations based on effective fetch length in combination with Weibull analyses of NCEP model data. A similar Weibull analysis of the significant wave height data provided from the ocean buoy was conducted in this report to compare the 10 and 50 year values from the measured data set with those in the site survey. The resulting Weibull analysis presented in figure 10.12 showed estimated 10 and 50 year significant wave height of 2.217 m and 2.373 m, which is significantly lower than the modelled values of 3.3 m and 3.5 m, respectively. This indicates that estimation of dimensioning wave height from the calculations and NCEP model data were more conservative than measurements at the actual location with corresponding long-term statistical analysis.

The values from the site survey and those determined from the ocean buoy are summarized in table 10.9.

Table 10.9: Comparison of extreme environmental parameters

Parameter	Site survey	Ocean buoy
10 year current velocity	82 [cm/s]	97 [cm/s]
50 year current velocity	91 [cm/s]	108 [cm/s]
10 year significant wave height	3.3 [m]	2.217 [m]
50 year significant wave height	3.5 [m]	2.373 [m]

10.3.2   Interaction Between Current and Waves

The interaction between current and waves were inspected in both irregular and regular conditions. Figure 10.21 show that the dynamic contribution from irregular waves was small compared to the static contribution from current, but the dynamic effects increased for the case of combined current and waves. The wave loads oscillate around a mean tension of 56 kN, which is only slightly higher than the pretension, while the mean tension due to current loads was about 100 kN. Current loads are dominating due to the large submerged area of the net, and the resulting drag loads acting on the net due to current were larger than the wave loads on the floater and the upper parts of the net.

By comparing the tension in the mooring line due to combined current and waves, and the summation of current and waves in figure 10.22, non-linear effects were observed. This non-linearity indicates that linear theory is not applicable for this particular study, and the superposition principle is not valid. The non-linear increase in response for combined current and waves corresponds to the effects of viscous drift, as illustrated in figure 10.35.
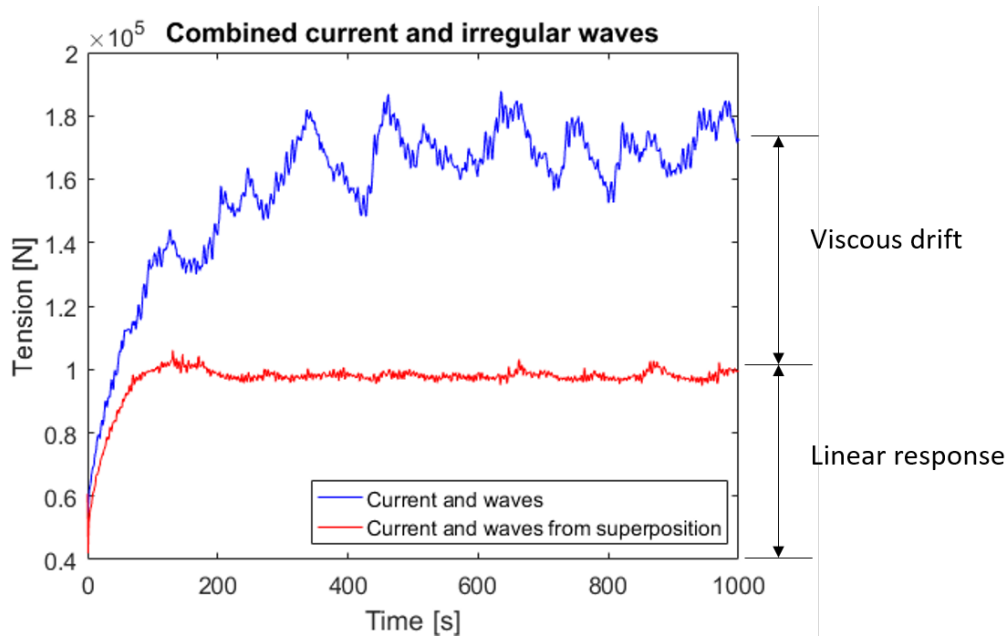
Figure 10.35: Irregular analysis - effect of viscous drift

Figure 10.24 show that the regular simulations do not capture the slowly-varying motions, only wave-frequency motions. Slowly-varying motions only occur for irregular wave conditions, since at least two waves with different frequency and amplitude are essential to get the effect. As seen in the response spectrum for irregular analyses in figure 10.19, low-frequency motions corresponds to the governing part of the response, while the wave-frequency motions have much lower effects on the mooring line tension. Also, the response was much higher for the combination of waves and current, than for waves only, which indicates the importance of viscous drift effects.

The mean drift force observed in figure 10.35, as well as the slowly-varying motions mentioned above, arise from the relative velocity term in Morison's equation, which represent the relative velocity between the fluid and the structure. For the simulation study, the relative velocity could not be determined, due to lack of information about structure velocity, V_S, in FhSim. By assuming $V_S = 0$, the relative velocity ranged between -0.73 m/s and 2.56 m/s for regular waves, which directly affect the drag loads calculated from Morison's equation.

In section 6.4.2, non-linear variations in submerged floater area was introduced as an effect that can cause viscous drift. The floater model in FhSim does not account for non-linear free-surface effects, and changing relative velocity was thus the only identified reason for second-order effects in this simulation study.

10.3.3   Static and Dynamic Response

The load factor applied in the partial coefficient method is dependent on whether static or dynamic analyses are conducted, and the effect of choice of analysis was inspected by comparing the design load, S_D, from the two approaches. Maximum dynamic response from the most unfavorable combination of irregular waves and current, as well as static response from 50 year current only, were multiplied with the appropriate load factor. The results are presented in table 10.10.

Table 10.10: Static and dynamic analysis

Type of analysis	Characteristic load S_C	Load factor γ_f	Design load $S_D = S_C \times \gamma_f$
Static	1.0621×10^5 [N]	1.6	1.6994×10^5 [N]
Dynamic	1.8578×10^5 [N]	1.15	2.1365×10^5 [N]

The analyses showed that the design load from the dynamic analysis was more than 25% higher than the resulting design load from the static analysis.

The standard does not specify which loads to include in a static (or dynamic) analysis. Here, it was assumed that static analyses includes sea loads due to current only, but the combination of current loads and mean loads from regular waves can also be considered a static force. This will increase the static response significantly, and thus the static analyses will be more conservative than dynamic analyses. Expectations regarding what to include in the different analysis options should be made clearer in the technical standard.

10.3.4   Regular and Irregular Response

Simulations in regular and irregular environments gave significant deviations in estimation of characteristic loads. According to NS9415, regular analyses are conducted by the design wave method, where $H_{max} = 1.9 \times H_S$, while irregular analyses are conducted by applying a JONSWAP spectrum with $H_{max} = H_S$. Table 10.11 show resulting design load from simulations of the most unfavorable load combination in regular and irregular environments, respectively.

Table 10.11: Regular and irregular analysis

Type of analysis	Characteristic load	Load factor	Design load
	S_C	γ_f	$S_D = S_C \times \gamma_f$
Regular - design wave	4.9458×10^5 [N]	1.15	5.6877×10^5 [N]
Irregular	1.8578×10^5 [N]	1.15	2.1365×10^5 [N]

The resulting design load in regular waves were more than 60% higher than the design load in irregular waves, which implies that regular wave analyses are very conservative.

For the regular simulation study, the period was set equal to peak period, T_p, as specified in NS9415. The standard does not specify any criteria in terms of wave steepness, which is the ratio between wave height, H_S, and wave length, λ. Maximum steepness of a regular wave is given by (Pettersen, 2007):

$$\frac{H_S}{\lambda} = \frac{1}{7} \tag{72}$$

or

$$H_S \leq \frac{g}{7 \times 2\pi} \, T_p^2 \tag{73}$$

It is important to satisfy equation 73 to simulate realistic conditions, and this should be specified in NS9415. For the regular simulation study presented here, load combination 2 with $T_p = 6.5 \ s$, gave maximum significant wave height of 9.4 m according to equation 73. This was in compliance with the criteria for wave steepness, and the simulated wave could thus be considered realistic.

Also, NS9415 does not specify the required duration of the simulations. The design wave method is based on assuming that the most probable largest wave amplitude is equal to (Larsen, 2014):

$$\zeta_{max,N} = \sigma_x \sqrt{2 \ln N} \tag{74}$$

where N equals number of sea states, and can be calculated from:

$$N = \frac{T}{T_z} \tag{75}$$

T equals duration of the sea state, and T_Z equals zero-upcrossing period. By assuming 3 hour sea states, equation 74 can be simplified to:

$$\zeta_{max,N} \approx 3.8 \times \sigma_x \tag{76}$$

and by introducing

$$\sigma_x = \frac{H_S}{4} \tag{77}$$

equation 76 becomes

$$\zeta_{max,N} = 3.8 \times \frac{H_S}{4} = 0.95 \times H_S \tag{78}$$

This gives maximum wave height of

$$H_{max} = 2 \times \zeta_{max,N} = 1.9 \times H_S, \tag{79}$$

which equals the design wave approach. This shows that the design wave approach is based on assuming that sea states have duration of 3 hours, which means that simulation length should also have a duration of 3 hours for the design wave approach to be accurate.

The length of the time series in this simulation study was restricted to 1000 seconds, due to very time-consuming simulations. To ensure an accurate piecewise stationary short-term description of the environment, the duration of the simulations should be extended to at least 20 minutes, and preferably 3 hours.

10.3.5 Extreme Value Distribution

The fitted extreme value distribution was based on 45 simulation runs of 10 and 50 year environmental conditions. Extreme values for each simulation run turned out to be very similar, and number of simulation runs were considered sufficient for this purpose. The sea loads were assumed to arise from the same direction, and from the most unfavorable direction with respect to mooring line tension. This would overpredict the response to some extent, and the extreme value distribution would thus be conservative.

The fitted extreme value distribution presented in figure 10.30 is valid for the specific mooring line and the specific simulation model, and based on 10 and 50 year environmental conditions from the site survey. To get a more accurate extreme value distribution of the mooring line tension, the All Sea States Approach presented in section 8.5.3 should be conducted for a wide range of significant wave height and peak period values.

However, the extreme value distribution obtained by simulation of two sea states gave an indication of the variability in mooring line tension. This variability is not captured in regular wave analyses, which is the standard approach conducted in the industry today. The industry should consider including irregular analyses in their design approach, to be able to capture load effects in realistic conditions.

10.3.6 Partial Coefficient Method

The partial coefficient method incorporates safety factors in the calculations to ensure that the structure meets the design requirements that are necessary to avoid technical failure. The method is based on requiring that the characteristic load, S_C, multiplied with some

load factor γ_f, must be less than or equal to the characteristic strength of the component, R_C, divided by some material factor γ_m.

Characteristic Load

The standard presents different methods for determining characteristic load, S_C, and in the simulation study this was done by three different approaches:

1. Static analysis in current only with load factor $\gamma_f = 1.6$

2. Dynamic analysis in irregular waves with load factor $\gamma_f = 1.15$ and $H_{max} = H_S$

3. Dynamic analysis in regular waves with load factor $\gamma_f = 1.15$ and $H_{max} = 1.9 \times H_S$

The result from each approach is summarized in table 10.12.

Table 10.12: Comparison of characteristic load by different design approaches

Type of analysis	Characteristic load S_C	Load factor γ_f	Design load $S_D = S_C \times \gamma_f$
Static - current only	1.0621×10^5 [N]	1.6	1.6994×10^5 [N]
Irregular	1.8578×10^5 [N]	1.15	2.1365×10^5 [N]
Regular - design wave	4.9458×10^5 [N]	1.15	5.6877×10^5 [N]

As seen from the resulting characteristic loads, choice of analysis highly affects the dimensioning load that the component must be able to withstand. Regular analyses with the design wave approach gave design load of more than three times the design load resulting from static analysis, and more than twice the design load from irregular analyses. In theory, the three methods for estimating design load should give similar results, and preferably equal. The differences in characteristic load arising from the different methods should be inherent in the load factor when determining design load.

NS9415 states that *"the characteristic values shall be determined as loads which the marine fish farm with a defined probability will not exceed during its design working life"*. The probability level is not specified in the standard, and probability of load exceedance will vary significantly for each of the analysis approaches presented above.

Characteristic Strength

The characteristic strength of the mooring lines was assumed equal to a minimum breaking load of 68.2 *tonnes*. This MBL value corresponds to standard 8-braided Aqualine rope with diameter 64 *mm*, while the mooring lines in the simulation model had diameter of 50 *mm*. Also, the weight in water was higher for the modelled lines than the standard mooring lines.

This would affect both the response of the structure and the minimum breaking load, but these assumptions were made to be able to compare the distribution of load with strength.

Similarly as for characteristic load, NS9415 states that *"The characteristic capacity for resistance shall be based on a defined probability that they will not be underreached during the dimensioned useful life of the fish farm"*. The requirements for probability level is not specified for characteristic strength.

Design Load and Strength

Figure 10.36 show the distribution of load and strength, design strength (blue dashed line), as well as design load from the three approaches presented above. The red dashed line represents the irregular environment, the pink dashed line represents the static load, while the green dashed line represents the regular design wave approach.
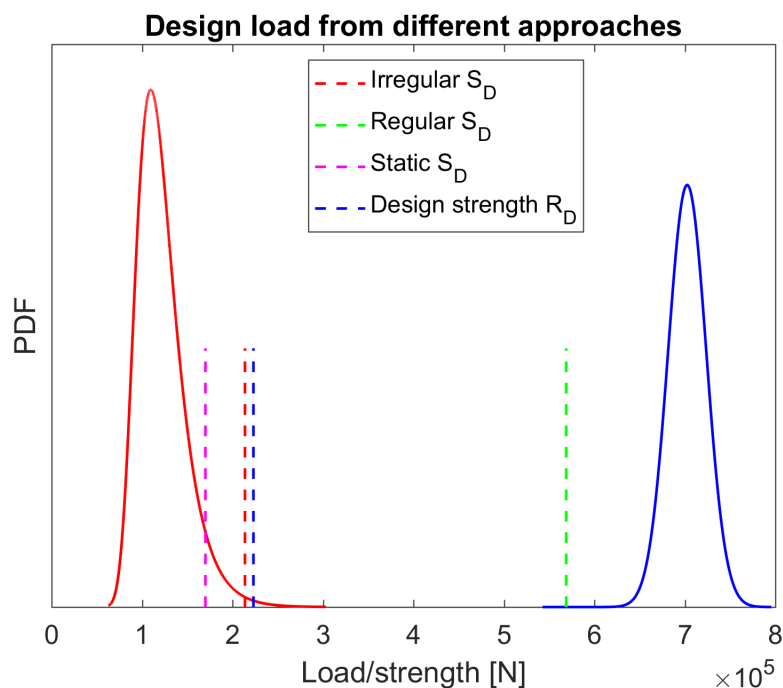
Figure 10.36: Comparison of design load in the partial coefficient method

The two distribution curves does not overlap at all, which indicates that the probability of failure, $P(S > R)$, is extremely small. Also, it can be seen that the design strength is very far out in the tail of the strength distribution. This indicates a large safety level. Design strength was determined by dividing the minimum breaking load by the material factor for synthetic rope, $\gamma_m = 3.0$. This resulted in design strength, R_D of 223 kN, which corresponds to 22.7 *tonnes*.

The design loads from the three approaches vary significantly. The load distribution is valid for the inspected irregular sea state, but could be compared to design load from both regular and static simulations for illustrative purposes. The regular design load is located far out in the tail of the load distribution, while the static design load is lower than the 90% quantile of the distribution.

Figure 10.37 illustrates how probability of load exceedance can be determined from the partial coefficient method. Load factor, γ_f is applied to characteristic load, S_C, to determine the design load, S_D. The Pf curve represents the load distribution based on simulations in irregular environmental conditions.
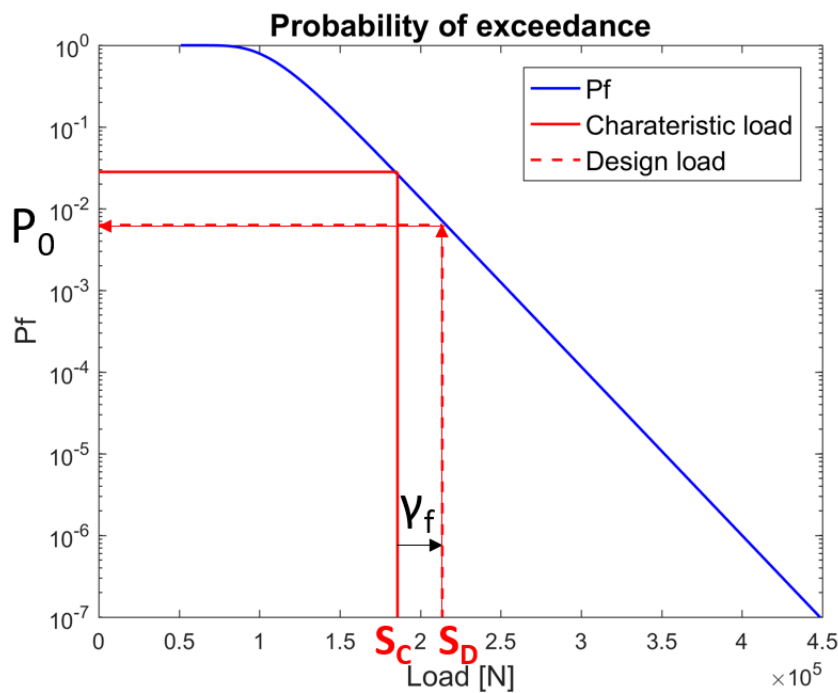
Figure 10.37: Concept for determining probability of exceedance

According to calculations in irregular conditions, design load of 214 kN gave corresponding probability of load exceedance, indicated as P_0 at the figure, of about $10^{-2.3}$. This corresponds to less often than once per 100 year.

Figure 10.38 show probability of exceedance for design load from irregular, regular and static analyses.
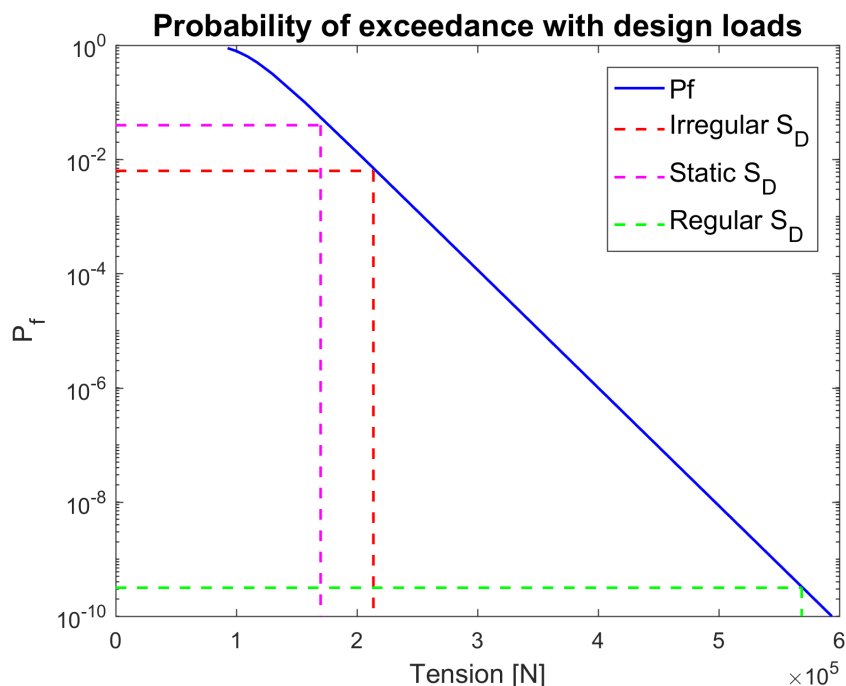
Figure 10.38: Probability of exceedance for the three design approaches

Static analyses indicates probability of exceeding the design load of about $10^{-1.5}$, which corresponds to once every 50 year. Regular analyses, on the other hand, indicates probability of exceeding the design load of $10^{-9.5}$, which can be considered as extremely low.

10.3.7   Calibration of Safety Factors

The safety factors in NS9415 is based on *Eurocode: Basis for Structural Design, NS-EN 1990*, which is valid for loads on structures. In general, safety factors are calibrated based on requirements for defined probability of failure. This defined probability must be seen in accordance with risk evaluation, as well as intended lifetime of the structure. An aquaculture installation has expected lifetime of about 20 years with the correct maintenance and service, and the safety level of design loads and strength should be seen in regard to this. In the oil and gas industry the defined probability level is set equal to 10^{-4}, which corresponds to acceptable failure once every 10 000 year.

The desired probability level should be inherent in the safety factors, and dimensioning load should be in the same range regardless of analysis approach. The partial coefficient method can be rewritten as:

$$R_C \geq S_C \times \gamma_f \times \gamma_m \tag{80}$$

For static conditions, with load factor $\gamma_f = 1.6$ and material factor $\gamma_m = 3.0$, this gives:

$$R_C^{stat} \geq S_C^{stat} \times 1.6 \times 3.0 = S_C^{stat} \times 4.80 \tag{81}$$

And similarly, for dynamic conditions, with load factor $\gamma_f = 1.15$ and material factor $\gamma_m = 3.0$:

$$R_C^{dyn} \geq S_C^{dyn} \times 1.15 \times 3.0 = S_C^{dyn} \times 3.45 \tag{82}$$

If the load factors were calibrated correctly, the ratio between static and dynamic loads should be equal to

$$\frac{S_C^{dyn}}{S_C^{stat}} = \frac{4.80}{3.45} \approx 1.39 \tag{83}$$

Simulations in irregular conditions and static simulations with current only gave ratio of 1.75, which is in the same range as the requirement in equation 83. However, simulations in regular conditions gave ratio of 4.66, which is far from the theoretical ratio. This implies that the load factor, γ_f, should be adjusted for simulations in regular conditions. The design wave approach overpredicts the loads, and by applying the dynamic load factor, the loads are additionally overpredicted.

The material factor, γ_m should reflect the uncertainties in component strength. In the standard design approach used in the industry today, the characteristic strength is set equal to minimum breaking load, which represents the 90% quantile of the strength distribution. This means that a safety level is already included in the choice of characteristic strength, before application of the material factor. As seen in figure 10.33, the design strength is situated far out in the tail of the strength distribution, which implies a very conservative safety level.

11   Conclusion

This chapter will summarize and conclude the results of the simulation study. Recommendations for further work is presented at the end.

11.1   Concluding Remarks

Dimensioning of components in the aquaculture industry is based on the *partial coefficient method*, which requires that the maximum load effect must be lower than the minimum strength of the component with sufficient probability. This requirement ensures that the loads imposed on the fish farm does not exceed the strength of the different components, by applying safety factors that account for uncertainties in load and response, as well as material properties.

The mooring analyses performed in the industry today are based on regular wave analyses, which implies that the variability in load conditions is not assessed. Simulations performed with only regular waves exclude the uncertainty in estimation of loads, and does not capture the slowly-varying motions that arise in irregular conditions.

A simulation study of mooring line tension was conducted to inspect the effects of irregular environmental conditions and the variability of the response. Interaction between waves and current in irregular conditions was dominated by non-linear effects due to viscous drift. Viscous drift arises from the relative velocity term in Morison's equation, which describes the relative motion between the structure and the fluid. Simulations in irregular conditions captured both wave-frequency motions and low-frequency motions, which cannot be identified in standard regular analyses.

An extreme value distribution of mooring line tension was developed based on the *Two Sea States Approach*, which is a useful method for estimating the load distribution when there is lack of simultaneous data available. The resulting extreme value distribution showed inherent variability and deviations from the design wave approach. Distribution of component strength was approximated by assuming that both standard deviation and mean value is dependent on the minimum breaking load of the component. The resulting distributions of load and strength showed that probability of overload was extremely small.

The characteristic load that will act on the structure was determined from three different approaches in this simulation study; (i) Static analyses with current only, (ii) Dynamic analyses in irregular waves, and (iii) Dynamic analyses in regular waves. The results showed that approach (iii) gave more than three times higher design load than approach (i), and

more than twice the design load from approach (ii). This implies that selection of analysis method has significant impact on the requirements concerning the load the components must withstand. By choosing the approach that gives the lowest design load requirement, money can be saved. The industry must consider whether it should be beneficial to choose one analysis approach over another.

The load factor applied to the characteristic load was the same for regular and irregular conditions. Due to the deviation in design load for the two approaches, a third load factor valid for regular analyses should be considered introduced in the technical standard. The material factor for synthetic rope also gave a very conservative design strength, due to the inherent safety level in the characteristic strength.

This report concludes that design analyses should be conducted with longer time series and irregular environmental conditions to be able to study the behavior of fish farms in more realistic sea states and capture the variability of sea loads. The industry should contribute to, and encourage, software development, such that state of the art analysis tools become commercial. The challenges that comes with more exposed sites must be modelled correctly to ensure that the installations are fit for harsher environmental conditions.

11.2   Recommendations for Further Work

For this simulation study, only the *Two Sea States Approach* was conducted, due to limited available time and time consuming simulations. For obtaining a more accurate extreme value distribution, the *All Sea States Approach* should be conducted, with a wide range of H_S and T_p values to capture the extreme effects. Also, the length of the simulations should be extended to at least 20 minutes to ensure an accurate piecewise stationary short-term description of the environment.

To achieve more comparable results, the simulation model should be modelled as a true copy of an existing system. The mooring lines were modelled without the anchor chain segment, and the weight of the mooring lines in water was made higher than polyethylene ropes usually are. This made comparison with component strength difficult, due to lack of breaking load data. By modelling mooring lines with known dimensions, weight in water, as well as breaking load, the distribution of load can be directly compared to the distribution of strength of the mooring lines. This applies for all types of components.

This simulation study only focused on mooring line tension, and analyses of all local components, as well as the global system, should be conducted to be able to generalize the conclusions. The results from this study can be seen as trends, and the response of the

global system in irregular conditions should be inspected more closely to understand the extent of irregular wave effects.

References

Bai, Y. and Bai, Q. (2012). *Subsea Engineering Handbook*. Elsevier, Amsterdam.

Berstad, A. J., Heimstad, L. F., and Walaunet, J. (2014). Model testing of fish farms for validation of analysis programs. In *Proceedings of the ASME 2014 33rd International Conference on Ocean, Offshore and Arctic Engineering*, OMAE2014. ASME.

Berstad, A. J., Tronstad, H., Sivertsen, S.-A., and Leite, E. (2005). Enhancement of design criteria for fish farm facilities including operations. In *The 24th International Conference on Offshore Mechanics and Arctic Engineering*, OMAE2005. ASME.

Brown, D. T. (2005). Mooring systems. *Handbook of Offshore Engineering (2-volume set)*, pages 663–708. Chapter 8.

Burns, G. E. (1983). Calculating viscous drift of a tension leg platform. In *Proceedings of the ASME 1983 Second International Conference on Ocean, Offshore and Arctic Engineering*, OMAE1983.

Chakrabarti, S. (2005). Ocean environment. *Handbook of Offshore Engineering (2-volume set)*, pages 79–131. Chapter 3.

Curtin, W. G., Shaw, G., Beck, J. K., and Bray, W. A. (2008). *Limit State Design*. Oxford, UK: Blackwell Science Ltd, Oxford, UK.

Directorate of Fisheries (2016). Utviklingstillatelser. *Web Page in Norwegian*, Downloaded 30.09.2016. http://www.fiskeridir.no/Akvakultur/Tildeling-og-tillatelser/Saertillatelser/Utviklingstillatelser.

Directorate of Fisheries (2017). Organisering. *Web Page in Norwegian*, Downloaded 14.02.2017. http://www.fiskeridir.no/Om-oss/Organisering.

Endresen, P. C. (2017). Research Scientist SINTEF Ocean. Personal Communication 26.05.2017.

Endresen, P. C., Birkevold, J., Føre, M., Fredheim, A., Kristiansen, D., and Lader, P. (2014). Simulation and validation of a numerical model of a full aquaculture net-cage system. In *Proceedings of the ASME 2014 33rd International Conference on Ocean, Offshore and Arctic Engineering*, number 23382 in OMAE2014.

Endresen, P. C., Føre, M., Fredheim, A., Kristiansen, D., and Enerhaug, B. (2013). Numerical modeling of wake effect on aquaculture nets. In *Proceedings of the ASME 2013 32nd International Conference on Ocean, Offshore and Arctic Engineering*, number 11446 in OMAE2013, page V003T05A027.

Enerhaug, B., Føre, M., Endresen, P. C., Madsen, N., and Hansen, K. (2012). Current loads on net panels with rhombic meshes. In *Proceedings of the ASME 2012 21st International Conference on Ocean, Offshore and Arctic Engineering*, number 83394 in OMAE2012, pages 49–60.

Faltinsen, O. M. (1990). *Sea Loads on Ships and Offshore Structures*. Cambridge Ocean Technology Series. Cambridge University Press, Cambridge.

Fredheim, A. (2016). Introduction to Marine Aquaculture. *Lecture Notes*, TMR4140.

Fredheim, A. and Langan, R. (2009). *Advances in technology for off-shore and open ocean finfish aquaculture*, book section 30, pages 914–944. Woodhead Publ. CRC Press, Oxford.

Føre, H. M. (2016). Structural Characteristics of Floating Open Net Cage Systems. *Lecture Notes*, TMR4140.

Føre, M. (2017). SINTEF Ocean. Personal Communication 31.03.2017.

Greco, M. (2012). *Sea Loads. Complementary material to "Sea Loads on Ships and Offshore Structures" by O. M. Faltinsen*, TMR4215. Lecture Notes.

Hairer, E., Nørsett, S. P., and Wanner, G. (1993). *Solving Ordinary Differential Equations I : Nonstiff Problems*, volume 8 of *Solving ordinary differential equations*. Springer Berlin Heidelberg, 2nd ed. edition.

Havbrukstjenesten AS (2015). *Lokalitetsrapport av Salatskjæra*. Report nr. LR-T-00515. In Norwegian.

Haver, S. (2011). *Prediction of Characteristic Response for Design Purposes*. Preliminary version.

Haver, S. (2012). From Probabilities to Design of Offshore Structures in 3 Lectures. *Lecture Notes*, TMR4225.

Hval, M. N. (2017). Marine Engineer in Aqualine. Personal Communication 17.03.2017.

Hørte, T. and Macke, M. (2014). NorMoor JIP - Test Data and a Probabilistic Model for Polyester Rope Strength. *DNV GL report no. 2014-0601*, rev. no. 0.

Karlsen, L. (2015). Open Aquaculture Installations. *Lecture Notes*, TMR4140.

Kristiansen, T. (2013). A numerical parameter study on current forces on circular aquaculture net cages. In *Proceedings of the ASME 2013 32nd International Conference on Ocean, Offshore and Arctic Engineering*, number 55430 in OMAE2013, page V009T12A035.

Kristiansen, T. and Faltinsen, O. M. (2012). Modelling of current loads on aquaculture net cages. *Journal of Fluids and Structures*, 34:218–235.

Kristiansen, T. and Faltinsen, O. M. (2015). Experimental and numerical study of an aquaculture net cage with floater in waves and current. *Journal of Fluids and Structures*, 54:1–26.

Langen, I. and Sigbjörnsson, R. (1999). *Dynamic Analysis of Structures*. Excerpt from Dynamic Analysis of Structures. s.n., Trondheim.

Larsen, C. M. (2014). *Marine dynamics : TMR4182 Marine dynamics*. Akademika forlag Kompendieforlaget, Trondheim.

Larsen, K. (2016). Station Keeping and Mooring Systems. *Lecture Notes*, TMR4225.

Li, P. and Faltinsen, O. M. (2012). *Wave-induced Vertical Response of an Elastic Circular Collar of a Floating Fish Farm. 10th International Conference on Hydrodynamics*, October 1-4, 2012 St. Petersburg, Russia.

Lie, H. and Kaasen, K. E. (2008). Viscous drift forces on semis in irregular seas - a frequency domain approach. In *Proceedings of the ASME 2008 27th International Conference on Ocean, Offshore and Arctic Engineering*, number 57313 in OMAE2008.

Løland, G. (1993). Current forces on, and water flow through and around, floating fish farms. *Journal of the European Aquaculture Society*, 1:72–89.

Marine Harvest (2015). *Salmon Farming Industry Handbook. Pamphlet*, pages 55–62.

McCool, J. I. (2012). *Using the Weibull Distribution: Reliability, Modeling and Inference*, volume v.950 of *Wiley Series in Probability and Statistics Ser.* Wiley, Hoboken.

Moe, H., Olsen, A., Hopperstad, O. S., Jensen, O., and Fredheim, A. (2007). Tensile properties for netting materials used in aquaculture net cages. *Aquacultural Engineering*, 37(3):252–265.

Morison, J. R., O'Brien, M. P., Johnson, J. W., and Schaaf, S. A. (1950). *The force exerted by surface waves on piles*, volume 189 of *Petroleum Transactions*. American Institute of Mining Engineers, USA.

Myrhaug, D. and Lian, W. (2009). *Marine dynamics : lecture notes 2009.* TMR4182 Marine dynamics : irregular waves. Akademika forlag Kompendieforlaget, Trondheim.

Naess, A. and Moan, T. (2005). Probabilistic design of offshore structures. *Handbook of Offshore Engineering (2-volume set)*, pages 197–277. Chapter 5.

Naess, A. and Moan, T. (2012). *Stochastic Dynamics of Marine Structures*. Cambridge University Press, Cambridge.

Norwegian Seafood Council (2016). *Laksefakta - Norske regler for miljø og oppdrett. Web page in Norwegian*, Downloaded 15.02.2017. https://laksefakta.no/laks-og-miljo/norske-regler-for-miljo-og-oppdrett/.

NSK Ship Design (2016). *NSK - 3417 Offshore Fish Farm. Web Page*, Downloaded 30.09.2016. http://www.nskshipdesign.com/designs/aquaculture/fish-farm/.

NYTEK (2011). *Forskrift om krav til teknisk standard for flytende akvakulturanlegg (NYTEK-forskriften). In Norwegian.* Norwegian Ministry of Trade, Industry and Fisheries.

Pettersen, B. (2007). *Marin teknikk 3 : Hydrodynamikk.* Marine hydrodynamics. Marine Technology Centre, Department of Marine Technology, Trondheim.

Pinkster, J. A. (1975). Low-frequency phenomena associated with vessels moored at sea. *Society of Petroleum Engineers Journal*, 15(06).

Priour, D. and Germain, G. (2005). Experimental study and numerical modelling of a cod-end. *Oceans Europe 2005*, 1:17–22.

Puente, I. J. and Lian, G. (2017). Draft: Long term Analysis of TLP Extreme Tendon Tension Using a Coupled Model and Comparison with the Contour Line Approach. In *Proceedings of the ASME 2017 36th International Conference on Ocean, Offshore and Arctic Engineering*, number 61213 in OMAE2017.

Rausand, M. (2013). *Risk Assessment : Theory, Methods, and Applications.* Statistics in Practice. Wiley, Hoboken.

Reite, K.-J., Føre, M., Aarsæther, K. G., Jensen, J., Rundtop, P., Kyllingstad, L. T., Endresen, P. C., Kristiansen, D., Johansen, V., and Fredheim, A. (2014). FhSim — Time Domain Simulation of Marine Systems. In *Proceedings of the ASME 2014 33rd International Conference on Ocean, Offshore and Arctic Engineering*, number 23165 in OMAE2014. ASME.

SalMar (2016). *Offshore fish farming - a new era! Web Page*, Downloaded 03.10.2016. http://www.salmar.no/en/offshore-fish-farming-a-new-era.

SINTEF, FHF, and FHL (2010). *Fortøyning med Fjellbolt.* Trondheim.

SINTEF Ocean (2017). *Manual: FhSim - Time Domain Simulation.* Rev. ed.

Standard Norway (2002). *NS-EN 1990. Eurocode: Basis of Structural Design.* Rev. ed.

Standard Norway (2009). *NS9415. Marine Fish Farms: Requirements for design, dimensioning, production, installation and operation.* Rev. ed.

Suwarno, G. and Lee, C. H. (2016). Wave Seed Selection on Irregular Wave Analyses and the Max Extreme Time Windows from 3 Hour Simulations. *Offshore Technology Conference.*

Søreide, M. (2016). Structural Design of Aquaculture Installations. *Lecture Notes*, TMR4225.

The Aquaculture Act (2006). *The Aquaculture Act.* Rev. ed.

Vryof Anchors, B. (2010). Anchor Manual 2010. Capelle a/d Yssel, Netherlands, rev. ed. edition.

A   Simplifying the Viscous Equations

Simplification of the viscous equations is described in the following section, and this procedure is based on Burns (1983).

For current and waves arising from the same direction, the drag force can be calculated by:

$$F = R \left[V_C + V_W \cos{(\theta + \psi)} - V_S \cos{(\theta)} \right] \times \left[V_C + V_W \cos{(\theta + \psi)} - V_S \cos{(\theta)} \right] \tag{84}$$

where V_C is the current velocity, V_W is the wave particle velocity, and V_S is the velocity of the structure. The phase shift ψ represents the shift of the structure centerline from the wave, plus the spacial shift of the member from the centerline.

By introducing a partial relative velocity, V_r, and a phase shift α:

$$V_r \cos{(\theta + \alpha)} = V_W \cos{(\theta + \psi)} - V_S \cos{(\theta)}, \tag{85}$$

Expanding equation 85, equating the like terms, and squaring, gives the expressions for V_r and α, respectively:

$$V_r = \sqrt{V_W^2 + V_S^2 - 2V_W V_S \cos\psi} \tag{86}$$

$$\alpha = \frac{V_W \sin\psi}{V_W \cos\psi - V_S}, \tag{87}$$

where V_R represent the amplitude of the relative velocity between the structure and water particle, and α is the phase shift measured from the wave phase. By letting $\theta + \alpha = \phi$, equation 84 becomes:

$$\frac{F}{R} = (V_C + V_r \cos{(\phi)}) \, |V_C + V_r \cos{(\phi)}| \tag{88}$$

Two expressions equivalent to equation 88 is then:

$$\frac{F}{R} = V_C^2 + V_r^2 \cos\phi^2 + 2V_C V_r \cos\phi, \qquad V_C \geq |V_r \cos\phi| \tag{89}$$

$$\frac{F}{R} = \left[V_C^2 + V_r^2 \cos\phi^2 \right] \frac{V_r \cos\phi}{|V_r \cos\phi|} + 2V_C V_r \cos\phi, \qquad V_C < |V_r \cos\phi| \tag{90}$$

It can be shown that by integrating equation 89 and 90 over a wave cycle, the mean viscous force, F_S, can be determined from:

$$\frac{F_S}{R} = V_C^2 + \frac{1}{2}V_r^2, \qquad V_C \geq |V_r \cos\phi| \tag{91}$$

$$\frac{F_S}{R} = 1.4 \, V_C V_r, \qquad V_C < |V_r \cos\phi|, \tag{92}$$

where equation 91 is a direct derivation, while 92 is an approximate solution. These two equations does not account for free-surface effects.

B   Site Survey: Salatskjæra

The simulations in this Master Thesis was based on the environmental conditions at the Salatskjæra locality. The site survey was conducted by Havbrukstjenesten AS and is owned by SalMar Farming. Table B.1 and B.2 present the key results from the site survey used for the simulation study.

Figure B.1: Site Survey for Salatskjæra

Table B.1: Site survey for 10 year return period

Return Period - 10 year			N	NE	E	SE	S	SW	W	NW
Current	5 m	cm/s	46	50	37	82	32	24	23	51
	Direction	degrees	0-15	15-30	90-105	135-150	165-180	240-255	255-270	330-345
	15 m	cm/s	30	13	20	73	23	9	29	45
	Direction	degrees	345-0	15-30	90-105	135-150	165-180	240-255	270-285	300-315
Wind-induced waves	Hs	m	2.7	2.8	2.7	2.6	2.0	2.0	2.2	2.4
	Tp	s	4.1	5.4	5.4	5.4	4.0	4.0	3.7	3.6
	Direction	degrees	22	59	85	114	170	227	279	337
Ocean Swells	Hs	m	1.2					0.7	1.0	1.2
	Tp	s	14.0					15.4	15.4	16.3
	Direction	degrees	63					44	61	65
Combined wave conditions	Hs	m		3.2	3.3					
	Tp	s		5.9	6.3					
	Direction	degrees		66	87					

Table B.2: Site survey for 50 year return period

Return Period - 50 year			N	NE	E	SE	S	SW	W	NW
Current	5 m	cm/s	52	56	41	91	36	27	26	57
	Direction	degrees	0-15	15-30	90-105	135-150	165-180	240-255	255-270	330-345
	15 m	cm/s	34	14	22	82	26	10	33	50
	Direction	degrees	345-0	15-30	90-105	135-150	165-180	240-255	270-285	300-315
Wind-induced waves	Hs	m	2.8	3.0	2.9	2.8	2.3	2.2	2.4	2.6
	Tp	s	4.1	5.7	5.7	5.4	4.0	4.0	4.0	4.0
	Direction	degrees	22	60	85	113	169	224	276	337
Ocean Swells	Hs	m	1.2					0.7	1.1	1.3
	Tp	s	14.5					16.3	16.3	16.3
	Direction	degrees	64					48	62	65
Combined wave conditions	Hs	m		3.4	3.5					
	Tp	s		6.3	6.5					
	Direction	degrees		66	87					

C   Simulation Model

C.1   Mooring System

Table C.1: Data for the mooring system of Aqualine Midgard®

Mooring System	Value	Unit
Polyethylene mooring lines		
Number	8	#
Length	300	m
Diameter	0.0499775	m
E-modulus	1.9×10^9	N/m^2
Weight in water	2.20694	kg/m
Anchor depth	100	m
Horizontal distance to anchor	355	m
Spring stiffness of bottom attachment	2×10^5	N/m
Bridles		
Bridles at each corner	3	#
Length outer bridle	53.091	m
Length mid bridle	47.7055	m
Diameter	0.0499775	m
E-modulus	2.0×10^{11}	N/m^2
Weight in water	2.20694	kg/m
Mooring frame		
Number	4	#
Length frame rope	100	m
Depth	8	m
Diameter	0.0499775	m
E-modulus	1.9×10^9	N/m^2
Weight in water	2.20694	kg/m
Buoys		
Number (one in each corner)	4	#
Buoyancy	2500	$litre$

C.2   Net

Table C.2: Data for the net of Aqualine Midgard®

Net	Value	Unit
Thread diameter	1.73×10^{-3}	m
E-modulus	1.9×10^9	N/m^2
Solidity	0.2232	-
Wall Depth	15	m
Cone Depth	13	m
Total Depth	28	m

C.3   Floater

Table C.3: Data for the floater of Aqualine Midgard®

Floater	Value	Unit
Number of tubes	2	#
Inner tube circumference	157	m
Diameter inner ring	50	m
Tube diameter	0.5	m
Tube area	0.052477	m^2
E-modulus	1.9×10^9	N/m^2
Weight in air	50.010737	kg/m

D   FhSim Input Files

The SimObjects corresponding to the different environments used in this simulation study is presented in the following sections. The complete input-files were uploaded together with the Master Thesis on DAIM.

D.1   50 year conditions

<Lib LibName="SFHBaseLibrary"
SimObject="DeepSeaGravityWaves"
Name="environment"
WaveTheory="Airy"
WaveSpecter="JONSWAP"
Spectrum="Spectrum"
LongCrestedPower="1000.0"
SignificantWaveHeight="3.5"
MeanWavePeriod="6.5"
MainWaveDirectionRad="0"
DepthLayerThickness="5,10,1000"
CurrentVelocity="0.91,0.91,0.82,0.82"
CurrentDirectionRads="0,0,0,0"
/>

D.2   10 year conditions

¡Lib LibName="SFHBaseLibrary"
SimObject="DeepSeaGravityWaves"
Name="environment"
WaveTheory="Airy"
WaveSpecter="JONSWAP"
Spectrum="Spectrum"
LongCrestedPower="1000.0"
SignificantWaveHeight="3.3"
MeanWavePeriod="6.3"
MainWaveDirectionRad="0"
DepthLayerThickness="5,10,1000"
CurrentVelocity="0.82,0.82,0.73,0.73"
CurrentDirectionRads="0,0,0,0"
/>

D.3 Load combination 1

```
<Lib LibName="SFHBaseLibrary"
SimObject="DeepSeaGravityWaves"
Name="environment"
WaveTheory="Airy"
WaveSpecter="JONSWAP"
Spectrum="Spectrum"
LongCrestedPower="1000.0"
SignificantWaveHeight="3.3"
MeanWavePeriod="6.3"
MainWaveDirectionRad="0"
DepthLayerThickness="5,10,1000"
CurrentVelocity="0.91,0.91,0.82,0.82"
CurrentDirectionRads="0,0,0,0"
/>
```

D.4 Load combination 2

```
¡Lib LibName="SFHBaseLibrary"
SimObject="DeepSeaGravityWaves"
Name="environment"
WaveTheory="Airy"
WaveSpecter="JONSWAP"
Spectrum="Spectrum"
LongCrestedPower="1000.0"
SignificantWaveHeight="3.5"
MeanWavePeriod="6.5"
MainWaveDirectionRad="0"
DepthLayerThickness="5,10,1000"
CurrentVelocity="0.82,0.82,0.73,0.73"
CurrentDirectionRads="0,0,0,0"
/>
```

D.5 Current only

```
<Lib LibName="SFHBaseLibrary"
SimObject="DeepSeaGravityWaves"
Name="environment"
WaveTheory="Airy"
WaveSpecter="JONSWAP"
```

Spectrum="Spectrum"
LongCrestedPower="1000.0"
SignificantWaveHeight="0"
MeanWavePeriod="0"
MainWaveDirectionRad="0"
DepthLayerThickness="5,10,1000"
CurrentVelocity="0.91,0.91,0.82,0.82"
CurrentDirectionRads="0,0,0,0"
/>

D.6   Waves only

<Lib LibName="SFHBaseLibrary"
SimObject="DeepSeaGravityWaves"
Name="environment"
WaveTheory="Airy"
WaveSpecter="JONSWAP"
Spectrum="Spectrum"
LongCrestedPower="1000.0"
SignificantWaveHeight="3.5"
MeanWavePeriod="6.5"
MainWaveDirectionRad="0"
DepthLayerThickness="5,10,1000"
CurrentVelocity="0,0,0,0"
CurrentDirectionRads="0,0,0,0"
/>

D.7   Regular 50 year conditions

<Lib LibName="SFHBaseLibrary"
SimObject="DeepSeaGravityWaves"
Name="environment"
WaveTheory="Airy"
Spectrum="Component"
WaveFrequency="0.9666"
WaveAmplitude="1.75"
WaveDirection="0"
PhaseAngle="0"
DepthLayerThickness="5,10,1000"
CurrentVelocity="0.91,0.91,0.82,0.82"
CurrentDirectionRads="0,0,0,0"

/>

D.8   Design wave approach - load combination 1

```
<Lib LibName="SFHBaseLibrary"
SimObject="DeepSeaGravityWaves"
Name="environment"
WaveTheory="Airy"
Spectrum="Component"
WaveFrequency="0.9666"
WaveAmplitude="3.135"
WaveDirection="0"
PhaseAngle="0"
DepthLayerThickness="5,10,1000"
CurrentVelocity="0.91,0.91,0.82,0.82"
CurrentDirectionRads="0,0,0,0"
/>
```

D.9   Design wave approach - load combination 2

```
<Lib LibName="SFHBaseLibrary"
SimObject="DeepSeaGravityWaves"
Name="environment"
WaveTheory="Airy"
Spectrum="Component"
WaveFrequency="0.9666"
WaveAmplitude="3.325"
WaveDirection="0"
PhaseAngle="0"
DepthLayerThickness="5,10,1000"
CurrentVelocity="0.82,0.82,0.73,0.73"
CurrentDirectionRads="0,0,0,0"
/>
```

E   Calculations of Drag Fore on Net Panel

The following simplified calculations are based on Exercise 12 in TMR4225 Marine Operations, spring 2016.

E.1   Method

Total drag force on a net panel can be determined from the Morison formula:

$$F_D = \frac{\rho}{2} \, C_D \, A \, U_L^2 \tag{93}$$

where

ρ	water density
C_D	drag coefficient for net with given solidity
U_L	local incident current velocity ahead of mesh
A	total net area

The current velocity will decrease as an effect of the conservation of mass, and the mean velocity behind several panels can be determined from:

$$u_i = U_\infty 0.9^i \tag{94}$$

where U_∞ is the velocity in front of the first panel and u_i is the velocity in front of panel number i.

A simplified model of a square net cage with two net panels are shown in figure E.1. The drag forces on the longitudinal and bottom part of the net, as well as floater and other components, are neglected in this model.
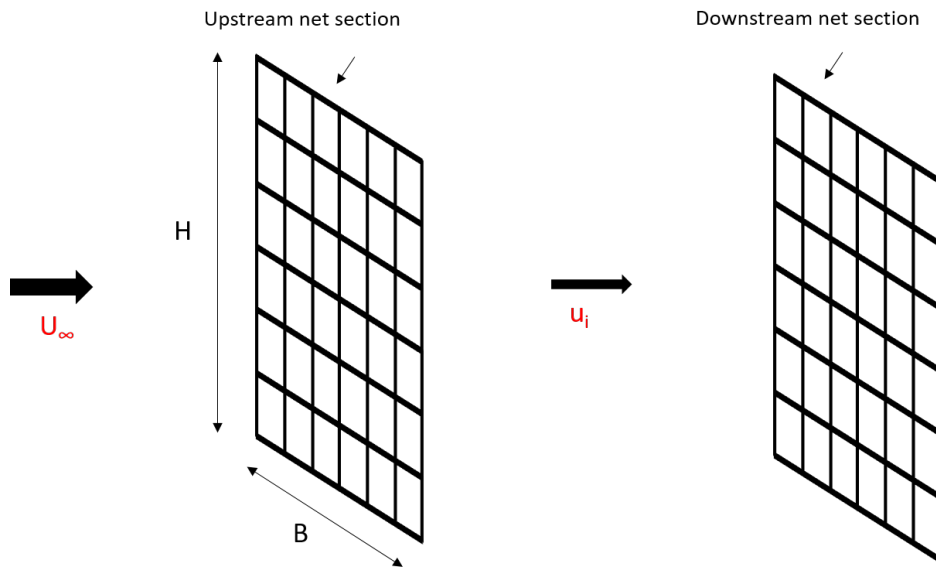
Figure E.1: Simplified model for calculations of drag force on net cage

The simplifications gives total drag force of

$$F_{D,TOT} = \frac{\rho}{2} \ B \ H \ C_D \ [U_\infty^2 + (0.9 \ U_\infty)^2] \tag{95}$$

for a square cage with two net panels.

E.2   Results

This simplified procedure was applied to the Midgard cage by assuming net sides of 30 m and depth of 15 m. The drag coefficient for the net section was assumed to be $C_D = 0.66$, based on Kristiansen and Faltinsen (2012). The results presented in figure E.2 showed good correlation with simulations.

```
---------------------------------
Calculated drag force on net structure
 F_D,calc = 228145.38 N
Drag force from simulations
 F_D,sim = 209837.80 N
Difference between calculated drag force and simulation
 delta = 18307.58 N
---------------------------------
```

Figure E.2: Results from hand-calculations

F   MATLAB

F.1   Inspect mooring line tension 50 year conditions

```matlab
%          MOORING LINE TENSION
% inspect and compare tension in all mooring lines

clc
clear all

%% Open data
path    = 'C:\Users\malinbjorkoy\Desktop\Master\FhSimPlayPen_vs14_6_4_student\bin';
header  = [path '\'];% '\env'];
filename = [header 'Midgard_env_50_1.csv'];
data    = dlmread(filename,';',3,0);

%% Extract forces in mooring lines
fid = fopen(filename,'r');
tags = split(fgetl(fid),';');           %Get tag names from first line (row)
ports  = split(fgetl(fid),';');         %Port names from second line (row)
indexes = zeros(1,size(tags,1));

for i = 1:1:size(tags,1)
    str = tags{i};
    if(~isempty(strfind(str,'ACable')))   %Find mooring line forces = ACable
        indexes(i) = 1;
    end
end

subset  = data(:,logical(indexes));
ports   = ports(logical(indexes));

indexes = zeros(1,size(tags,1));

for i = 1:1:size(ports,1)
    str = ports{i};
    if(~isempty(strfind(str,'ForceA')))   %Forces in point A
        indexes(i) = 1;
    end
end

subset  = subset(:,logical(indexes));

%% Make vectors of mooring line forces
```

F.1 Inspect mooring line tension 50 year conditions

```matlab
x = subset(:,1:3:end);          %First column in each ACable
y = subset(:,2:3:end);          %Sencond column in each ACable
z = subset(:,3:3:end);          %Third column in each ACable


%% Mooring line tension in all 8 lines
for i = 1:8
    T(:,i) = sqrt((x(:,i)).^2 + (y(:,i)).^2 + (z(:,i)).^2);
end %for


%% Plot tension in all mooring lines
figure
plot(data(:,1), T,'LineWidth',1.2);
title('Tension in all mooring lines');
set(gca,'fontsize',12)
xlabel('Time [s]');
ylabel('Tension [N]');
legend('1','2','3','4','5','6','7','8');


%% Windward mooring lines
figure
plot(data(:,1), T(:,2),'b','LineWidth',1.2);
hold on
plot(data(:,1), T(:,3),'r','LineWidth',1.2);
hold off
title('Tension in windward mooring lines');
set(gca,'fontsize',12)
xlabel('Time [s]');
ylabel('Tension [N]');
legend('Line # 2','Line # 3');


%% Leeward mooring lines
figure
plot(data(:,1), T(:,1),'c','LineWidth',1.2);
hold on
plot(data(:,1), T(:,4),'m','LineWidth',1.2);
hold off
title('Tension in leeward mooring lines');
set(gca,'fontsize',12)
xlabel('Time [s]');
ylabel('Tension [N]');
legend('Line # 1','Line # 4');


%% Inspect tension in mooring line # 2
%cut time series
n = length(data);
tt = data(300:n,1);
T2 = T(:,2);
T2cut = T2(300:n);
```

F2

```
midt = mean(T2cut);

%Plot
figure
plot(tt,T2cut,'b','LineWidth',1.2)
hold on
line([tt(1) n],[midt midt]);
title('Tension in mooring line # 2');
set(gca,'fontsize',12)
xlabel('Time [s]');
ylabel('Tension [N]');
```

F.2 Interaction between current and waves

```
%       STATIC AND DYNAMIC COMPARISON
%inspect interaction between current and waves in regular and irregular
%conditions

clear all
clc

%% Load static and dynamic tension for regular and irregular sea states
load static dynamic.mat
load load combinations.mat

%% IRREGULAR ENVIRONMENT
% Plot current only, waves only and a combination of current and waves
figure
plot(Tstep,Tw,'r', 'LineWidth',1.2)
hold on
plot(Tstep,Tc,'g', 'LineWidth',1.2)
hold on
plot(Tstep,Tcomb,'b', 'LineWidth',1.2)
hold off
axis([0 Tstep(n) 0 2*10^5])
set(gca,'fontsize',12)
title('Static and dynamic loads')
xlabel('Time [s]')
ylabel('Tension [N]')
legend('Waves only','Current only', 'Current and Waves');

% Plot superposition principle
pretension = Tc(1);
superpos = Tw + Tc   pretension;
```

```matlab
figure
plot(Tstep,Tcomb,'b', 'LineWidth',1.2)
hold on
plot(Tstep,superpos,'r', 'LineWidth',1.2)
hold off
title('Combined current and irregular waves')
set(gca,'fontsize',12)
xlabel('Time [s]')
ylabel('Tension [N]')
legend('Current and waves', 'Current and waves from superposition');

%% REGULAR AND IRREGULAR ENVIRONMENT
% Plot regular and irregular together
figure
plot(Tstep,Tcomb,'b', 'LineWidth',1.2)
hold on
plot(Tstep,Trcomb,'m', 'LineWidth',1.2)
hold off
title('Regular and irregular response')
set(gca,'fontsize',12)
xlabel('Time [s]')
ylabel('Tension [N]')
legend('Irregular','Regular' );

% Plot close up of combined response, regular and irregular
Tstep2 = Tstep(401:n);
Tcomb2 = Tcomb(401:n);
Trcomb2 = Trcomb(401:n);
mean = sum(Tcomb2)/length(Tcomb2);
meanr = sum(Trcomb2)/length(Trcomb2);

figure
plot(Tstep2,Tcomb2,'b', 'LineWidth',1.2)
hold on
plot(Tstep2,Trcomb2,'m', 'LineWidth',1.2)
line([Tstep2(1) n1],[mean mean], 'LineWidth',1.2);
line([Tstep2(1) n1],[meanr meanr], 'LineWidth',1.2);
hold off
title('Regular and irregular response')
set(gca,'fontsize',12)
xlabel('Time [s]')
ylabel('Tension [N]')
legend('Irregular','Regular');
```

F.3   Response spectrum

F4

```matlab
%                RESPONSE SPECTRUM
% calculate and plot response spectrum for the mooring line tension
clc
clear all
%% Get data   Static and dynaic contributions
load static dynamic.mat
%% Calculate response spectrum   MATLAB fft description
% Signals to inspect
d = Tw;              %Waves only
x = Tcomb;           %Current and waves
dmean = mean(d);
xmean = mean(x);
d = d dmean;         %remove mean from wave signal
x = x xmean;         %remove mean from combo signal

% Cut response to converged part
n = length(d);     %vector length
stab = 300;        %converged response
d = d(stab:n);     %Remove first segment
x = x(stab:n);     %Remove first segment
L = n stab;        %Length of signal

% Compute the Fourier transform of the signal.
z = 10*pow2(nextpow2(n));   %transform length
Y = fft(x);                 %combined response
A = fft(d);                 %response due to waves

%Frequnecy specifications
Fs = 1.0;                 %Sampling frequency, 1 per second
f = Fs*(0:(L/2))/L;       %frequency area
w = 2*pi*f;
nn = length(f);

Y2 = abs(Y/L);
Y1 = Y2(1:L/2+1);
Y1(2:end 1) = 2*Y1(2:end 1);     %combined current and waves

A2 = abs(A/L);
A1 = A2(1:L/2+1);
A1(2:end 1) = 2*A1(2:end 1);     %waves only

%% JONSWAP spectrum
%50 year conditions
Tp = 6.5;          %peak period
Hs = 3.5;          %significant wave height
wp = 2*pi/Tp;      %peak frequency
gamma = 3.3;       %peakedness paramete
g = 9.81;          %gravity constand
```

F.3 Response spectrum

```matlab
for i = 1:length(w)
    if w(i)<wp
        sigma = 0.07;
    else
        sigma = 0.09;
    end
    aw = exp( (w(i) wp)^2/2*sigma^2*wp^2);
    as = 5.058*(Hs^2/Tp^4)*(1 0.287*log(gamma));
    Sw(i) =  as*g^2/w(i)^5*exp( 1.25*(wp^4/w(i)^4))*gamma^(aw);
 end %for

[maxValue, index] = max(Sw(:));
wmax = w(index);

%% Plot JONSWAP
 figure
 plot(w,Sw, 'LineWidth',1.2)
 hold on
 line([wmax wmax],[0 maxValue],'Color','green', 'Linestyle','  ', 'LineWidth',1.2)
 hold off
 title('JONSWAP Spectrum');
 set(gca,'fontsize',12)
 xlabel('frequency \omega [rad/s]');
 ylabel('S_F (\omega)');

%% Plot the one sided spectrum:
figure
plot(w,Y1,'b',w,A1,'r', 'LineWidth',1.2);
hold on
line([wp wp],[0 max(Y1)/4],'Color','green', 'Linestyle','  ', 'LineWidth',1.2);
hold off
title('Response Spectrum')
set(gca,'fontsize',12)
xlabel('frequency \omega [rad/s]')
ylabel('S_x (\omega)')
legend('Combined waves and current','Waves only', 'Peak frequency');

%% Plot only wave spectrum
figure
plot(w,A1,'r', 'LineWidth',1.2);
hold on
line([wp wp],[0 max(A1)/2],'Color','green', 'Linestyle','  ', 'LineWidth',1.2);
hold off
title('Response Spectrum for waves only')
set(gca,'fontsize',12)
xlabel('frequency \omega [rad/s]')
ylabel('S_x (\omega)')
```

F6

```matlab
legend('Waves only', 'Peak frequency');
```

F.4   Convergence test

```matlab
%              CONVERGENCE TEST
% Check if the Gumbel parameters converge and determine how many
% simulation runs that are nescessary
clc
clear all
%% Open data
%Load tension in mooring line 2 for all simulation runs
load tension.mat
 %% Gumbel Parameters
 %Check if the number of storm samples is adequate, i.e. if the Gumbel parameters converge
 n = length(T2_50);           %vector length
 N = [1:1:n];                 %vector with # of storm samples
 Qlim = 0.9;                  %90% quantile
 p = log ( log(Qlim));        %logarithmic 90% quantile

for i=1:n
    %      For 50 year storm condition
    Text_50(i) = max(T2_50{1,i});                    %Extreme 50 year
    sigma_ext_50 = std(Text_50);                     %standard deviation of extreme values
    mu_ext_50 = mean(Text_50);                       %mean of extreme values

    %Gumbel parameters
    beta_50(i) = (sqrt(6)/pi) * sigma_ext_50;        %parameter beta
    alpha_50(i) = mu_ext_50   0.5772 * beta_50(i);   %parameter alpha

    %90% quantile
    ev50_fit = evfit(Text_50);                        %EVD parameters
    Xx_50(i) = evinv(Qlim, ev50_fit(1),ev50_fit(2));  %Built in function for 90% quantile
    Q_50(i) = alpha_50(i)   beta_50(i)*p;             %90% quantile function

    %      For 10 year storm condition
    Text_10(i) = max(T2_10{1,i});                    %Extreme 10 year
    sigma_ext_10 = std(Text_10);                     %standard deviation of extreme values
    mu_ext_10 = mean(Text_10);                       %mean of extreme values

    %Gumbel parameters
    beta_10(i) = (sqrt(6)/pi) * sigma_ext_10;        %parameter beta
    alpha_10(i) = mu_ext_10   0.5772 * beta_10(i);   %parameter alpha

    %90% quantile
    ev10_fit = evfit(Text_10);                         %EVD parameters
```

F.4 Convergence test

```matlab
    Xx_10(i) = evinv(Qlim, ev10_fit(1),ev10_fit(2));    %Built in function for 90% quantile
    Q_10(i) = alpha_10(i)   beta_10(i)*p;               %90% quantile function

end %for

%% Save Gumbel parameters
%Converged Gumbel parameters alpha and beta
a50 = alpha_50(n);
b50 = beta_50(n);
a10 = alpha_10(n);
b10 = beta_10(n);
%Sort extreme forces in entire time series
Text_50 = sort(Text_50);
Text_10 = sort(Text_10);

save('gumbel parameters','a50','b50','a10','b10',...
    'Text_50','Text_10','Q_50','Q_10','n','Qlim','p')
%% Plot Gumbel parameters to ensure that they converge
%   1 . Alpha
figure
plot(N,alpha_50, 'o ', 'LineWidth',1.2);
hold on
plot(N,alpha_10, 'x ', 'LineWidth',1.2);
hold off
title('Gumbel parameter \alpha');
ylabel('\alpha');
xlabel('# storm samples, N');
set(gca,'fontsize',13)
legend('50 year conditions', '10 year conditions')

%   2 . Beta
figure
plot(N,beta_50,'o ', 'LineWidth',1.2);
hold on
plot(N,beta_10, 'x ', 'LineWidth',1.2);
hold off
title('Gumbel parameter \beta');
set(gca,'fontsize',13)
ylabel('\beta');
xlabel('# storm samples, N');
legend('50 year conditions', '10 year conditions')

%   3 . 90% quantile plots
%50 year conditions
figure
plot(N,Xx_50,'^  g', 'LineWidth',1.2);
hold on
plot(N, Q_50,'^ b', 'LineWidth',1.2)
```

F8

```matlab
hold off
title('Gumbel 90% quantile 50 year conditions');
set(gca,'fontsize',13)
ylabel('CDF');
xlabel('# storm samples, N');
legend('Fitted', 'Calculated')

%10 year conditions
figure
plot(N,Xx_10,'* m', 'LineWidth',1.2);
hold on
plot(N, Q_10, '* c', 'LineWidth',1.2);
hold off
title('Gumbel 90% quantile 10 year conditions');
set(gca,'fontsize',13)
ylabel('CDF');
xlabel('# storm samples, N');
legend('Fitted', 'Calculated')
```

F.5   Gumbel distribution in 10 and 50 year conditions

```matlab
%              GUMBEL DISTRIBUTTION
% plot Gumbel PDF & CDF and Gumbel Q Q plot for 10 and 50 year conditions
clc
clear all
%% open data
load gumbel parameters.mat
%% Gumbel PDF & CDF for 10 and 50 year environment
for m = 1:n
    %50 year conditions
    z_50 = (Text_50(m) a50)/b50;                    %z parameter in distribution
    Gpdf50(m) = (1/b50)*exp( (z_50 + exp( z_50)));   %Gumbel PDF
    Gcdf50(m) = exp( exp( z_50));                    %Gumbel CDF

    %10 year conditions
    z_10 = (Text_10(m) a10)/b10;
    Gpdf10(m) = (1/b10)*exp( (z_10 + exp( z_10)));   %Gumbel PDF
    Gcdf10(m) = exp( exp( z_10));                    %Gumbel CDF
end %for

%Fitted extreme value distribution
%(1) location parameter alpha, (2) scale parameter beta
ev50_fit = evfit( Text_50);
ev10_fit = evfit( Text_10);
```

F.5   Gumbel distribution in 10 and 50 year conditions

```matlab
%Built in pdf
Gpdf50_fit = evpdf( Text_50,ev50_fit(1),ev50_fit(2));    %PDF 50 year
Gpdf10_fit = evpdf( Text_10,ev10_fit(1),ev10_fit(2));    %PDF 10 year

%Built in pdf with converged alpha and beta
Gpdf50_semifit = evpdf(Text_50,a50,b50);
Gpdf10_semifit = evpdf(Text_10,a10,b10);

%Built in CDF
Gcdf50_fit = 1 evcdf( Text_50,ev50_fit(1),ev50_fit(2));
Gcdf10_fit = 1 evcdf( Text_10,ev10_fit(1),ev10_fit(2));

%Quantile line
Xquant50 = [Q_50(n) Q_50(n)];
Yquant50 = [0 0.5*max(Gpdf50)];
Xquant10 = [Q_10(n) Q_10(n)];
Yquant10 = [0 0.5*max(Gpdf10)];

%% Plot PDF and CDF
%     Plot Gumbel PDF
figure
hold on
plot(Text_50,Gpdf50,' s', 'LineWidth',1.2);
hold on
plot(Text_50,Gpdf50_fit,' o', 'LineWidth',1.2)
hold on
line(Xquant50,Yquant50, 'LineWidth',1.2)
hold off
title('Gumbel PDF  50 year conditions');
set(gca,'fontsize',13)
ylabel('PDF');
xlabel('Tension [N]');
legend('Calculated PDF','Fitted PDF','90% Quantile')

figure
plot(Text_10,Gpdf10,' s', 'LineWidth',1.2);
hold on
plot(Text_10,Gpdf10_fit,' o', 'LineWidth',1.2)
hold on
line(Xquant10,Yquant10, 'LineWidth',1.2)
hold off
title('Gumbel PDF   10 year conditions');
set(gca,'fontsize',13)
ylabel('PDF');
xlabel('Tension [N]');
legend('Calculated PDF','Fitted PDF','90% Quantile')

%     Plot Gumbel CDF
```

F10

```matlab
figure
plot(Text_50,Gcdf50,' s', 'LineWidth',1.2);
hold on
plot(Text_50,Gcdf50_fit,' o', 'LineWidth',1.2)
hold on
line([Text_50(1) Text_50(n)],[Qlim Qlim],'Color',...
    'blue', 'LineStyle','  ', 'LineWidth',1.2);
hold off
title('Gumbel CDF   50 year conditions');
set(gca,'fontsize',13)
ylabel('CDF');
xlabel('Tension [N]');
legend('Calculated CDF','Fitted CDF', '90% Quantile')


figure
plot(Text_10,Gcdf10,' s', 'LineWidth',1.2);
hold on
plot(Text_10,Gcdf10_fit,' o', 'LineWidth',1.2)
hold on
line([Text_10(1) Text_10(n)],[Qlim Qlim],'Color','blue',...
    'LineStyle','  ', 'LineWidth',1.2);
hold off
title('Gumbel CDF   10 year conditions');
set(gca,'fontsize',13)
ylabel('CDF');
xlabel('Tension [N]');
legend('Calculated CDF','Fitted CDF', '90% Quantile')

%% Gumbel plot procedure, Naess chapter 16.6
for r = 1:n
    yax(r) =  log(log((n+1)/r));        %logarithmic y axis
    Mk_50(r) = Text_50(r);              %Extreme value 50 year
    Mk_10(r) = Text_10(r);              %Extreme value 10 year
end %for

%90% quantile line
x2_50 = [Mk_50(1) Mk_50(n)];
x2_10 = [Mk_10(1) Mk_10(n)];
y2 = [ p  p];

%fit linear polynomial
p1_50 = polyfit(Mk_50,yax,1);       %Linear fitting
p2_50 = polyfit(x2_50,y2,1);        %90% quantile line

p1_10 = polyfit(Mk_10,yax,1);       %Linear fitting
p2_10 = polyfit(x2_10,y2,1);        %90% quantile line

%calculate intersection
```

F.5 Gumbel distribution in 10 and 50 year conditions

```matlab
x_intersect_50 = fzero(@(x) polyval(p1_50 p2_50,x),3);    %intersection x coordinate
y_intersect_50 = polyval(p1_50,x_intersect_50);           %intersection y coordinate

x_intersect_10 = fzero(@(x) polyval(p1_10 p2_10,x),3);    %intersection x coordinate
y_intersect_10 = polyval(p1_10,x_intersect_10);           %intersection y coordinate

for s = 1:n
    lin_50(s) = p1_50(1)*Mk_50(s) + p1_50(2);     %Linear fit line
    lin_10(s) = p1_10(1)*Mk_10(s) + p1_10(2);     %Linear fit line
end %for

%% Gumbel plot with intersection point and lines
%     50 year conditions
figure
%Variables
plot(Mk_50, yax,'x', 'LineWidth',1.2);
hold on
%Linear fit
plot(Mk_50,lin_50, 'LineWidth',1.2)
hold on
%90% quantile
line([Mk_50(1) x_intersect_50],[y_intersect_50 y_intersect_50],...
    'Color','blue', 'LineStyle','  ', 'LineWidth',1.2);
%line from intersection to x axis
hold on
line([x_intersect_50 x_intersect_50],[yax(1) y_intersect_50],...
    'Color','blue', 'LineStyle','  ', 'LineWidth',1.2);
hold on
%Intersection point
plot(x_intersect_50,y_intersect_50,'r*')
hold off
title('Q Q Gumbel Plot for 50 year conditions');
set(gca,'fontsize',13)
xlabel('Extreme value');
ylabel(' ln(ln(1 CDF))');
legend('Data','Linear fit', '90% Quantile');

%     10 year conditions
figure
%Variables
plot(Mk_10, yax,'x', 'LineWidth',1.2);
hold on
%Linear fit
plot(Mk_10,lin_10, 'LineWidth',1.2)
hold on
%90% quantile
line([Mk_10(1) x_intersect_10],[y_intersect_10 y_intersect_10],...
    'Color','blue', 'LineStyle','  ', 'LineWidth',1.2);
```

F12

```matlab
%line from intersection to x axis
hold on
line([x_intersect_10 x_intersect_10],[yax(1) y_intersect_10],...
    'Color','blue', 'LineStyle','  ', 'LineWidth',1.2);
hold on
%Intersection point
plot(x_intersect_10,y_intersect_10,'r*')
hold off
title('Q Q Gumbel Plot for 10 year conditions');
set(gca,'fontsize',13)
xlabel('Extreme value');
ylabel(' ln(ln(1 CDF))');
legend('Data','Linear fit', '90% Quantile');
```

F.6   Two Sea States Approach

```matlab
%            METHOD 2: TWO SEA STATES APPROACH
% fit Gumbel distribution from two known sea states
clc
clear all
%% Load parameters
load gumbel parameters.mat
load load combinations.mat
%% Fit Gumbel distribution
T50 = Q_50(n);      %90% quantile from 50 year conditions
T10 = Q_10(n);      %90% quantile from 10 year conditions

%New Gumbel parameters estimated from 2 equations with 2 unknowns
F_X50 = 0.98;       %50 year CDF
F_X10 = 0.9;        %10 year CDF

F50 = log ( log(F_X50));   %constant
F10 = log ( log(F_X10));   %constant

beta90 = ((T10 T50)/F50)*(1/(1 (F10/F50)));       %new beta
alpha90 = beta90*F10 + T10;                       %new alpha

%New Gumbel distribution for new alpha and beta parameters
F_T = [0:0.0001:1];        %CDF vector
f = length(F_T);           %number of entries in CDF vector
Q = alpha90   beta90*p;    %90% quantile of new distribution

for i = 1:f
    t(i) = beta90 * ( log ( log(F_T(i)))) + alpha90;  %calculates tension for new distr
    z_T(i) = (t(i) alpha90)/beta90;                   %Gumbel entry
```

```matlab
    f_T(i) = exp( (z_T(i) + exp( z_T(i))));        %new Gumbel PDF
end %for

%Save variables
save('method2.mat','alpha90','beta90','F_T','f_T','t')

%% Plot fitted Gumbel distribution
%    new Gumbel CDF
figure
plot(t,F_T,'b', 'LineWidth',1.2)
title('Fitted Gumbel CDF');
set(gca,'fontsize',13)
xlabel('Tension [N]');
ylabel('CDF');

%    new Gumbel PDF
figure
plot(t,f_T,'r', 'LineWidth',1.2)
title('Fitted Gumbel PDF');
set(gca,'fontsize',13)
xlabel('Tension [N]');
ylabel('PDF');
```

F.7 Partial coefficient method

```matlab
%                PARTIAL COEFFICIENT METHOD
% Distribution of load and strength with load and material factors
% Comparison of characteristic load
clc
clear all
%% Load parameters
load method2.mat
load load combinations.mat
%% Plot quantiles in the tail region
Quantile = [0:0.0000001:1.0];
qn = length(Quantile);

for j = 1:qn
    pq(j) = log( log(1 Quantile(j))); %CDF
    Qq(j) = alpha90   beta90*pq(j); %Quantiles
    Pf(j) = (Quantile(j));          %1 CDF
end % for

% Plot probability of exceedance
figure
```

```matlab
semilogy(Qq, Pf, ' b', 'LineWidth',1.2)
title('Probability of exceedance', 'FontSize', 14);
xlabel('Tension [N]', 'FontSize', 12);
ylabel('P_f', 'FontSize', 12);

%% Partial coefficient method
%safety factors
gamma_load = 1.15;              %load factor, dynamic analysis
gamma_load_stat = 1.6;         %load factor, static analysis
gamma_mat = 3.0;               %material factor, polyethylene mooring lines

%Characteristic laod and design load
Sd = Sc*gamma_load;                    %irregular design load
Sc_reg = 4.9458e+05;                   %regular characteristic load
Sd_reg = Sc_reg*gamma_load;            %regular design load
Sc_stat = 1.0621e+05;                  %static characteristic load
Sd_stat = Sc_stat*gamma_load_stat;  %static design load

%Characteristic strength
MBL = 6.6904*10^5;
%MBL = 6.6904*10^5*(0.050/0.064)^2;
MBL_gamma = MBL/gamma_mat;

save('characteristic load.mat', 'Sc', 'Sd', 'Sc_reg', 'Sd_reg', 'Sc_stat', 'Sd_stat')
%% Load PDF with load factor
figure
plot(t,f_T,'r', 'LineWidth',1.2)
hold on
Cplot = line([Sc Sc], [0 0.5*max(f_T)], 'Color','red', 'LineWidth',1.2);
Dplot = line([Sd Sd], [0 0.5*max(f_T)], 'Linestyle','  ', 'Color','red', 'LineWidth',1.2);
hold off
title('Distribution of load with effect of safety factor');
set(gca,'fontsize',12)
xlabel('Load [N]');
ylabel('PDF');
legend([Cplot, Dplot], {'Characteristic load S_C','Design load S_D'})
%% Pf with characteristic load
figure
Pfplot = semilogy(Qq,Pf,'b', 'LineWidth',1.2);
hold on
Scplot = line([Sc Sc], [10^(1.55) 10^(7)],...
    'Color','red', 'LineWidth',1.2);
Sdplot = line([Sd Sd], [10^(2.2) 10^(7)],...
    'Color','red', 'Linestyle','  ', 'LineWidth',1.2);
hold on
line([0 Sc], [10^(1.55) 10^(1.55)],...
    'Color','red', 'LineWidth',1.2);
line([0 Sd], [10^(2.2) 10^(2.2)],...
```

```matlab
    'Color','red', 'Linestyle',' ', 'LineWidth',1.2);
hold off
title('Probability of exceedance', 'FontSize', 14);
xlabel('Load [N]', 'FontSize', 13);
ylabel('Pf', 'FontSize', 13);
legend([Pfplot, Scplot, Sdplot],{'Pf','Charateristic load', 'Design load'}, 'FontSize', 12)
%% Strength distribution
mu = 1.05*MBL;              %assuming mean value
sigma = 1.05*0.03*MBL;      %assuming standard deviation
var = sigma^2;
Rmin = MBL 6*sigma;        %calculation range min
Rmax = MBL+6*sigma;        %calculation range max
range = [Rmin:Rmax];
m = length(range);

const = 1/(sqrt(2*pi*var)); %normal distrbution constant

for x = 1:m
    ex(x) = ((range(x) mu).^2)/(2*var);   %exponential value
    f_X(x) = const*exp( ex(x));           %assuming normal distribution
    f_R(x) = f_X(x)*10^4.2;               %for plot purposes
end %for

%plot strength distribution
figure
plot(range,f_X, 'LineWidth',1.2);
title('Distribution of strength');
set(gca,'fontsize',12)
xlabel('Strength [N]')
ylabel('PDF')
legend('Distribution of strength')

%% Plot distirbution of load and strength together
figure
plot(t, f_T,'r',range,f_R,'b','LineWidth',1.2);
hold on
line([Sc Sc], [0 0.5*max(f_T)], 'Color','red', 'LineWidth',1.2);
line([Sd Sd], [0 0.5*max(f_T)], 'Linestyle',' ', 'Color','red', 'LineWidth',1.2);
hold on
line([MBL MBL],[0 0.5*max(f_T)], 'Color','blue', 'LineWidth',1.2)
line([MBL_gamma MBL_gamma],[0 0.5*max(f_T)],...
    'Linestyle',' ', 'Color','blue', 'LineWidth',1.2)
hold off
title('Distribution of load and strength with safety factors');
set(gca,'fontsize',12)
set(gca,'YTick',[]);
xlabel('Load/strength [N]')
ylabel('PDF')
```

F16

```matlab
legend('Distribution of load','Distribution of strength')

%% Distribution of load and strength with different characteristic loads
figure
plot(t, f_T,'r',range,f_R,'b','LineWidth',1.2);
hold on
irreg = line([Sd Sd], [0 0.5*max(f_T)],...
    'Linestyle','  ', 'Color','red', 'LineWidth',1.2);
hold on
reg = line([Sd_reg Sd_reg], [0 0.5*max(f_T)],...
    'Linestyle','  ', 'Color','green', 'LineWidth',1.2);
hold on
stat = line([Sd_stat Sd_stat], [0 0.5*max(f_T)],...
    'Linestyle','  ', 'Color','magenta', 'LineWidth',1.2);
hold on
mbl = line([MBL_gamma MBL_gamma],[0 0.5*max(f_T)],...
    'Linestyle','  ', 'Color','blue', 'LineWidth',1.2);
hold off
title('Design load from different approaches');
set(gca,'fontsize',12)
set(gca,'YTick',[]);
xlabel('Load/strength [N]')
ylabel('PDF')
legend([irreg, reg, stat, mbl],...
    {'Irregular S_D','Regular S_D','Static S_D','Design strength R_D'})

%% Distribution of strength with characteristic strength and design strength
figure
plot(range,f_R,'b','LineWidth',1.2);
hold on
mbl = line([MBL MBL],[0 0.5*max(f_T)],...
    'Color','blue', 'LineWidth',1.2);
mbl_load = line([MBL_gamma MBL_gamma],[0 0.5*max(f_T)],...
    'Linestyle','  ', 'Color','blue', 'LineWidth',1.2);
hold off
title('Distribution of strength with effect of safety factor');
set(gca,'fontsize',12)
xlabel('Strength [N]')
ylabel('PDF')
legend([mbl, mbl_load], {'Characteristic strength R_C','Design strength R_D'})
```